Some Investigations on Metasurface Based Microwave Absorber and their Applications

A Thesis submitted

In fulfilment of the requirement for the award of the degree

of

DOCTOR OF PHILOSOPHY

in

Electronics and Communication Engineering

Submitted by:

Vishal Puri
Reg. No. 951706001

Under the Supervision

of

Dr. Hari Shankar Singh
Assistant Professor
Electronics and Communication Engineering Department
Thapar Institute of Engineering and Technology
Patiala-147 001 (Punjab), India

ELECTRONICS AND COMMUNICATION ENGINEERING DEPARTMENT
THAPAR INSTITUTE OF ENGINEERING AND TECHNOLOGY
PATIALA – 147 004 (PUNJAB), INDIA

OCTOBER-2022

DECLARATION

I, **Vishal Puri** hereby declare that the work contained in the thesis entitled "**Some Investigations on Metasurface based Microwave Absorber and their Applications**" in fulfilment of the requirement for the award of degree "**Doctor of Philosophy**" submitted at **Department of Electronics and Communication Engineering, Thapar Institute of Engineering and Technology, Patiala** is an authentic record of research work carried out under the supervision of **Dr. Hari Shankar Singh**, Assistant Professor, Thapar Institute of Engineering and Technology (TIET), Patiala, Punjab, India. The matter presented in this thesis does not incorporate any material previously published or written by any other person except where due references are made in text. The results obtained in this thesis have not been submitted in part or full to any other institute or university for award of degree or diploma.

Date: 19th Oct 2022

Vishal Puri

(Reg. No. 951706001)

CERTIFICATE

It is certified that the work contained in the thesis entitled **"Some Investigations on Metasurface based Microwave Absorber and their Applications"** by Vishal Puri (Reg. No. 951706001) has been carried out under my supervision and this work has not been submitted elsewhere for any other degree.

Date: 19/10/2022

Dr. Hari Shankar Singh

Assistant Professor

Electronics and Communication Department

Thapar Institute of Engineering and Technology, Patiala

Punjab, India

To start with, first and foremost I would like to bow my head in gratitude while remembering Mata Vaishno Devi, Katra the place from where the blessings of both Shiv and Shakti constantly reach me at any place, any time and at any moment and then I remember Baba Ghulam Shah Badshah the revered saint whose blessing always guide me in my endeavours. The blessings of Mata Vaishno Devi flourished upon me the day I got the opportunity to work under Dr. Hari Shankar Singh (my supervisor). I wish to express my deep sense of gratitude with reverence towards my supervisor Dr. Hari Shankar Singh, Assistant Professor, Department of Electronics and Communication Engineering, Thapar Institute of Engineering and Technology, Patiala for his valuable guidance and inspiring encouragement in pursuance of this work. The research work carried during these years is only and only attributed to his constant support and guidance and today I came to understand the true meaning of well-known lines "Guru bin gyan adhura". I am thankful to Dr. Soumendu Jana (Professor, School of Physics and Materials Sciences), Dr. Amanpreet Kaur, (Assistant Professor, ECED), Dr. R. P. Yadav (Former Assistant Professor, ECED) and Dr. Mayank Agarwal (Assistant Professor, ECED) for being in my doctoral research committee, and encouraging me by giving valuable suggestion when I need it most. I am thankful to Dr. K. R. Jha (Associate Professor, SMVDU, Katra) for extending laboratory facilities in completing experimentation part at SMVDU Katra, J&K. I would like to thank the management and administration of Baba Ghulam Shah Badshah University, Rajouri, J&K for giving me all important permissions to pursue my research work. Further, I would also like to offer my sincere thanks to all Teaching staff and non-teaching staff of ECED at TIET, Patiala, and also staff of the central library, TIET, Patiala for their kind support. The acknowledgement part will be incomplete if I fail to remember my father Mr. L. C. Puri whose always want me to pursue Ph.D. degree and remains instrumental in shaping my thought process and then my mother Mrs. Rita Puri who always believe and trust me. The contribution of my wife Mrs. Shaveta Puri is beyond words and with her all-time support and continuous encouragement surely is responsible for all my achievements in life. The love of my children Lakshya Puri and Shriya Puri is surely a tonic for re-energising my thought process. I would like to extend special thanks to my colleagues and friends Mr. Abishek Mishra, Mr. Rohit Arora, Ms. Manpreet Kaur and Ms. Harleen Kaur for their valuable suggestions, support, and encouragement. Finally, again my humble thanks to my supervisor, the stage reached is only because of his guidance and nothing else. The moment I got the opportunity to work under your guidance my life changed and I reckon this event to be the special blessing from divinity.

The available materials demonstrate only a small portion of Electromagnetic properties that are theoretically discussed and studied. Initially, J. C. Bose realised and emphasised the possibility of artificial material by arranging twisted structures such materials with 'meta' properties were given the term 'Metamaterial'. The metamaterial are engineered materials which are developed artificially. The artificially design metamaterial provides negative permeability and negative permittivity which result in found its usage in many engineering applications one of such application is metamaterial absorber. In 2004, researcher Smith and his team realised the significance of Metamaterial in various applications. Soon after, researcher Landy and his group provided the information about metamaterial based microwave absorber, the work mentioned was notified with special term 'Prefect metamaterial absorber'. The work formed a base on which latter researchers and scientists experimentally demonstrated and applied Absorption principle in various reported work. When an electromagnetic wave is incident at the boundary interface of two regions then some part of the wave is reflected back in first region, some part gets transmitted in the second region and the remaining part gets absorbed provided no scattering and/or diffraction is occurred. The waves which get absorbed in the material if effective properties like permittivity and permeability are tailored to needs, resulting the absorption of the wave at a particular band. The optimization of physical parameters of metallic layer, thickness of dielectric substrate etc. led to coupling of Electric and magnetic fields to specific input impedance and this input impedance can further be matched to free space impedance for maximum absorption. This complete absorption of electromagnetic wave is realised by minimisation of *reflection coefficient*. This properties can be utilized for various strategic and important engineering applications.

The need of low profile absorber in microwave frequency range results in motivation towards metamaterial absorbers for applications demanding isolation in engineering applications. The thesis work was cantered on the attainment of two objectives, the first being design, development, and characterization of the multiband and wideband absorber and the second one is the application part involving the designed absorber in attaining isolation for MIMO setup. The work completed in various stages is summarized as follows;

a. The design of first structure in multiband category focusses on the attainment of multiband absorption with the design and development of a metasurface-based

microwave absorber having polarisation insensitivity, broad angle of incidence, low profile, and compactness in the microwave frequency range.

b. The second structure focuses on the design of super compact polarization insensitive with wide angular stability, ultrathin triple-band metamaterial absorber. The unit cell comprising patches achieves almost perfect absorption (close to 100%) at C-, X-, and Ku-bands.

c. The third structure is a wideband absorber designed and developed with the attainment of more than 99% absorption for ultra-wideband covering a bandwidth of 8.23 GHz from 11.17 GHz to 19.40 GHz. The structure exhibits polarization insensitive behaviour with wide angular stability.

d. The application part is completed with the incorporation of metasurface based absorber as an isolator. The mutual coupling of unwanted fields between MIMO antenna elements acts as a major deterrent to exploiting the optimum performance of the MIMO antenna. The work focus on the design and development of MIMO elements and then incorporation of metasurface-based isolator (acting as absorber) clearly with an intention to provide high order optimum isolation levels between two antenna elements. The work succeeded in incorporating a designed absorber in a practical designed MIMO setup with the attainment of good isolation results.

A. Peer Reviewed International Journals (Published)

A1. V. Puri and H. S. Singh, "Design of super compact ultrathin perfect wide-angle polarization independent metamaterial absorber for C, X and Ku band applications," *Microwave Optical Technology Letters*, vol.63, pp. 2782-90, 2021. **DOI:** https://doi.org/10.1002/mop.32972. **(Impact Factor: 1.311)**

A2. V. Puri and H. S. Singh, "Design and analysis of a compact ultrathin ultra-wideband metamaterial absorber with near to unity absorption for Ku-band," *International Journal of RF Microwave Computer-Aided Engineering*, vol.32, no. 4, 2022. **DOI:** https://doi.org/10.1002/mmce.23069**. (Impact Factor: 1.987)**

A3. V. Puri and H. S. Singh, "Design of an isolation improved MIMO antenna using metasurface based absorber for wireless applications," *Optik- International Journal for Light and Electron Optics*, vol. 259, Mar. 2022. **DOI:** https://doi.org/10.1016/j.ijleo.2022.168963. **(Impact Factor: 2.84)**

A4. V. Puri and H. S. Singh, "Design of quad-band polarization insensitive ultra-thin compact metamaterial based absorber for terahertz applications" *Results in Optics*, vol. 8, no. 100248, pp. 1-8, 2022.
DOI: https://doi.org/10.1016/j.rio.2022.100248

B. Peer Reviewed International Journals (Under-Review)

B1. V. Puri and H. S. Singh, "The C, X and Broad Ku Band Ultrathin Triple-Band Metamaterial Absorber with Wide Angular Stability and Polarisation Insensitive Behaviour for Applications in Microwave Frequency Regime," *Frequenz-Journal of RF Engineering and Telecommunications*. **(Revision Submitted)**

B2. V. Puri and H. S. Singh, "The Near Perfect Wideband Metamaterial Absorber using Conductive Ink with Wide Angular Stability and Polarization Insensitive Behaviour for Applications in Microwave Frequency Regime," *IETE Journal of Research*. **(Under Review)**

C. International Conferences

C1. V. Puri and H. S. Singh, "A Compact Ultrathin Metamaterial Absorber for C, K and Ka Band Microwave Frequency Regime," 2020 *IEEE MTT-S Latin America Microwave Conference (LAMC 2020)*, 2021, pp. 1-3. **DOI:** 10.1109/LAMC50424.2021.9602614.

5G : Fifth Generation

BS : Base Station

CPA : Coherent Perfect Absorption

dB : Decibel

DG : Diversity Gain

DNG : Double Negative

DPS : Double Positive

DPS : Double Positive

EBG : Electromagnetic Band Gap

ECC : Envelope Correlation Coefficient

EDG : Effective Diversity Gain

EM : Electromagnetic

EMC : Electromagnetic Compatibility

EMI : Electromagnetic Interference

ENG : Epsilon Negative

FIT : Finite Integration Technique

FSS : Frequency Selective Surface

FWHM : Full Width Half Maximum

GPS : Global Positioning System

HIS : High Impedance Surfaces

LHM : Left Handed Material

LTE : Long Term Evolution

MEG : Mean Effective Gain

MIMO : Multiple Input and Multiple Output

MNG : Mu Negative

MTM : Metamaterial

PBG : Photonic Band Gap

PEC : Prefect Electric Conductor

PIFA : Planar Inverted-F Antenna

RHM : Right Handed material

S/N : Signal to Noise

SRRR : Square Split Ring Resonator

TARC : Total Active Reflection Coefficient

TE : Transverse Electric

TM : Transverse Magnetic

VNA : Vector Network Analyzer

WPAN : Wireless Personal Area Network

TABLE OF CONTENT

1.1 Introduction to Metamaterial

The term "meta" means beyond and therefore the word "Metamaterial (MM)" signifies artificial composite materials. While a lot of research going on tailoring the properties of material to achieve desired results. The artificial materials are designed to give a new colour to research domain. The effective permittivity ε_{eff} and μ_{eff} represent materials characteristics. The effective permittivity (ε_{eff}) and effective permeability (μ_{eff}) is the basis of classification [1].

The theoretical background metamaterial is linked to negative indexed refractive index and the base is linked to Maxwell's equations of electromagnetism which act as a foundation for realising metamaterials. The four general Maxwell equations are [2],

$$\nabla . E_s = 0 \tag{1.1}$$

$$\nabla . H_s = 0 \tag{1.2}$$

$$\nabla \times E_s = -\mathrm{j}\omega\mu H_s \tag{1.3}$$

$$\nabla \times H_s = (\sigma + \mathrm{j}\omega\epsilon) E_s \tag{1.4}$$

The application of curl on both sides of Eq. (1.3) will provide lossy dielectric electric field and we are to achieve Eq. (1.5) and (1.6);

$$\nabla^2 E_s - \gamma^2 E_s = 0 \tag{1.5}$$

$$\nabla^2 H_s - \gamma^2 H_s = 0 \tag{1.6}$$

where, $\gamma = \sqrt{j\omega\mu + (\sigma + j\omega\epsilon)}$ and is known as propagation constant for any material. The Eq. (1.5) and (1.6) are known as wave equation or Helmholtz equation and act as base equations for understanding the behaviour of any material.

If *z*-axis is taken as axis of propagation and electric and magnetic field is travelling along *x*- and *y*-direction then we simplify earlier equations such that we are able to achieve;

$$E_s = E_x a_x \tag{1.7}$$

On substitution of value of E_s in Eq. (1.5), we are able to achieve;

$$E_x(z) = E_o e^{\gamma z} + E_o' e^{-\gamma z} \tag{1.8}$$

The representation of electric field vector will be of the form;

$$(\mathrm{E(z,t)} = Real(E_x(z) a_x e^{j\omega t}) \tag{1.9}$$

We know that $\gamma = \alpha + j\beta$ thus substituting the above parameters in the equation we deduce that;

$$E(z,t) = E_o e^{-\alpha z} cos(\omega t - kz) a_z \quad (1.10)$$

The similar interpretation can be achieved for magnetic field and is given by;

$$H(z,t) = H_o e^{-\alpha z} cos(\omega t - kz) a_y \quad (1.11)$$

The intrinsic medium impedance 'η' draws relationship governing electric and magnetic fields and can be interpreted as,

$$\eta = \frac{E_0}{H_0} \quad (1.12)$$

If the medium is lossless then the value of $\sigma \approx 0$ and electric field and magnetic field are in phase to each other with $\alpha = 0$ and $k = \omega\sqrt{\mu\varepsilon}$ thus

$$|\eta| = \sqrt{\frac{\mu}{\varepsilon}} \quad (1.13)$$

The, velocity of wave becomes,

$$v = \frac{1}{\sqrt{\mu\varepsilon}} \quad (1.14)$$

The material properties denoted permittivity (ε) and permeability (μ) will determine the movement of electric and magnetic line of force through a material and if direction of wave vector 'k' and Poynting vector 'p' are following same direction then movement of propagating wave with A as transmitter and B as receiver will obey right-hand rule and such materials are called as right handed materials (RHM). The materials for which constituents parameters ε and μ are such that the wave vector 'k' and Poynting vector 'p' are in opposite direction, the material will be interpreted as left-handed material (LHM) as shown in Fig. 1.1. The interpretation lies in the fact that constituent parameters ε and μ will decide propagation of wave and such materials are organized to form four broad divisions as shown in Fig. 1.2.

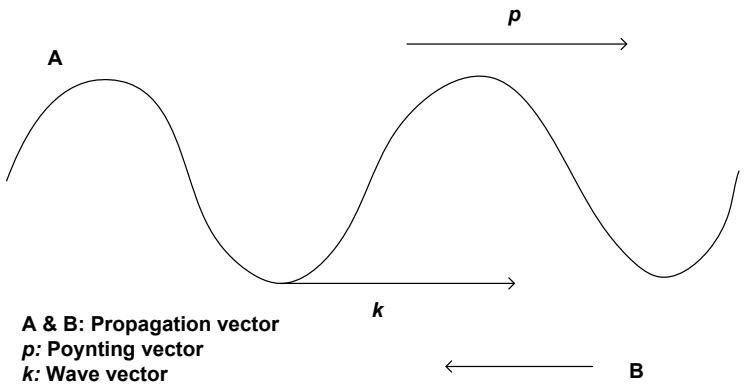

(a)

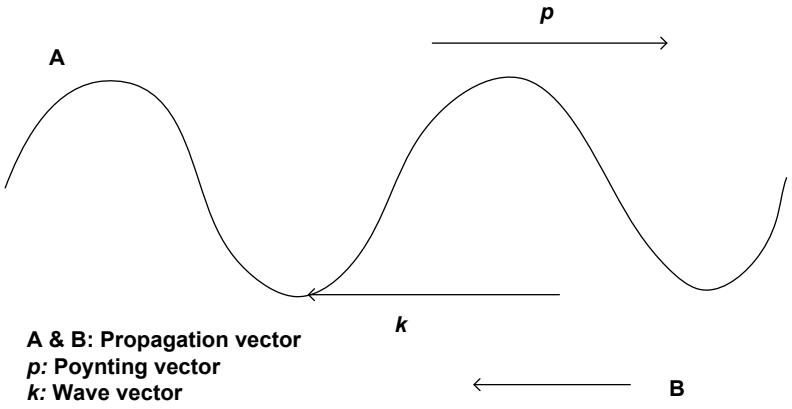

(b)

Fig. 1.1: (a) Wave propagation in Right-handed material (RHM) and (b) Wave propagation in Left-handed material (LHM).

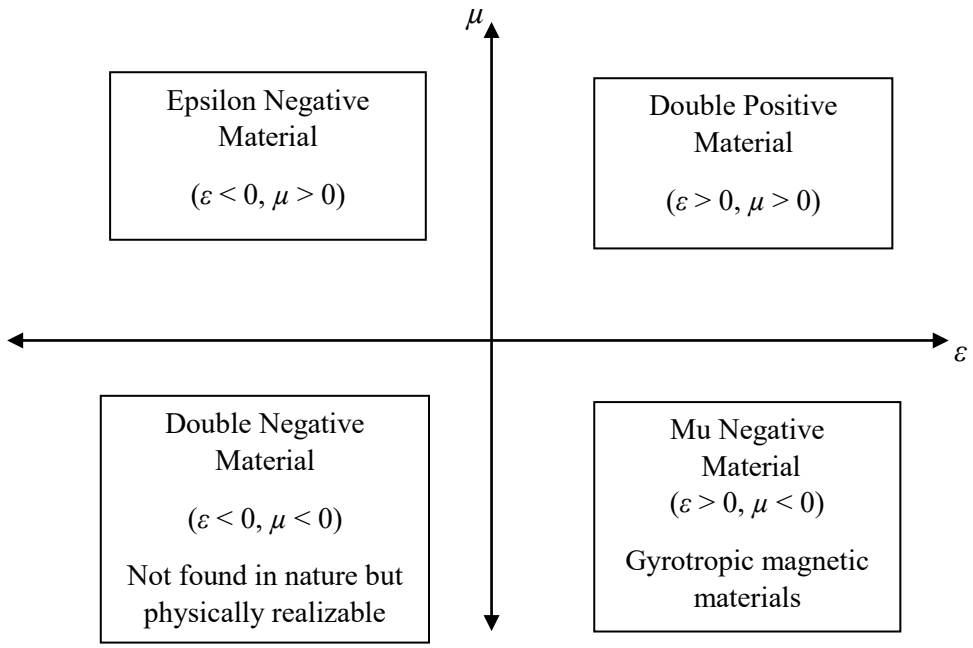

Fig. 1.2: Material classifications on quadrants [1].

Depending upon the signs of permittivity (ε) and permeability (μ) the classification of metamaterials is as follows [1]:

1. Double positive (DPS) materials with $\varepsilon > 0$, and $\mu > 0$ *i.e.* naturally existing dielectric materials lies in quadrant–I. In such materials, the direction of Poynting vector and wave vector is same. However, such type of materials exhibit positive refractive index. All the quadrant–I materials are also known as right-handed materials.

2. Epsilon negative (ENG) materials ($\varepsilon < 0$, $\mu > 0$) such as plasmas and metals at optical frequencies belong to quadrant–II. The wave travels in evanescent mode in these materials.
3. Double negative (DNG) materials ($\varepsilon < 0$, $\mu < 0$) known as ***metamaterials lies in quadrant–III***. These materials are not available in nature. The Poynting vector direction is in anti-direction to that of wave vector. The materials are known as left-handed materials. However, the refractive index is negative in these materials.
4. Mu-negative (MNG) materials ($\varepsilon > 0$, $\mu < 0$) like ferromagnetic and gyrotropic materials belong to the quadrant-IV.

The effective ε and μ of a material can be tailored to design an artificial structure for any specific application. The effective parameters of epsilon (ε_{eff}) and mu (μ_{eff}) of a material are expressed as [1]:

$$\varepsilon_{eff}(\omega) = \varepsilon'(\omega) + j\varepsilon''(\omega) \tag{1.15}$$

$$\mu_{eff}(\omega) = \mu'(\omega) + j\mu''(\omega) \tag{1.16}$$

The 'ε' measures change in electric field within materials. The dielectric constant is defined by permittivity (real part) and the attenuation is understood by material (imaginary part). The electric loss tangent of a material is given as;

$$\tan(\delta_e) = \varepsilon''(\omega)/\varepsilon'(\omega) \tag{1.17}$$

The loss tangent is important parameter to decide the practical relevance of material in applications. Further, the "μ" defines change in magnetic field within materials. The real part of permeability defines the energy stored in the magnetic field and imaginary part measures dissipation of energy in the material for the incident magnetic field. The magnetic loss tangent behaviour is given as:

$$\tan(\delta_m) = \mu''(\omega)/\mu'(\omega) \tag{1.18}$$

Therefore, by combining the structural elements of electric and magnetic response together in a unit cell, an artificial material with effective material properties can be designed. The electric and magnetic responses can also be generated by coupling between metamaterial elements. The unit cell is the basic building block of metamaterial. Its periodicity (p) is much less than the operating wavelength (λ). The periodic arrangement explanation of unit cell is made with the condition i.e. $p \leq \lambda/4$ makes the structure effectively uniform along the direction of incident electromagnetic radiations.

1.1.1 Classification of Metamaterial

The mathematical approach forms the basis to division of metamaterial into two major classes [3]. The first group includes double negative and single negative materials, whereas the second is the Photonic band-gap materials or photonic crystals that also named as photonic band gap materials. Linear size of constituents in double negative and single negative structures materials is much lesser than the wavelength of operation. Thus, such media generally form background to homogeneity and best understood through effective medium concept. The constituent elements in PBG-structures are maintained such that distance between them is equal to about half the wavelength or more. Therefore, homogeneous media approach is not considered in photonic crystals. They are interpreted through Bragg reflection, which does not have any implication in double negative and single negative structures, and periodic media approach. The classification of metamaterials is shown in Fig. 1.3.

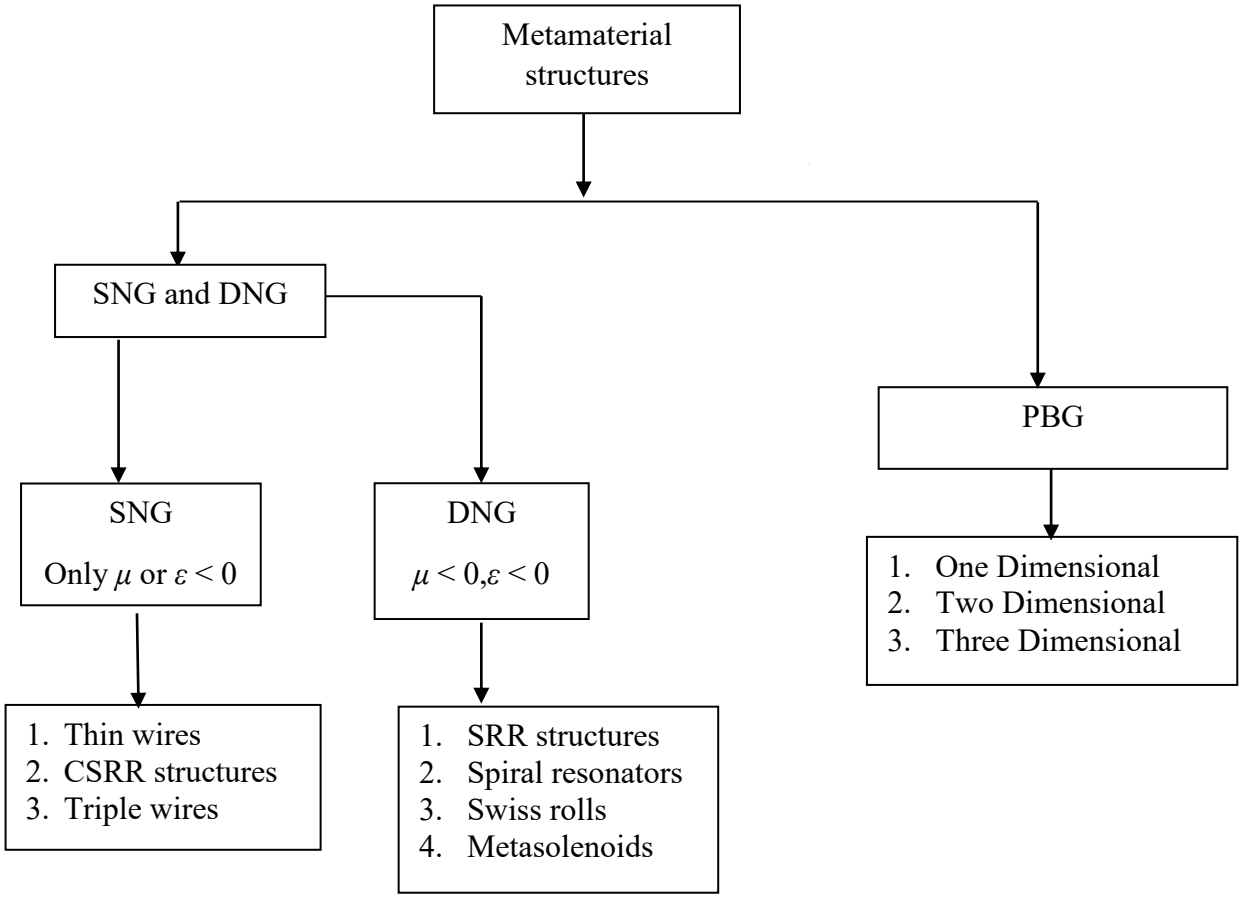

Fig. 1.3: Metamaterial structures [3].

1.1.1.1 Epsilon-negative (ENG) Metamaterial

The matrix structure in square shape of long parallel thin metal wires(infinite approach) embedded in a dielectric medium, is taken in propagation of electromagnetic waves and such a structure is similar to propagation in plasma. The lattice of infinitely connected wires produce element as shown in Fig.1.4. The composite material permittivity is negative at frequency $\omega < \omega_p$, where plasma frequency is denoted by ω_p for the structure in relation to radius and placement period of wires, so decision on selection of structure plasma frequency is calculated by designer. The effective permittivity can be described as;

$$\varepsilon_{eff} = 1 - ((\omega_p^2)/\omega(\omega - [i(\omega_p^2\alpha^2\varepsilon)\sigma\pi r^2]) \quad (1.19)$$

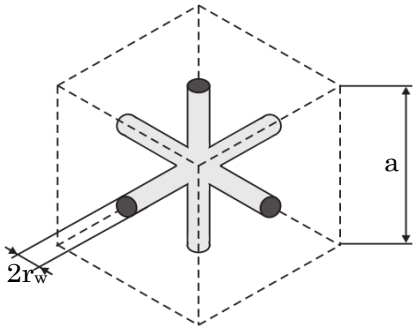

Fig. 1.4: Triple wire isotropic structure [4].

1.1.1.2 Mu-negative (MNG) Metamaterial

The split-ring resonator (SRR) is widely-used MNG-structure is [4-5]. The geometry of split ring resonator can be taken in the shape of circular and square. These resonant structure with high-conductivity are such that, in which inductance is balanced by capacitance between the two rings. The secondary magnetic field is produced by current induced by magnetic field (time varying) applied perpendicular to the rings surface. The resonant property of structure will decide, that it will either oppose or enhance the incident field, thereby deducing positive or negative μ_{eff}. The MNG metamaterial is shown in Fig. 1.5.

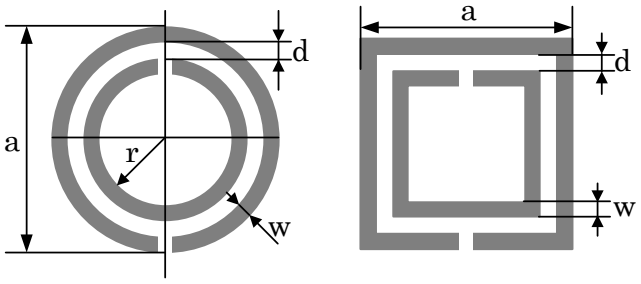

Fig. 1.5: MNG material unit cell [4].

1.1.1.3 Photonic band gap (PBG) Metamaterial

Artificially fabricated structures Photonic crystals or photonic bandgap materials (PBG) can manoeuvre the electromagnetic propagation. The design of photonic crystals can be used to disallow the electromagnetic waves propagation, or permit desired direction propagation. A possibility of localisation of electromagnetic energy is also possible using PBG structure [6]. The vibration of refractive index results in restricted energy range in which desired wavelength light has proceed [6] as shown in Fig. 1.6.

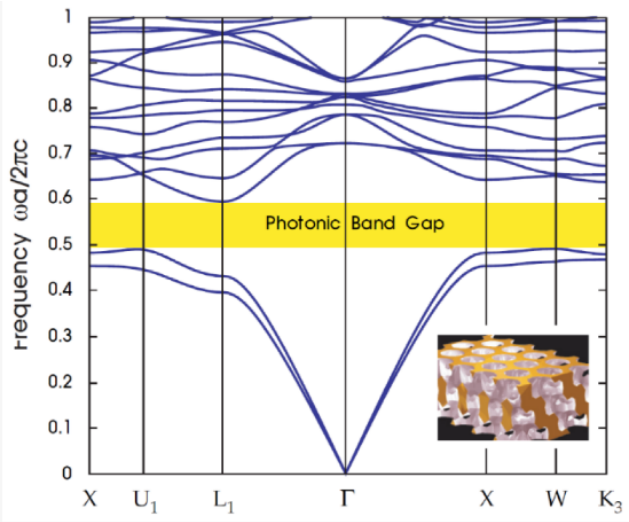

Fig. 1.6: Photonic band gap sample [6].

1.1.1.4 Double negative (DNG) Metamaterial

Double negative materials (DNG) are the metamaterials that have negative index of refraction with negative permittivity and permeability shown in Fig.1.7. These are also known as negative index metamaterials (NIM) [4], [7]. The left handed media is the terminology used for DNGs, media with a negative refractive index. The metamaterial can act as absorber at resonant frequency [8] providing absorption necessarily at a wide angle [9].

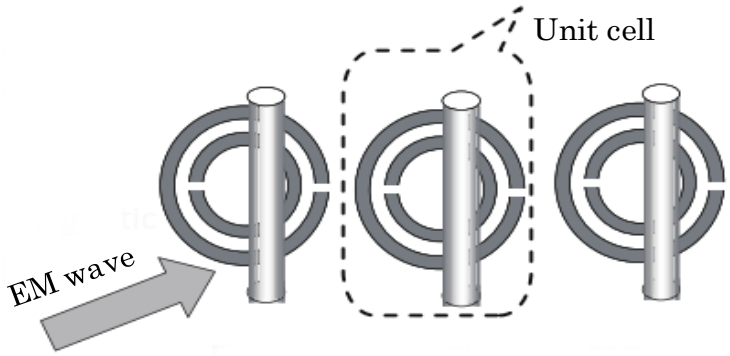

Fig. 1.7: DNG- metamaterial [4].

1.1.1.5 Electromagnetic band gap (EBG) Metamaterials

EBG metamaterials manoeuvre the propagation of light and the achievement is attributed to either by photonic crystals (PC), or left-handed materials (LHM)with artificial structures having the capacity to control and manipulate the propagation of electromagnetic waves. The realization of EBG can be in the form of one-, two- and three-dimensions [4]. The dimensionality dependency on the periodicity directions [10] is shown in Fig. 1.8. The complete band-gap can be achieved through three dimensional EBG and the reason being coverage of all incident angles for waves. The band-gap in EBG is analogous to a forbidden energy gap in electronic crystals therefore photonic crystals (PCs) terminology is also used for EBG.

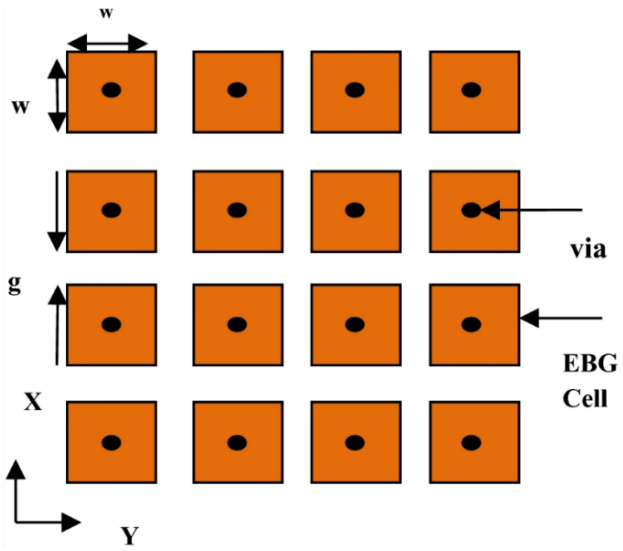

Fig. 1.8: Geometry of EBG structure [10].

1.2 Electromagnetic Absorbers

An ideal electromagnetic absorber is one which absorbs all the incident radiations at the operating frequency and provides zero reflection, transmission, and scattering. Electromagnetic absorbers have motivated the researchers due to their range of applications which covers from microwave to optical frequency regime. At microwave frequency, absorbers are used for reducing radar signature [11-13] and for power imaging [14]. In terahertz range, EM absorbers are used in solar cells [15], phase modulators [16] and bolometers [17]. At optical frequency regime, absorbers are used as thermal emitters [18]. However, the electromagnetic absorbers are classified into two types:

a) Resonant Absorbers.
b) Broadband Absorbers.

1.2.1 Resonant Absorbers

The resonant absorbers are generally composed of multiple layers separated by quarter of the operational wavelength. In these absorbers, the incident radiations are absorbed by the material at a specific frequency only. The conventional techniques to develop resonant absorbers include Salisbury screen [19], Jaumann absorber [20], Dallenbach layer [21], crossed grating absorber [22], and circuit analogue absorber [23]. The basic concept in the design of a conventional narrowband resonant absorber such as Salisbury screen is to place as resistive screen at a distance of λ/4 in front of a metallic ground plane separated by a lossless dielectric substrate as shown in Fig. 1.9(a). When the electromagnetic wave is incident on the Salisbury screen then some part of the wave is reflected by the resistive sheet and remaining part enters into the dielectric which is further reflected from the metal ground plane and get back into the air.

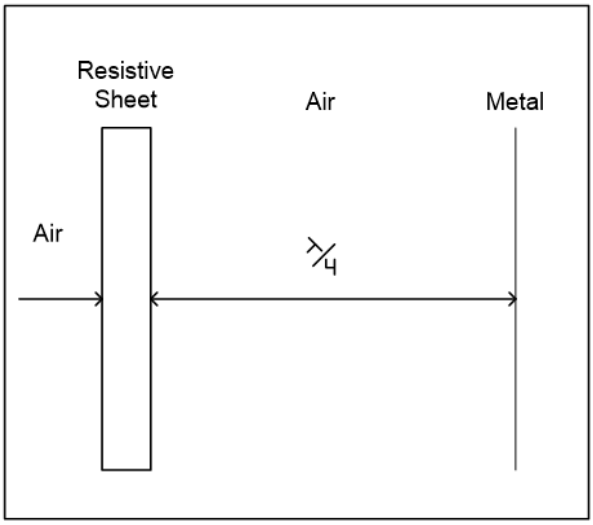

(a)

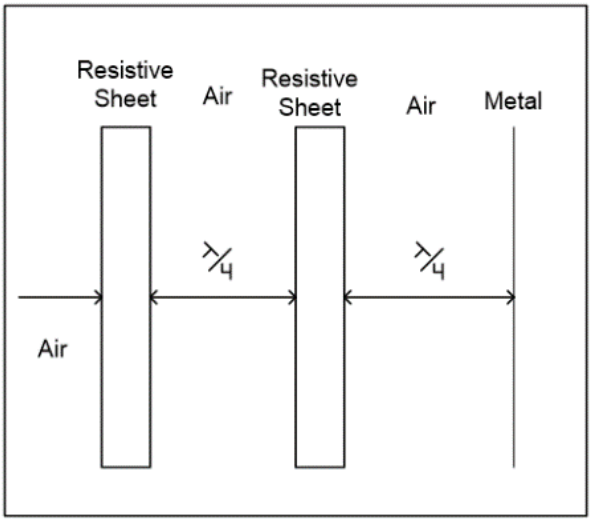

(b)

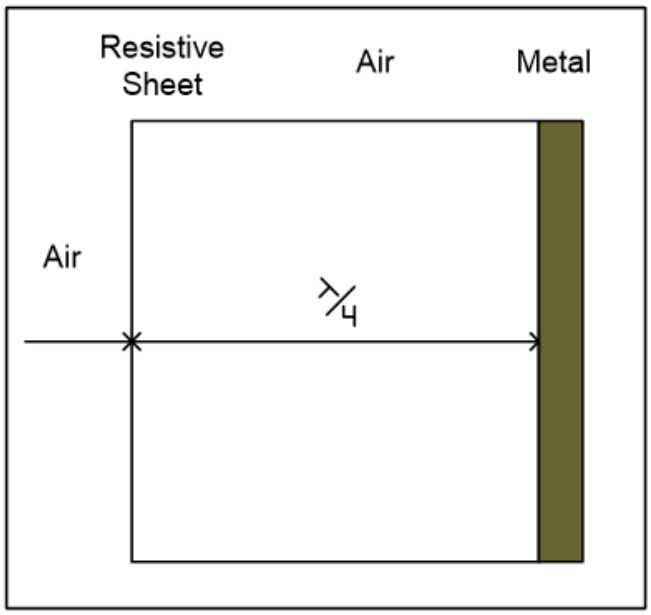

(c)

Fig. 1.9: (a) Salisbury Screen, (b) Jaumann absorber, and (c) Dallenbach absorber.

This reflected part of the wave travels λ/2 distance and so it is 180^0 out of phase *w.r.t.* the first wave reflected by the resistive sheet. Therefore, when the second wave reaches the surface, both the waves cancel each other and the net result is no reflection from the structure. The other type of resonant absorber known as Jaumann absorber as shown in Fig. 1.9(b). It is basically an advancement of the Salisbury screen in which multiple resistive sheets separated by λ/4, are placed in front of the metallic ground plate and are designed to operate at distinct wavelength to produce multiple reflections for the enhancement of absorption bandwidth. Further, Dallenbach resonant absorber design is shown in Fig. 1.9(c). It has a different mechanism of absorption as compared to Salisbury and Jaumann absorber. In this, a homogeneous layer of particular loss value is placed at a λ/4 distance in front of the metallic ground plane. The concept is to match the impedance by minimizing the reflection from the homogenous layer and the incident energy absorption due to the loss in the layer. Further, a crossed grating absorber is made up of a reflective metal plane with an etched periodic grid. An extension of Salisbury absorber is circuit analogue resonant absorber. Its basic structure consists of one or more lossy frequency selective sheet arranged in a periodic pattern at a distance of λ/4 in front of a ground plane. It is noticed that, a resonant absorber can provide near to perfect absorption due to its resonating behaviour, but one of the common features of all the conventional resonant absorbers is the larger thickness. At least λ/4 thickness is required for absorption at even specific frequency. Except, of circuit analogue absorbers, all resonant absorbers provide limited control over the specific absorption properties.

1.2.2 Broadband Absorbers

In broadband absorbers, the absorption response is generally independent of frequency and the absorption occurs for a large range of frequency spectrum. For broadband absorber design, the geometric transition and low density absorption methods are generally used [24]. A model of the geometric transition type of absorber as shown in Fig. 1.10(a).

(a) (b)

Fig. 1.10: (a) Geometric transition absorber design and (b) Low density absorber.

These types of absorbers provide broadband absorption and therefore generally used in anechoic chambers. The design consists of transition from free space into lossy material in slow variation. These absorbers are commonly of Pyramid or Wedge shape. Further, low density absorber is a type of broadband absorber which is shown in Fig. 1.10(b). The low density absorber is made up of multiple layers of some light weighted and porous composite materials such as carbon nanotubes filled with ferromagnetic alloys. Such types of absorbers are broadband, but they have large thickness and heavy weight result in fabrication complexity in processes to development. The geometric transition based low density broadband absorbers are also suffering from the problem of large thickness. Moreover, these traditional approaches to design electromagnetic (resonant and broadband) absorbers have adverse effects on the radiation performance of the RF systems like antennas used for in-band RCS reduction. These types of absorbers are confined to microwave regime below 30 GHz. Therefore the ideal solution to these issues is the metamaterial based absorbers.

1.3 Metamaterial Absorber

In the last decade, many absorber design based on artificially engineered structures have been proposed [24]. Among these designs, a popular configuration has been implemented by a periodic metallic surface fabricated on a grounded dielectric substrate. These periodic designs are popularly known as high impedance surfaces (HIS) [25]. Such sub-wavelength

structures are able to provide narrowband or wideband absorption if an adequate content of losses is introduced. There are different techniques for introducing the losses. One of the techniques to introduce the loss is to use some resistive elements like resistors or resistive inks [26-30]. In another technique, intrinsic loss component of permittivity (ε) and permeability (μ) of dielectric substrates are exploited to synthesize absorbers [8]. The former technique is based on introducing the resistive losses by external means and the latter is referred as metamaterial-based absorber design approach. Due to their numerous applications and advantages, metamaterial based electromagnetic absorbers are the best alternative of the conventional absorbers. The metamaterial absorbers are broadly classified in three different groups based on applications in different frequencies. The classification is as follows;

a. Microwave Frequency
b. Terahertz Frequency
c. Optical Frequency

The applications related to microwave frequency cover sensors, antennas etc. while for terahertz frequency it find applications in imaging and sensing. The applications related optical frequency is optical absorption, solar cell and cloaking. When a metamaterial absorber is exposed to electromagnetic radiations then there is matching of free space impedance with absorber impedance under ideal conditions with minimization of reflections. The concurrent absorption of electric and magnetic fields provides higher attenuation, and higher power loss due to electromagnetic absorption in all EM wave absorption applications. EM absorbers have many potential commercial and defence applications. Electromagnetic shielding and/or absorbers have been developed in order to minimize electromagnetic interference (EMI) in stealth technology [31] and to provide operational security to EM wave-based systems. Other applications uses include reduction of undesirable radiations and side lobe level suppressions in antennas [32]. Further, EM absorbers are also used for wireless communication by preventing the exposure to health hazards radiations. Moreover, they are also used to absorb spurious radiations for reducing the electromagnetic interference. The metamaterial absorber can be classified as [33];

a. Narrow band metamaterial absorber
b. Broadband metamaterial absorber
c. Frequency tunable metamaterial absorber
d. Coherent metamaterial absorber

In 2008 Landy *et al.* [5] proposed absorber involving full width half maximum (FWHM) of around 4%. The desire to increase width of absorption led researchers to incorporate various methodologies multi-layer stacked structures, multi-resonant cells, lumped elements to improve bandwidth of metamaterial absorber, the concept of tunablity was attained by using medium with adjustable material properties into passive absorber such as ferroelectric, ferrites, graphene, varactor diode etc. The main drawback of metamaterial absorber is fixed absorptivity at design level only the coherent perfect absorption (CPA) [33] technique is possible solution.

1.3.1 Absorption in Metamaterial

The mechanism of absorption of electric and magnetic field is linked to manipulation of two component that is permittivity (ε) and permeability (μ). The permittivity and permeability are the basic constituent for defining the property of material. The matching of components permittivity (ε) and permeability (μ) with free space is possible through designs. The design of metamaterial absorber is based on simultaneous resonant excitations of electric and magnetic dipole. The metamaterial absorber consists of three layers with top metallic layer in the form of patches and the ground conducting layer is completely metallic in nature to nullify transmission. The upper and ground layer is separated by substrate. The close proximity of top layer having patches with completely metallic ground plane results in symmetric hybrid mode electric field that oscillates in phase to two metallic patch normal to their axis. The asymmetric low frequency oscillates in opposite phase to two metallic patches normal to axis. The induced magnetic dipole couple to the external magnetic field and gives rise to desired dispersion in magnetic permeability of the effective medium. In this way, one can obtain a magnetic resonance as well as an electric response at a desired frequency by appropriate design of the metamaterial structure as shown in Fig. 1.11. The geometrical proximity of top layer with metallic patches and completely metallic bottom layer is instrumental in changing the behaviour of structure since there is existence of coupled fields between the structured patch as top layer and bottom metal film resulting in a phenomenon responsible for achieving symmetric high-frequency hybrid mode with the behaviour of the electric field oscillating in phase to the two metallic patch normal to their axis and a asymmetric low frequency hybrid mode providing a behaviour in which electric field oscillates in such a fashion as to form a opposite phase in the two metallic patch normal to their axis. The behaviour of the structure is such that frequencies of the two modes of oscillation for the coupled system are analogous to a coupled harmonic oscillator.

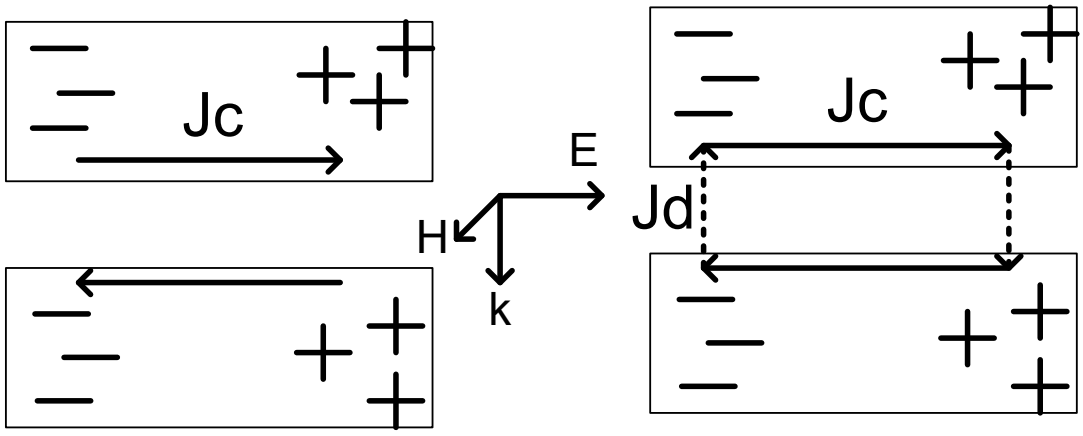

Fig. 1.11: Mechanism of absorption in metamaterial.

1.3.2 Impedance Matching Theory of Absorber

A metamaterial absorber is a composition of three layers as shown in Fig. 1.12 in which a dielectric is sandwiched between upper layer comprising patches and bottom layer with ground plane. The electric permittivity and permeability of metamaterial is defined as $\varepsilon = \varepsilon_o \varepsilon_r(\omega)$ and $\mu = \mu_o \mu_r(\omega)$, where ε_o and μ_o are permittivity and permeability of free space, $\varepsilon_r(\omega)$ and $\mu_r(\omega)$ are frequency dependent permittivity and permeability of medium, respectively.

The mathematical expression for defining absorption of proposed metamaterial-based absorber is as follows; [5]

$$A(\omega) = 1 - R(\omega) - T(\omega) \tag{1.20}$$

$$A(\omega) = 1 - |S_{11}(\omega)|^2 - |S_{21}(\omega)|^2 \tag{1.21}$$

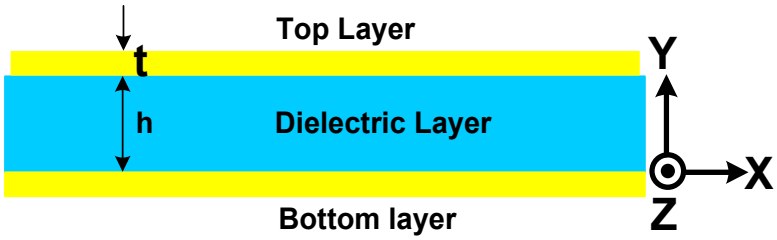

Fig. 1.12: Layers of metamaterial based absorber.

where, absorption, reflectance, and transmittance are represented by $A(\omega)$, $R(\omega)$, $T(\omega)$ are respectively. From Eq. (1.20), it is evident that the parameter absorption [$A(\omega)$] is linked to S_{11} the parameter reflection coefficient and S_{21} the transmission coefficient. The methodology of using complete metallic bottom layer as ground plane the value S_{21} or $T(\omega)$ becomes zero

and taking the value of S_{21} or $T(\omega)$ = 0, this permits dependence on reflectance parameter only. The Eq. (1.20) is modified as;

$$A(\omega) = 1 - |S_{11}(\omega)|^2 \tag{1.22}$$

The Fresnel formula for reflection for metamaterial is given as [5]

$$R_{TE} = |r_{TE}|^2 = \left|\frac{(\mu_r \mathrm{Cos}\theta - \sqrt{(n^2 - \mathrm{Sin}\theta)}}{(\mu_r \mathrm{Cos}\theta + \sqrt{(n^2 - \mathrm{Sin}\theta)}}\right|^2$$

$$R_{TM} = |r_{TM}|^2 = \left|\frac{(\varepsilon_r \mathrm{Cos}\theta - \sqrt{(n^2 - \mathrm{Sin}\theta)}}{(\varepsilon_r \mathrm{Cos}\theta + \sqrt{(n^2 - \mathrm{Sin}\theta)}}\right|^2$$

where, TE and TM indicate polarized waves and are indicated as Transverse Electric (TE) and Transverse Magnetic (TM). For a condition with $\theta = 0°$ that is the case of normal angle of incidence, the above equations reduces to;

$$A = 1 - R = 1 - \left|\frac{Z - Z_o}{Z + Z_o}\right|^2 = 1 - \left|\frac{\sqrt{\mu_r - \varepsilon_r}}{\sqrt{\mu_r + \varepsilon_r}}\right|^2$$

Where, $Z = \sqrt{\frac{\mu}{\varepsilon}}$ being impedance of structure and $Z_o = \sqrt{\frac{\mu_o}{\varepsilon_o}}$ being impedance of free space. The impedance matching is achieved by $Z = Z_0$ or $\mu_r = \varepsilon_r$ and it is referred as perfect condition for maximum absorption.

The effective permeability $\mu(\omega)$ and effective permittivity $\varepsilon(\omega)$ is matched and it results in reduction of transmission parameter. The frequency range for which value of $R(\omega)$ is minimized is through matching of free space impedance to normalized impedance consequently enhancing the absorption parameter. The normalised input impedance is calculated using Eq. (1.23);

$$z = \pm\sqrt{\frac{(1+S_{11})^2 - S_{21}^2}{(1-S_{11})^2 - S_{21}^2}} \tag{1.23}$$

The metamaterial absorber is made of complete metallic ground plane thereby making the value $|S_{21}|^2 = 0$ and on substituting the value S_{21} = 0, then Eq. (1.23) reduces to

$$z = \pm\frac{1+S_{11}}{1-S_{11}} \tag{1.24}$$

The 2008, Landy et al. [5] practically achieved absorption of 88% at 11.5GHz and the geometric dimensions were able to fix the absorption parameters of the structure. The initial absorber were narrow band and anisotropic structures having polarization sensitive behaviour

and were classified as single band [34], dual band [35-40], multiband [41-46] etc. subsequently the wideband [47-54] were also realized.

The modification of narrowband into multi-band and wideband can be possible by following approaches;

a) Combining structures with different resonance in a single unit.
b) Using structure with multi Resonance.
c) An approach to use multilayer for design.
d) Using resonant magnetic inclusions.
e) Using scaling approach in resonant structures.
f) Use of lumped elements.

The above said factors act as preliminary indicators while designing a metamaterial absorber. Each factor has its own limitation which makes its applicability bounded under some limitation.

1.4 Introduction to MIMO Antenna

The present wireless system has witness quantum change with numerous applications in different arenas like mobile communication, wireless communication, global positioning system (GPS), wireless personal area network (WPAN) etc. The Shannon's -Hartley capacity acts as principle equation for giving understanding on channel capacity [55]

$$C = B * log_2\left(1 + \frac{S}{N}\right) \tag{1.25}$$

where, *B* is bandwidth of system and *S/N* is signal to noise ratio. The increased channel capacity can be attained by either increasing bandwidth or improving signal to noise ratio (S/N). The capacity of channel can be enhanced by bandwidth improvement for a channel in communication system through increasing symbol rate of modulated carrier but that is prone to multipath fading. The signal to noise ratio cannot be increased in unrestricted fashion as communication channel introduces noise in channel thus single antenna system provide limitations to performance of channel on account of low capacity, bandwidth and multipath fading. The MIMO stands for Multiple Input and Multiple output and it is technology meant for transmission and reception of signal in modern communication system such as long term evolution (LTE), wireless local network (WLAN) and massive MIMO will be key in 5G communication [55-56]. The MIMO system is gaining relevance in present era on account of present requirements of multiple functionalities, requirement of huge data rate and large capacity. The system demands less multipath fading and to meet the demand of superiority in

communication channel, MIMO provides solution as more than one antenna is deployed at transmitter and receiver side as shown in Fig. 1.13 setup thereby mitigating fading, improved capacity and higher data rates, less signal loss etc. The fading problem in channel can be solved by MIMO through diversity techniques involving space, polarization and pattern diversity. The multipath environment is covered through MIMO setup where connection in transmitter and receiver is established through number of antennas. The multipath terminology is self-explanatory term describing that signal will reach the destination many routes involving multiple antennas, through processing at receiving section the original signal is produced having originality in term of transmitted data. The methodology of multiple data transmission and reception deliver speed, coverage and reliability improvement in fading environment. The practical locations for MIMO setup is at mobile terminals and base stations (BS). The practical requirement demands limited space on account of miniaturized dimensions in present era. The space constraints results in mutual coupling between various antenna elements thereby restricting the performance of MIMO setup in practical applications.

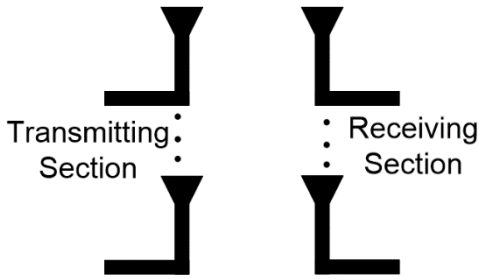

Fig. 1.13: MIMO configuration.

1.4.1 Block Diagram of MIMO System

The block diagram of MIMO system is shown in Fig. 1.14. The block diagram is divided in two sections as transmitter and receiver. The input data meant for transmission is encoded and interleaved followed by modulation, the next step is space time encoding for spatial multiplexing and then data is transmitted by different antennas represented as 'x' while the receiver section starts with reception of signal through receiving antenna denoted as 'y' the received data undergo spatial demultiplexing followed by demodulation and de-interleaving and then at last decoding for recreation of output bits. The MIMO channel can defined as matrix with mathematically representation as Eq. (1.26),

$$Y = Hx + n \tag{1.26}$$

where, y represents received signal , x is transmitted information, H is channel matrices and n is additive noise.

The MIMO channel is modelled as;

$$H = \begin{bmatrix} H_{1,1} & H_{1,2} & \dots\dots\dots\dots\dots\dots\dots & H_{1,M_T} \\ H_{2,1} & H_{2,2} & \dots\dots\dots\dots\dots\dots\dots & H_{2,M_T} \\ & & \vdots & \\ H_{M_R,1} & H_{M_R,2} & \dots\dots\dots\dots\dots\dots\dots & H_{M_R,M_T} \end{bmatrix}$$

where, $H_{m,n}$ is channel behaviour for transmitting and receiving antenna represented by M_T transmitter and M_R receiver, the MIMO channel modelling is shown in Fig. 1.15.

1.4.2 MIMO Mutual Coupling

The MIMO consist of various antenna elements and these elements are closely spaced to cause interference that will lead to coupling among the various elements of MIMO antenna. Therefore, it makes poor performance of MIMO setup by degrading radiation pattern and other efficiency pattern making MIMO system inefficient for implementation in practical scenario.

The various types of mutual coupling are;

a) Coupling due to near field.

b) Coupling due to far field.

c) Surface wave coupling.

The near field zone is the area in vicinity of antenna, the field is reactive in nature and the field is in the closed vicinity of antenna and can avoided by maintain suitable distance between antenna elements. The present era demand miniaturisation of communication setup therefore limiting the performance of MIMO setup.

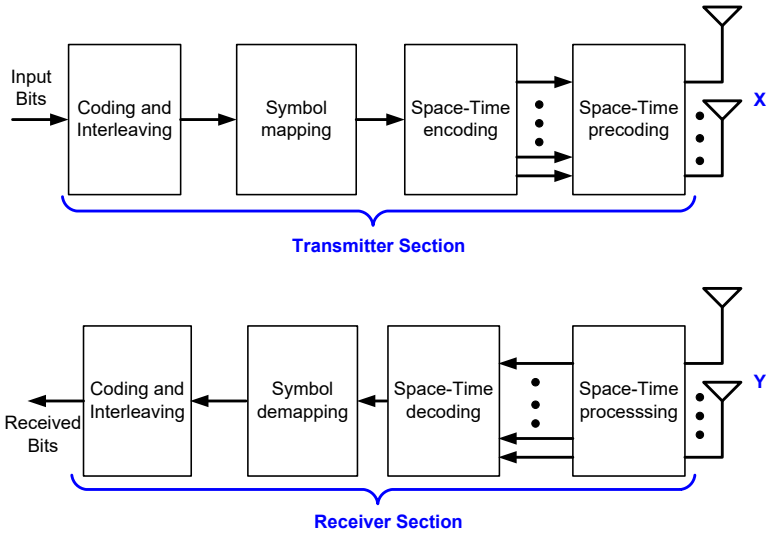

Fig. 1.14: Transmitter and receiver sections of MIMO setup.

The far-field coupling is prevalent in those structures with common ground plane. The far-field coupling can be avoided by suppressing the coupling current in ground plane.The reason for hindrance to maximum exploitation of MIMO setup is miniaturisation of dimensions in mobile environment and is the main source of mutual coupling mong antennas of MIMO setup as shown in Eq. (1.27) [56]

$$C_{mn} = \exp\left(-\frac{2d_{mn}}{\lambda}(\alpha + j\Pi)\right), m \neq n$$

$$C_{mm} = 1 - \frac{1}{N}\sum_m \sum_{n \neq m} C_{mn} \quad (1.27)$$

where, C_{mn} and d_{mn} are mutual coupling and distance between m^{th} and n^{th} antenna elements and α is parameter controlling coupling level thus mutual coupling tend to alter input impedance, reflection coefficient and radiation pattern of array elements. In order to enhance the performance of communication system for present generation setup and future 5G communication system, the researchers are striving for various techniques that can provide isolation among various element of MIMO antenna.

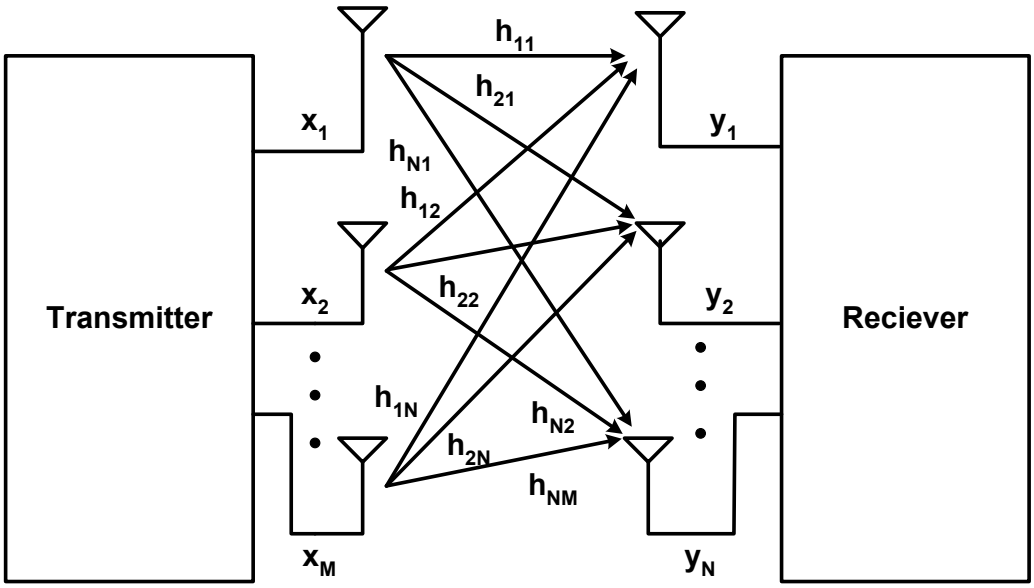

Fig. 1.15: MIMO channel modelling.

The surface current is linked to substrate thickness the thick substrate surface wave travel through substrate and discontinuity in surface results in scattering which extract power and results in the formation of undesired radiation that again get mutually associated with antenna elements, surface wave is also associated with dielectric constant of substrate

The main factors linked to mutual coupling are;

a) Geometrical shape of elements of MIMO setup
b) Radiation pattern of various elements
c) Common ground plane induced surface current
d) Thickness of substrate
e) Dielectric constant of substrate
f) Near field scatter

1.5 **Motivation for Thesis**

The involvement of metamaterial absorber in various practical applications was the initial source of motivation. The study various absorbers clearly indicate that despite numerous single, dual and multiband absorbers [34-46] are available the necessity for prefect absorption rate that too with ultrathin dimensions is still a bottleneck and to achieve near perfect absorption in wideband with simple geometry is very difficult task. The various approaches to increase absorptivity in the wideband segment [47-54] have been tried initially and tested. The wideband provide desired absorption with broad bandwidth. The approach from meander lines to lumped elements are tried but at the cost of complexity in design and fabrication. The appropriate thickness of substrate remains a bottleneck for compact structure for achieving the desired absorption. The researchers have achieved the stage where the transition from multiband to wideband is made possible but to attain high absorption values (more than 97%) in bands with geometrically simple and compact structure is still yet to be explored. The practical implementation of absorber is applicability aspect of designed absorbers in practical MIMO setup. The high isolation levels demand in practical applications of MIMO setup are marred with size and dimension constraint [57-59]. In the recent years the work on incorporation of MIMO antenna systems in practical setup is carried on with the aim of enhancing performance of communication setup but this opinion is restricted by isolation problem in MIMO setup. The desire of simultaneously achievement of both dimension compactness and high isolation is the need of practical applications. The different approaches [60-69] have been attempted in past but the duality of compactness and high isolation is extremely difficult to be achieved. The decoupling network, metamaterial and defected ground provide better isolation in comparison to neutralization and parasitic methods but advantage of size reduction is achieved through incorporation of metamaterial- based technique [70]. The inference drawn from above paragraph clearly suggest metasurface based

absorber can provide dual advantage of optimum level of isolation vis-a vis optimization of dimensions involved in practical real environment.

Thus the prime motivation of thesis work is divided in two themes the first portion of work will be to practically conceptualize the idea of design of multiband and wideband metasurface absorber with near perfect absorption and having polarization insensitive behaviour with workability of structure over wide angle of incidence. The second aspect of the work will be practical implementation of metasurface absorber to attain highest form of isolation with intent to resolve practical implications associated with incorporation of MIMO setup in communication environment.

1.6 Organisation of the Thesis

The thesis work is organised in six different chapters to address the problem formulation in systematic manner.

1. **Chapter-1: Introduction** of the thesis work covers introduction portion covering three important aspects;
   a) *Introduction to Metamaterial:* An introduction to metamaterial with its classification. The various types of metamaterials are discussed to give brief view to the readers on negative materials. Further absorber portion is discussed to acquaint user with electromagnetic absorbers and fundamental mechanism of absorption.
   b) *Introduction to MIMO Antenna:* This portion focuses on introduction to MIMO antenna. The portion also introduces readers with utility of MIMO setup to cater on ever rising demand of multiple applications with increasing user base. The part also brings into picture various practical issues that restrict the performance of MIMO antenna.
   c) *Motivation and Organisation of the Thesis*: The part of the thesis brings into light the key areas that motivated the work and provide insight to organisation aspect of thesis and finally a summary is given at the end of chapter.
2. **Chapter-2: Literature Review** is a review portion of earlier reported work and it is sub-divided into two broad groups
   a) *Review of Absorbers*: An insight to absorber is taken for review in this section. Various absorbers are discussed based on its performance parameters and classification on different types like multiband and wideband absorbers. The

tabular classification based on type of absorber, absorption level attained, number of peaks, dimensions etc. is taken for study in this section.

b) *Review of MIMO Antenna*: The section is an attempt to review the literature of various MIMO antenna in term of its performance parameter taking mutual coupling parameter as its prime focus. The section discusses the various literatures available to bring into light various techniques incorporated to provide maximum possible isolation among various antenna elements. The tabular classification based on size of antenna, frequency band, isolation level attained, and various parameters like ECC etc. to evaluate performance is taken for study in this section.

3. **Chapter-3: Design, Optimization and Development of Multiband Absorbers** of the thesis work are dedicated to development of multi-band absorber. In this section, two multi-band absorbers were designed, analysed, and developed for desired multi-band results. The theory section for design of multi-band absorber is taken for discussion. The various aspects for parameterisation are taken into analysis. The distribution of surface current and electric field is taken into consideration to provide the insight to development of multi-band absorber. The performance of multi-band absorbers is compared for interpretation with existing absorbers. Finally, the prototype of multi-band absorbers is taken for experimental analysis to verify its performance and compare it with simulated results.

4. **Chapter-4: Design, Optimization and Development of Wideband Absorber** of the thesis work is dedicated to development of wideband absorber. In this section, a wideband absorber was designed, analysed, and developed for desired results. The theory section for design of wideband absorber is taken for discussion. The distribution of surface current and electric field is taken into consideration to provide the insight to development of wideband absorber. The performance of wideband absorbers is compared for analysis with existing absorbers. Finally, the prototype of wideband absorbers is taken for experimental analysis to verify its performance and compare it with simulated results.

5. **Chapter- 5: Application of Metamaterial Absorber to Improve Isolation** of thesis work is the application part of work to establish the importance of multi-band absorber in achieving highest form of isolation in MIMO setup. The chapter is sub divided into three important sections;

a) The first section is evaluation of MIMO antenna designed without isolator through various *S*-parameters and results analysis based on established parameters.

b) The second section deals with performance evaluation of MIMO antenna designed with isolator through metasurface based absorber here again the results are analysed through *S*-parameters and other established parameters.

c) The third section is dedicated to performance evaluation through practical prototype implementation and comparison of results to establish outcome of the work.

6. **Chapter-6: Conclusion and Future Scope** is focussed on conclusion and future scope of the presented work. The chapter is focused on achievement part on account of work and to discuss future scope of work that can be beneficial for those who intent to take this work as reference for understanding and extending the research to achieve future objectives. The chapter is followed by reference section and the publication part on account of the research.

This thesis focuses on the design and development of metamaterial-based absorber and their application to improve isolation between multi-antenna systems. Initially, multiband and wideband metamaterial absorber is designed and investigated. Further, a multiband absorber is utilized to enhance the isolation between two or more antenna elements. Therefore, the complete literature review is divided into two parts. The first part focused on research progress related to the metasurface absorbers, and the second part focused on research progress based on MIMO antenna systems. The detailed literature review is given in the below sections.

2.1 Review of Metasurface Absorbers

In this section, the research works carried in the absorber field are discussed. The review of various absorbers is focused on the level of absorptivity achieved, dimensional aspect of structure with the determination of characteristics of structure like polarization behaviour and angle of incidence for the structure. All these parameters are prerequisites for determining the practical usability of absorber. The brief overview of various absorbers is subdivided into two sections as follows;

2.1.1 Multiband Absorbers

The section focusses on the research work of researchers in the past years for design, development and characterisation of metasurface based absorber. The absorber discussed in this section provide multiple peaks of high absorptivity in different bands. The performance of absorber is visualised on polarization parameter and angle of incidence as these parameters are essential components for practical implementation of absorber in any application. The review of metasurface absorber in multiband category is as follows,

Landy *et al*. (2008) [5] proposed absorbing metamaterial generating near-unity absorbance achieved in simulation. The basic composition of metamaterial structure is two resonators with different fields (electric and magnetic) with an ultimate aim to enhance absorption within the unit cell. The fabricated structure is achieving an absorption level of 88% at 11.5 GHz. The geometrical shape is 4.2 mm × 12 mm × 11.8 mm. The design is polarization sensitive and has a low angle of incidence.

Further, Cheng *et al*. (2009) [62] examined a structure with an absorptivity greater than 98% at 10.4 GHz. Two resonators and a metal wire are coupled with absorbing incident Electric and magnetic fields. An electric split ring resonator structure was proposed to achieve the

goal of higher Absorptivity. The dimension of the structure is 12 mm × 4.2 mm × 0.6 mm, and the design is polarization sensitive and has a low angle of incidence.

After that, Li *et al*. (2010) [63] described work on the absorber, which shows the Absorber achieve two absorption peaks with perfect absorption near 11.15 GHz and 16.01 GHz. The absorptions consideration with different polarizations are measured with a attainment of 97% at one peaks and 99% at other peaks. The structure size is 12 mm × 12 mm × 0.56 mm, and the design is polarization sensitive and has a low angle of incidence. Soon after, Zhu *et al*. (2010) [64] illustrated an absorber with high absorptivity. More than 95% is witnessed at 10 GHz. The approach is to use a dendritic structure disordered structures metamaterial absorber. It can be used for the infrared metamaterial absorber design, which controls the radiative heat energy collection with directional transfer enhancement. The dimension of the structure is 4.2 mm × 4.2 mm × 0.8 mm, and the design is polarization sensitive and has a low angle of incidence.

Further, Sun *et al*. (2011) [65] demonstrated an absorber that is based on antireflection theory provides high absorbance due to the theory applied for achieving destructive interference in reflection waves from the metamaterial having surfaces composition. A 60GHz absorptive bandwidth is achieved between 0 to 70GHz. The dimension of the structure is 6.4mm×6.4mm×2.5mm. The design is polarization sensitive and has a low angle of incidence. Thenceforth, Li *et al*. (2011) [66] proposed that a metamaterial absorber comprises a six-fold symmetricity for modified snow flake shaped resonators periodic array of with top layer having strip spiral line load printed and on the other side of dielectric substrate is metallic ground plane. The structure succeed in providing near-unity absorption peaks three in number. Thus, due to the six-fold symmetry, the structure is providing an absorption of 99.8% at 9.19 GHz and 12.35 GHz with 98.9% absorption. The geometrical shape is 5 mm × 5 mm × 1 mm, and the absorber structure is sensitive to the polarization of the incident radiation and has broad angle of incidence operation. Then, Huang *et al*. (2011) [67] proposed a multiband absorber polarization-insensitive metamaterial absorber. The structure constituting the closed rings having a number of six, the top and bottom is separated by FR4 substrate. The result conform attainment of 93.3% absorption for bands representing different frequencies. The dimension of the structure is 9 mm × 9 mm × 0.5 mm, and the structure is polarization sensitive and has a low angle of incidence.

After that, Lee *et al*. (2012) [68] illustrated an absorber based on the approach of periodic system of a resonator with a symmetrical structure. The five cells with different geometry enhance absorption bandwidth. The experimentation was performed after fabrication of

structure having a thickness of 0.8 mm thereby achieving an absorption of 93% (for 10 GHz) and 970 MHz bandwidth FWHM signifying the value achieved for full width half maximum. Then, Abdalla *et al*. (2012) [69] demonstrated a new application of metamaterial for radar absorbers for X-band. There are two arrangements, one having resonator absorber with a shape of fan and other one is metamaterial absorber having high impedance. The technique introduces a thin radar absorber (5.3% at a center frequency) with wide bandwidth and high absorption level. The dimension of the structure is 11 mm × 11 mm × 1.6 mm, and the design is polarization sensitive with a low angle of incidence.

In the subsequent year, Cheng *et al*. (2013) presented a metamaterial absorber with broadband characteristics based on multilayer cross-structure resonators with periodic array. The stacking phenomenon is instrumental in achieving absorption band of design. The four-layer structure has different geometrical dimensions [70]. Then, Feng *et al.* (2013), in this paper, a varactor is used and designed the to attain 80% absorption within the band from 9.8GHz to 10.4GHz. The dimension of the structure is 10 mm × 17 mm, and the design is polarization sensitive and has a low angle of incidence [71]. After that, Bhattacharyya *et al.* (2013) [72] discussed a complementary ring resonator proposed having a absorber within two bands in C and X. Optimization of geometric parameters is done so that greater absorption is obtained at two distinct absorption peaks. The 98.5% and 94.2% absorption are achieved at 5.04 and 5.28 GHz. The dimension of the structure is 5 mm × 5 mm × 1 mm. The design is polarization insensitive and has a broad angle of incidence. In the same year, Wen *et al.* (2013) [73] proposed a structure of size is 8 mm × 8 mm × 0.45 mm with polarization-insensitive and broad angle of incidence. The unit cell of the broadband metamaterial absorber with a composition of three dual-band sub-cells such that one cell gives two resonant frequencies and forms a broad-spectrum absorption on stacking. The unit size is thin, the structure is behaving polarization insensitive and is stable and adaptive for wide oblique incident angles of electromagnetic waves. The absorptivity level attained is close 80% between 8.8 and 10.8 GHz thereby exhibiting broad band characteristics. Soon after, Lee *et al*. (2013) [74] illustrated the mechanism of absorbing bandwidths by manoeuvring resonant peaks produced by two different resonance effects on the frequency selective surface. Then, by managing change in dimension parameters, the dual-band, 3dB and 10dB band absorbers were designed. The dimension of the structure is 14.2 mm × 14.2 mm × 0.6 mm, and the design is polarization insensitive with a broad angle of incidence. Then, Ghosh *et al*. (2013) [75] discussed absorber with ultrathin dimensions with design analysis which consists of a shape printed on FR4 dielectric substrate that is periodic array of swastika-like

structures backed by copper ground. At 10.10 GHz the simulation is performed to succeed in 99.64% absorption.The dimension of the structure is 10 mm × 10 mm × 1 mm. The design is polarization insensitive and has a broad angle of incidence. Thereafter, Shrekenhamer *et al.* (2013) [76] discussed the usage of active liquid crystals in important segments of unit cells based on metamaterial properties. This structure resonates at 2.62 THz by incorporation of active liquid was able to achieve 80% at 2.62 THz, and in the same year, Park *et al.* (2013) [77] discussed the usage of the donut-shaped resonator for achieving resonance at various peaks, thereby achieving 99%, 98% and 99% absorption at 6.51 GHz, 7.0 GHz, and 7.61 GHz, respectively. The design is polarization insensitive. Further, in the same year, Dincer *et al.* (2013) [78] proposed a structure with 99% and 79% at 4.0 GHz and 5.6 GHz. There exists a strong case that a metamaterial absorber could achieve high absorption at wide angles of incidence for both transverse Electric (TE), and transverse magnetic (TM) waves. The dimension of the structure is 15 mm × 15 mm × 1.6 mm and design is polarization sensitive with low angle of incidence. Ayop *et al.* (2013) [79] analysed a metamaterial absorber having wide incident angle of 70^0, to attain high absorbance of 88% and polarization insensitive behaviour. The circular patch is used for the design of said absorber.

In the next year, Ma *et al.* (2014) [80] discussed the usage of the donut-shaped resonator for achieving resonance at various peaks, thereby achieving 99.87%, 99.98%, and 99.99% absorption at 6.16 GHz, 8.76 GHz, and 12.54 GHz, respectively. The design was reported to be polarization insensitive and has a broad angle of incidence.

In the subsequent year, Bhattacharya *et al.* (2015) [81] discussed using a donut-shaped resonator for achieving resonance at various peaks, achieving 98.6%, 96.6%, 90.1%, 97.8%, and 93.1% absorption at 3.4 GHz, 8.34 GHz, 9.46 GHz, 14.4 GHz and 16.62 GHz, respectively. The geometry is of 16 mm × 16 mm × 1.2 mm. The design is polarization insensitive and has a broad angle of incidence.

The year was marked by the contribution of Zhai *et al.* (2015) [82] discussed triple band metamaterial-based absorbers at various peaks, thereby achieving above 90% absorption at 3.25 GHz, 9.45 GHz, and 10.90 GHz. Also, design is polarization insensitive and has a broad angle of incidence.

In the next year, Ramya *et al.* (2016) [83] discussed a C- and X-bands dual-band metamaterial absorber. The periodic arrangement of circles acting as resonator is included in a square resonator. This structure is providing absorption of 99.8 % and 99.97 % at 5.5 GHz and 8.9 GHz. The geometry is 10 mm × 10 mm × 1 mm and design is polarization insensitive with broad angle of incidence and then Ozden *et al.* (2016) [84] presented the metamaterial

based absorber through design, simulation, and measurements within frequency range from 8–12 GHz. An absorber working in X-band is determined by using the different dimensions of unit cells and placing their resonant frequencies close to each other. The measurement of structure is 6.67 mm × 6.67 mm × 0.75 mm. The design is polarization sensitive and has a low angle of incidence. Then, Agarwal *et al.* (2016) [85] proposed an absorber structure having dual resonance. The design parameters are optimized to attain desired results with absorption in C-and X-band. The geometry is 6 mm × 6 mm × 1.6 mm and structure is polarization sensitive in nature with broad angle of incidence. In the same year, Montaser *et al.* (2016) demonstrated a different metamaterial absorber (MA) supporting microwave and terahertz ranges applications. In the microwave range, three absorption peaks were attained that is focussed at around 99% at 2.8 GHz for the first resonance and 99% at 4.1 GHz for the second resonance, and 89% at 5.8 GHz for the third resonance[86]. The dimension of the structure is 30 mm × 30 mm × 1.6 mm. The design is polarization sensitive and has a low angle of incidence, and then Tak *et al.* (2016) [87] proposed absorber with working range 8–12 GHz. The results exhibit two absorptivity peaks of 98.5% in relation to 8.2 GHz and 12 GHz, respectively. Additionally, high Absorptivity is achieved at various incident angles. The dimension of the structure is 8 mm × 8 mm × 0.8 mm, also design is polarization insensitive and has a broad angle of incidence. The year saw Kadir *et al.* (2016) [88] demonstrated metamaterial absorbers with absorptive peaks of 99.9% and 99.3% at 7.90 GHz and 8.90 GHz. The measured results match with simulations for different polarizations of EM waves. The metamaterial absorbers can be used in stealth technology applications.

In the subsequent year, Sen *et al.* (2017) [89], the work stretched with the attainment of absorption bandwidth of 79% (with more than 85% absorption) . The three absorption peaks are achieved are at 8.48 GHz, 15.4 GHz, and 17.48 GHz. The dimension of the structure is 9 mm × 9 mm × 2.7 mm and design is polarization sensitive with broad angle of incidence. Agarwal *et al.* (2017) [90] concluded the absorption of 99.5% (7.20GHz), 99.8%(9.3GHz), 99.5%(12.61GHz), and 99.9%(13.07GHz). The bands covered are C-, X-, and Ku microwave band width applications pertaining to mobile communication, satellite communication, and radar platforms using absorbers as design constituent. Then, Marathe *et al.* (2017) [91] examined the creation of negative region at three frequencies 4.32 GHz, 7.55 GHz, and 9.76 GHz. This metamaterial structure has negative regions in C-and X-Frequency bands. The design is polarization sensitive and has a low angle of incidence. The year was marked by the contribution of Xin *et al.* (2017) [92]. The work focussed on the design of ultrabroad band metamaterial structure. The absorption of the MA is of the range of 83%, having frequency

range from 20.59 to 43.73 GHz at a normal angle of incidence. The 25.64 GHz full width at half maximum (FWHM) absorption bandwidth is achieved from proposed ultra-broadband MA.The structure is fabricated to decide the authenticity of results. The size of unit cell is 4 mm × 4mm × 0.9 mm and design is polarization insensitive with broad angle of incidence. Subsequently, Bagci *et al.* (2017) [93] presented a design within a range from 2.45 and 5 GHz.The dimension of the structure is 10 mm × 10 mm × 1 mm. The polarization insensitive nature of design and has a broad angle of incidence. In the same year, Naser *et al.* (2017) [94] developed a prototype structure of polarization independent absorber, and analysis of absorber is checked for 0^0 to 60^0 incident wave angle. The work is done in the time domain with CST, and the structure is fabricated with an FR4 substrate. The dimension of the structure is 24 mm × 24 mm × 1.6 mm and design are polarization insensitive with low angle of incidence. Then, Thummaluru *et al.* (2017) [95] demonstrated a C-band application oriented ultrathin triple-band polarization-insensitive metamaterial absorber. The proposed structure is interpreted as a combinational effect of two absorbers. It exhibits 91% (4.2 GHz), 98.9% (7 GHz), and 99.5% (7.4 GHz) absorptivity. The geometry is 28.2 mm × 28.2 mm × 1.6 mm. The design is polarization insensitive and has a broad angle of incidence. The work was analysed to demonstrate effectiveness in practical implementation. In the same year, the work on design of absorber was performed by Tak *et al.* (2017) [96] and in its work it demonstrated the design of absorber structure attains 97.8% (24.1 GHz) and 74.5% (25.2 GHz) absorptivity. The structure is polarization insensitive and tested at a wide angle of incidence. The Absorber is proposed for 24 GHz automotive radar application. Then, Mishra *et al.* (2017) [97] proposed ultra-thin triple band absorber peak at 4.19 GHz, 9.34 GHz and 11.48 GHz with Absorptivity of 99.67%, 99.48%, and 99.42%, respectively. The structure was reported to be polarization insensitive and tested at a wide angle of incidence.

The next year saw, Sekar *et al.* (2018) [98] investigated an ultra-thin, wide absorption based compact metamaterial absorber with operational range within microwave segment. The basic structure consists of circular and rectangular split rings. The absorptivity of more than 90% is attained for wide band absorber of 3.84 GHz from 12.80 GHz to 16.64 GHz with absorptivity level achieved is of close to 90% absorption, and peak resonance is obtained at 13.2 GHz and 16.5 GHz. Thereafter, Sabah *et al.* (2018) [99] proposed a structure in terahertz regime. The multiband terahertz metamaterial absorber is realized and by numerical simulation method. The design is polarization insensitive and has a low angle of incidence. In the same year, Huang *et al.* (2018) [100] described a THz metamaterial absorber with the absorption of more

than 93.7% at 9.05 THz. The structure is polarization insensitive. It is studied at a different angle of incidence. At oblique incidence, absorptivity is still exceeding 90%.

The next year witnessed, Cao *et al.* (2019) [101] investigated a structure that comprises of graphene metamaterial absorber. The structure, as claimed, can attain absorption with 99.95%, 99.28%, and 96.36% at 8.115 GHz, 11.4 GHz, and 15.12 GHz. The dimension of the structure is 23.2 mm × 23.2 mm × 1mm. The design is polarization insensitive and has a broad angle of incidence.

The year witnessed the work of Amiri *et al.* (2020) [102] which demonstrated a structure that comprises the crescent-shaped resonator. The structure, as claimed, can attain absorption at 99% at 5.17 GHz. The dimension of the structure is 18 mm × 18 mm × 1.6 mm. The design is polarization insensitive and has a broad angle of incidence, and then Wu *et al.* (2020) [103] investigated a structure that comprises three layers of the resonator. The structure as claimed can attain absorption with 99.25%, 99.68%, 97.83%, 97.54%, and 99.95% at 5.984 GHz, 12.232 GHz, 18.128 GHz, 18.414 GHz, and 20.592 GHz, respectively. The dimension of the structure is 17 mm × 17 mm × 1.2 mm. The design is polarization insensitive and has a broad angle of incidence.

In the next year, Jaradat *et al.* (2021) [104] discussed triple band metamaterial-based absorber at various peaks, achieving above 99% absorption at 1.67 THz. The dimension of the structure is 20 μm × 11 μm × 2.3 μμm. The design is polarization insensitive and has a broad angle of incidence.

The year followed was marked by the work of Hakim *et al.* (2022) [105], which investigated a Jerusalem structure that comprises two square split-ring resonators, four microstrip lines. The structure, as claimed, can attain absorption with more than 97%, 99.51%, 99%, and 99.5% absorption at 12.62 GHz, 14.12 GHz, 17.53 GHz, and 19.91 GHz, respectively. Then, Wang *et al.* (2022) [106] investigate a structure that is comprised of periodically arranged surface structure on an insulating slab. The structure, as claimed, can attain absorption with more than 98.75% and 99.46% absorption at 0.61 THz and 1.68 THz, respectively. The dimension of the structure is 120 μm × 120 μm × 15 μm. The design is polarization insensitive with broad angle of incidence. The work was followed by the contribution of Banerjee *et al.* (2022) [107], that investigated a structure that comprises four circular patches resonator. The structure, as claimed, can attain absorption with more than 99%, 99.75%, and 98%and 99.46% absorption at 2.36 THz, 2.675 THz, and 2.97 THz, respectively. The dimension of the structure is 100 μm × 100 μm × 5 μm. The design is polarization insensitive and has a broad angle of incidence. The structure found in applications related to terahertz

regime the attainment of desirable parameter for polarization and angle of incidence is good for practical applications.

2.1.2 Wideband Absorbers

The section focusses on the research work in the past years for design, development and characterisation of wideband metasurface based absorbers. The absorbers discussed in this section provide insight to the work done in past years for the achievement of wideband having high absorptivity in frequency spectrum through various techniques. To understand the practical viability of structure, the performance of absorber is visualised on polarization and angle of incidence parameter. The review of metasurface absorber in wideband category is as follows,

Gu *et al.* (2013) [108] presented a type of isotropic broadband metamaterial absorber having single-layer hexagonal dendritic units that is geometrically arranged with different dimensions. The 80% absorption is attained in X-band and the absorption level is more than 80% from 9.05 GHz to 11.4 GHz frequency range. The angle insensitivity is defined by evaluation the performance at oblique incidence and the structure is providing good absorption level at oblique incidences less than 45°. The absorption attained for S-band within the range from 3.02 GHz to 4 GHz is of the order of 50% in the desired frequency range. The dimension of the structure is 11 mm × 11 mm × 2 mm. The design is polarization insensitive and has a broad angle of incidence, and then Wang *et al.* (2013) [109] demonstrated an ultra-thin narrow-band metamaterial absorber with periodicity achieved circular metal patch array. The MA could exhibit an absorption peak at 5.91 THz with peak absorption of 99.9%. The absorption level exhibited with the 80 μm × 80 μm × 200 nm structure. The design is polarization sensitive and has a low angle of incidence.

The year followed by the work of Dincer *et al.* (2014) [110] designed, characterized, and analysed a new kind of metamaterial absorber for solar cell applications in desired frequency regions. This structure which is metamaterial based is localised for applications in solar spectrum in order to utilize solar energy effectively. The dimension of the structure is 30 mm × 30 mm × 1.5 mm. The design is polarization sensitive and has a low angle of incidence. Bhattacharyya *et al.* (2014) [111] proposed a absorber witnessing insensitivity to polarization parameter and wide angle of incidence. The absorption peaks are obtained at 98%(6.65 GHz), 81.4%(6.88 GHz), 90.9%(7.19 GHz), 90.3%(8.58 GHz), 87.2%(8.98 GHz), 82%(9.42 GHz), 99.4%(9.86 GHz) and 62.3%(10.14 GHz).The geometry is 10 mm × 10 mm × 1.6 mm. The design is polarization insensitive and has a broad angle of incidence. The work was followed

by the contribution of Wang *et al.* (2014) [112] metasurface based absorber, a continuous metal of 1m separated by only 1mm dielectric substrate. The structure is ultra-thin triple-band metamaterial absorber working in the microwave region. The structure is fabricated to analyse effectiveness of results and it is observed that fabricated structure exhibits 98.8%(4.88 GHz), 96.5%(7.88 GHz), and 95.9%(11.32 GHz). The behaviour of triple-band absorber is polarization-insensitive at the normal incidence. The dimension of the structure is 14 mm × 14 mm × 7.5 mm the design is polarization sensitive and has a low angle of incidence. Then, Wang *et al.* (2014) [113] investigated a metamaterial absorber having absorption above 90% (8.85 GHz -14.17 GHz). The dimension of the structure is 9 mm × 9 mm × 1.2 mm. The design is polarization insensitive and has a low angle of incidence.

The year followed with the contribution of Ayop *et al.* (2015) [114] illustrated a wideband absorber with a dual-band absorber with an absorbance of 98.66%, and 99.84 % arrived at 9.81 GHz and 10.41 GHz. The result is polarization-insensitive and has perfect dual resonances. Two peaks absorbance of respectively with full width half maximum (FWHM) bandwidth calculated to be 1050 MHz or 10.38% at normal incident wave. The structure was analysed with variation of polarization is performed at different polarization angles. The achievement of two resonant peaks and with wider bandwidth achieved justified its claim for dual wideband absorption.

The experimental data of it is conforming to the results, and two peaks of absorbance are achieved with magnitudes of 99.88% and 99.67% at 10.14 GHz and 10.79 GHz, respectively. Thereafter, Agarwal *et al.* (2015) [115] proposed a X-band operated compact metamaterial absorber. The proposed structure is behaving in dual-band and the attainment of peak absorptivity of 8.70 GHz (95.16%) and 8.70 GHz (97.84%).The dimension of the structure is 12 mm × 12 mm × 0.56 mm and design is polarization insensitive with broad angle of incidence. The contribution of Song *et al.* (2015) [116] illustrated a numerical approach to design the frequency selective surface (FSS) based metamaterial absorbers (MAs). The dimension of the structure is 9.8 mm × 9.8 mm × 0.4 mm and the design is polarization sensitive with low angle of incidence.

In the next year, Kong *et al.* (2017) [117] investigated a new structure with nested cross rings. Simulation results are providing a result of attaining absorption band from 6.08 to 13.04 GHz and 90% value of high absorption. The Absorber behaviour is broadband in nature having relative absorption bandwidth achieved to be 72.8%. Moreover, the proposed Absorber was insensitive to the polarization of the TE and TM waves. The dimension of the structure is 14.4 mm × 14.4 mm × 3.5 mm and the design are polarization insensitive with

broad angle of incidence, and then Lee *et al.* (2017) [118] investigated metamaterial absorber working as switch using a PIN diode. The performance of the proposed absorber is gauged by the ON/OFF state of the PIN diode. The PIN diode ON/OFF state provide varied absorption levels with PIN diode working in ON state, the structure attained 90% absorption bandwidth from 8.45–9.3 GHz. Similarly OFF state PIN diode provides more than 90% absorption from 9.2–10.45 GHz. The switching of the Absorption band is instrumental through PIN diode using ON/OFF state. Further, Sood *et al.* (2017) [119] investigate a wideband metamaterial absorber. The structure, as claimed, can attain absorption of 90% from 10.45 to 17.64 GHz. The dimension of the structure is 5.5 mm × 5.5 mm × 1.6 mm and the design is polarization sensitive in nature.

The next year Huang *et al.* (2018) [120] designed a tuneable broadband metamaterial absorber based on graphene. The Jerusalem cross is used as a shape. A tuneable broadband graphene structure is investigated in infrared regions. The dimension of the structure is 3 μm × 3 μm × 0.1 μm. The design is polarization insensitive and has a low angle of incidence. Alkurt *et al.* (2018) [121] proposed an octagonal-shaped broadband metamaterial absorber. The 99.97 % absorption at 5.5 GHz involving a bandwidth of 1 GHz between 5 GHz and 6 GHz in Transverse Electric (TE) mode is achieved. The structure is polarization insensitive. The dimension of the structure is 7.6 mm × 7.6 mm × 3.2 mm. Thereafter, Lei *et al.* (2018) [122] investigated a structure that is a thin nanostructure with titanium-silica (Ti-SiO2) cubes and an aluminium (Al) bottom film. The structure, as claimed, can attain perfect absorption and average absorbance of 97% is exhibited. The geometry of frame is 250 nm × 250 nm × 300 nm. The design is polarization insensitive and has a broad angle of incidence.

In the subsequent year, Wang *et al.* (2019) [123] investigated a simple structure of a rectangular-shaped resonator with elongated slots. The structure, as claimed, can attain near-perfect absorption with 100% at 1.04 THz and 2.65 THz. The dimension of the structure is 88 μm × 88 μm × 14 μm. The design is polarization sensitive and has a narrow-angle of incidence. After that, Ranjan *et al.* (2019) [124] investigated a wideband metamaterial structure. The structure, as claimed, can attain absorption with more than 90% absorption from 5.94 GHz to 11.92 GHz. The dimension of the structure is 9 mm × 9 mm × 3 mm and the design is polarization sensitive with narrow-angle of incidence. In the same year, Zhang *et al.* (2019) [125] investigated a structure that comprises of metal patch loading resistor with a variable capacitor. The structure, as claimed, can attain absorption with 90% at 0.68 GHz to 2.13 GHz. The dimension of the structure is 24 mm × 30 mm × 6 mm. The design is polarization sensitive and has a narrow-angle of incidence. Qi *et al.* (2019) [126]

demonstrated a structure that comprises of graphene metamaterial absorber. The structure, as claimed, can attain absorption with 90% at 8.7 THz to 11.9 THz. The dimension of the structure is 3.6 μm × 3.6 μm × 1.76 μm. The design is polarization insensitive and has a broad angle of incidence.

The next year, Nochian *et al.* (2020) [127] investigated a structure that comprises three layers of the resonator. The structure, as claimed, can attain absorption with more than 94% absorption from 6.5 GHz to 12 GHz. The dimension of the structure is 5.85 mm × 5.85 mm × 3.2 mm and design is polarization insensitive with broad angle of incidence. Thereafter, Barde *et al.* (2020) [128] demonstrated a structure that is a wideband metamaterial absorber. The structure, as claimed, can attain absorption with more than 88% absorption from 12 GHz to 18 GHz. The dimension of the structure is 10 mm × 10 mm × 1.6 mm and design is polarization sensitive with a narrow-angle of incidence.

The year followed with the work of Wang *et al.* (2021) [129] investigated a structure that comprises a VO2 disk, polyimide substrate, and gold ground plane. The structure, as claimed, can attain absorption with more than 90% absorption from 3 THz to 8 THz. The dimension of the structure is 12 μm × 12 μm × 7 μm. The design is polarization insensitive and has a broad angle of incidence, and then Luo *et al.* (2021) [130] investigated a structure that is a cross-band metamaterial absorber. The structure, as claimed, can attain absorption with more than 90% absorption from 1.18 THz and 1.85 THz. The dimension of the structure is 120 μm × 120 μm × 270 μm. The design is polarization insensitive and has a broad angle of incidence. Further, Kim *et al.* (2021) [131] analysed a wideband metamaterial absorber. The structure, as claimed, can attain absorption with more than 90% absorption from 6.3 GHz to 30.1 GHz. The dimension of the structure is 21 mm × 21 mm × 4 mm and the design is polarization insensitive with broad angle of incidence. The work was followed by the contribution of Kaur *et al.* (2021) [132] investigated a wideband metamaterial absorber. The structure, as claimed, can attain absorption with more than 97% absorption from 12 GHz to 21 GHz. The dimension of the structure is 5 mm × 5 mm × 1.54 mm and the design is polarization insensitive with broad angle of incidence.

2.2 Review of Isolation Techniques

In this section, the research works that have been done in the field of MIMO isolation techniques are discussed. The study of MIMO isolation techniques was primarily focused on understanding established techniques through which isolation in MIMO setup can be achieved. These techniques can be broadly classified as based on [61];

a) Decoupling Network.

b) Parasitic Elements.

c) Defective Ground analogy.

d) Neutralization Line.

e) Metamaterial based.

The review on MIMO isolation techniques is focused on the level of isolation achieved, methodology incorporated, and attained values of ECC, DG, and EDG. All these parameters will determine the practical usability of techniques for establishing the desired level of isolation in the MIMO setup. A brief overview of various absorbers is as follows;

In the year 2007, Chiu *et al.* (2007) [133] proposed that the isolation is achieved through the slitted ground, an isolation level of around -20 dB is achieved through the incorporation of defective ground methodology. The frequency of operation is 2.27-2.35GHz.

In the subsequent year, Chen *et al.* (2008) [134] proposed an isolation improved level of more than -30 dB that is achieved through a compact decoupling network thereby making the design suitable for practical applications. In the same year the work of Wang *et al.* (2008) [135] used parasitic structure methodology with highest isolation level of more than -21 dB at 4.2 GHz for making structure practical viable.

Thereafter, Lee *et al.* (2011) [137] proposed that the isolation is achieved through an array of metamaterial unit cell, and an isolation level of around 22.2 dB is achieved through the incorporation of the metamaterial-based unit cell at 2.45 GHz.

The next year through effort of Su *et al.* (2012) [138] saw incorporation of neutralisation line technique to achieve isolation level of -15 dB at 2.5 GHz. The gain achieved is 2.1 dBi and radiation efficiency of 81%. Moreover, diversity parameters are evaluated to test the diversity performance. In the same year isolation technique using dual-mode 1800 hybrid de-coupler was investigated by Lin *et al.* (2012) [139] and an isolation level above than -20 dB is achieved through network at 2.45 GHz and 5.25 GHz. In work of Li *et al.* (2012) [140] established an isolation through sleeve coupled rectangle stepped impedance resonator, an isolation level of around -23 dB is achieved over broad operating frequency (3.1 GHz to 10 GHz). The year witness isolation enhancement through the design of an EBG structure comprising slots through the research work of Margaret *et al.* (2012) [141],the highest level of isolation is around -36 dB using through parasitic element over wide operating band (5.2

GHz to 6.2 GHz). The year also witnessed U- shaped slots ground, an isolation level around -15 dB is achieved through incorporation of defective ground methodology over operating band of 1.7 GHz to 2.7 GHz with ECC attained as 0.01 and the work credit is effort of Zhou *et al.* (2012) [142].

In the next year, Yu *et al.* (2013) [144] proposed that the isolation is obtained using the slitted ground. An isolation level of around -18 dB is achieved through the incorporation of defective ground methodology. The frequency of operation is 2.7 GHz, and the value of diversity gain (DG) achieved is 9.88. In the same year Singh *et al.* (2013) [145] proposed to enhance the isolation between ports by using non-radiating folded shorting strip by interconnecting each antenna element with ground plane. The results achieved are isolation values of -28 dB from 2.4-2.48 GHz and -26 dB in the range from 5.15-5.85 GHz covering lower and higher WLAN band. The year also witnessed electromagnetic band gap technique of S-EBG with vias to achieve an isolation level greater than -25 dB at 2.42 GHz through the work effort of Suntives *et al.* (2013) [146]. Subsequently, Xia *et al.* (2013) [147] investigated that the isolation is achieved using two directional couplers and two sections of the transmission line. An isolation level of more than - 58 dB is exhibited through a decoupling network at 7.5 GHz thereby confirming the practical utility of structure in applications.

In the same year, Khan *et al.* (2014) [150] proposed the isolation is achieved through a digitated parasitic decoupling structure to obtain high isolation. They found isolation greater than -20 dB over ultra-wideband frequency (3.1 GHz to 10.6 GHz). Then, Chen *et al.* (2014) [151] investigated an isolation technique using a capacitor (range of 1.8 pF to 3.3 pF). The operating frequency range is from 704 MHz to 960 MHz and 1710 MHz to 2170 MHz having a value of isolation achieved greater than -10 dB and -15 dB, respectively. In the same year 2014, a -15db isolation is achieved with T-shaped ground stub and a vertical slot cut on a T-shaped ground stub through the efforts of Liu *et al.* (2014) [152] with achievement of ECC value of 0.1.

The next year is marked by the contribution of Zhao *et al.* (2015) [154] employed a decoupling network technique having coupled resonator decoupling network, thereby achieving an isolation level of -15 dB at 2.48 GHz. The radiation efficiency arrived is 75%. The parameters ECC achieved equal to 0.23 and DG parameter is 9.73 dB and then in the same year a technique to employ parasitic and slot element technique of two coplanar strip line feed staircase shaped radiating elements thereby achieving an isolation level of -20 dB at 3.1 GHz was employed by Roshana *et al.* (2015) [155]. The year witnessed the work of Singh

et al. (2015)[156] using folded shorted strips between elements and ground plane to obtain enhancement of isolation level by -13 dB at 2.45 GHz, -5 dB at 4.4 GHz band and -12 dB at 5.5 GHz. Further, Yu *et al.* (2015) [157] proposed an isolation technique to high isolation level around -18 dB and -21 dB using defective ground methodology for frequency of 2.7 and 3.95 GHz, respectively. The ECC is calculated as 0.15 which is well below the defined limit. The year witness isolation achieved through wideband neutralization line, isolation level around -22 dB is achieved through proposed methodology over 3.1 GHz to 5 GHz through the research work of Zhang *et al.* (2015) [158]. The work of Singh *et al.* (2015) [53] involving defected ground methodology to attain high isolation of -20 dB between antennas for WLAN applications. The contribution of Wang et al. (2015) [159] employed the neutralization line technique to achieve an isolation level of -23 dB at 750 MHz. Further, Lee *et al.* (2015) [160] employed the electromagnetic band gap technique to achieve an isolation level greater than -53.7 dB at 2.54 GHz. The radiation efficiency is 82%, ECC is 0.002, and DG is 9.98 dB at designated frequency. In the same year, Zhai *et al.* (2015) [161] employed a metamaterial-based technique to achieve an isolation level of -42 dB at 2.45 GHz. The work of Singh *et al.* (2015) [162] employed two non-radiating folded shorting strips are connected between each antenna element and ground plane resulting an isolation level to a maximum of -24dB in the range of frequencies cover WLAN (2.46–2.6 GHz), WiMAX (3.37–3.75 GHz), and HIPERLAN (5.2–5.87 GHz).

The following year witnessed the contribution of Agarwal *et al.* (2016) [163]. They proposed an isolation technique using an array of metamaterial unit cell to obtain isolation level around -33 dB and -32.5 dB over operating band from 5.15 GHz to 5.35 GHz and 5.72 GHz to 5.82 GHz, respectively. They proposed an isolation technique using an array of metamaterial unit cell to obtain isolation level around -33 dB and -32.5 dB over operating band from 5.15 GHz to 5.35 GHz and 5.72 GHz to 5.82 GHz, respectively. The same year saw incorporation of S-shaped defected ground structure and was able to achieve isolation of -55 dB at 2.57 GHz by the effort Wei *et al.* (2016) [164]. Then Chen *et al.* (2016) [165] employed open-ended defected ground slots to achieve isolation of greater than -20 dB at 1 GHz. The gain achieved is 2 dBi with radiation efficiency 80%. Moreover, ECC value at the designated frequency is 0.075, while DG achieved for reference frequency is 9.97 dB. Thereafter, Ibrahim *et al.* (2016) [166] demonstrated a metamaterial-based technique to achieve an isolation level of -28 dB at 5.55 GHz and Krishna *et al.* (2016) [167] employed parasitic or slot element technique of stepped feed line and square ring slots, thereby achieving an isolation level of -

20 dB at 3.0 GHz in the same year. The year witness parasitic or slot element technique of stepped slot feed line and open-ended ground slot, thereby achieving an isolation level of -22 dB at 3.2 GHz. The value of gain calculates as 4 dBi and radiation efficiency as 80% by the effort Srivastava *et al.* (2016) [168]. Then, in the same year, Diallo *et al.* (2016) [169] proposed that the isolation is achieved through suspending line between PIFA feeding and/or shorting points and by virtue of technique an isolation level around -22 dB is achieved through incorporation of neutralization line methodology at 1.95 GHz.

In the next year, Xu *et al.* (2017) [173] employed a metamaterial-based technique to achieve an isolation level of -15 dB at 4.75 GHz. However, the value of radiation efficiency is 77%, the value of ECC is 0.02, and the value of DG is 9.89 dB at designated frequency. The technique has wider applications in mobile handset applications. The same year also witnessed a decoupling network technique having a reactive dummy load, thereby achieving an isolation level of -27.6 dB at 2.18 GHz through the contribution of Wu *et al.* (2017) [174]. Further, Khan *et al.* (2017) [175] employed parasitic or slot element technique of meandered feed line and stub to ground connection thereby achieving an isolation level of -15 dB at 3.0 GHz. The value of gain achieved is 1.5 dBi and the radiation efficiency arrived is 82%. The parameter ECC is calculated as 0.42 and DG is 9.07dB thereby establishing practical utility of structure.

In the subsequent year, Li *et al.* (2018) [176] demonstrated an isolation technique through an array of metamaterial unit cell to achieved isolation around -24 dB at 5.8 GHz. Then in the same year, a decoupling network technique having pattern diversity, achieving an isolation level of -15 dB at 3.6 GHz was proposed by Ding *et al.* (2018) [177]. The radiation efficiency achieved through technique was 50%.

In the year 2009, Rezapour *et al.* (2019) [178] investigated that the isolation is achieved through an array of metamaterial unit cell, and an isolation level of around -23 dB is achieved through the incorporation of the metamaterial-based unit cell over dual band operating frequency bands from 2.02 GHz to 2.7 GHz and from 2.18 GHz to 3.8 GHz.

Subsequently, the next year a -41 dB isolation at 5.3 GHz is witnessed through the contribution of Khan *et al.* (2020) [179] that employed a defective ground analogy.The value of gain achieved is 8.4 dBi and the radiation efficiency arrived is 98.01%. The diversity parameters are calculated and found ECC as 0.01 while DG as 10 dB. In the same year, spatial diversity technique was employed by Hadri *et al.* (2020) [180] with the achievement

of -35 dB isolation at 28 GHz. The year also saw the contribution of Kaur *et al.* (2020) [181] proposed that the isolation is achieved through an array of metamaterial unit cell, an isolation level around - 25 dB is achieved through incorporation of the metamaterial-based unit cell at 5.65 GHz resonating frequency band.

The year 2021 was marked with the work of Dey *et al.* (2021) [182] employed the electromagnetic band gap technique with the achievement of - 32.7dB isolation at 28 GHz. Further, incorporation of decoupling structures by Rajmohan *et al.* (2021) [183] with the achievement of -82 dB isolation at 28 GHz. Also, radiation performances are tested and found the gain as 5.7 dBi and the efficiency as 82%. The same year were marked by the contribution of Roy *et al.* (2021) [184]. They employed a meander line isolator in order to achieve high isolation of -19 dB over 2.8 GHz to 4.2 GHz. The diversity parameters is calculated and found ECC equal to 0.2 and DG equal to 9.6 dB.

The year 2022 is also witnessing various novel techniques to enhance isolation level for various applications suffering from mutual coupling due to interference in various elements of MIMO setup. The year 2022 witnessed the contribution of Khurshid *et al.* (2022) [185], who employed the slotted ground technique to achieve isolation of -20 dB over wide operating frequency range from 2.3 GHz to 23 GHz. Further, in the same year T-shaped ground branch which is acting as a decoupling network was tested for results by Mu *et al.* (2022) [186] and the highest level of isolation is obtained in the range of -20 dB at 5.4 GHz. The close to -20dB isolation level attainment and effectively be incorporated in practical setup for desired resuts. The ECC value achieved is 0.075. The antenna efficiency arrived is 93%, while the antenna gain is 5.35 dBi. The work was followed by the contribution of Nithya *et al.* (2022) [187], that employed a decoupling element acting as an isolator to achieve isolation of -15 dB in the frequency range from 3.3 GHz to 5.0 GHz. The contribution of Kaur *et al.* (2022) [188] paved the way for incorporation of a reverse T-shaped rectangular strip in the central portion of the substrate inter-connecting CPW grounds. The centralised reverse T-shaped rectangular strip is effectively providing an isolation level of the order of -17.5dB from 1.92 GHz to 3.3 GHz and 4.6 GHz to 6 GHz falling within the range of Wi-Fi/WLAN standards and therefore justifying its relevance for practical implementation in setups demanding incorporation of isolators.

CHAPTER 3 DESIGN, OPTIMIZATION AND DEVELOPMENT OF MULTIBAND ABSORBERS

3.1 Introduction

The innovation of metamaterial absorbers with the rising need for application-oriented absorbance at microwave regimes involving cloaking, mutual coupling reduction, reduced radar cross section, EMI/EMC (Electromagnetic interference/Electromagnetic compatibility), and stealth technology is well known today [34-47]. The geometry of the unit cell is a restricting condition to explore the possibility of multiband, wideband with optimized dimensions in coherence to requirement of the highest form of absorptivity. This condition restricts the practical usability of metamaterial-based absorbers for exploitation in commercial applications. The miniaturization and absorptivity are the prime region to focus and paramount necessity for researchers using metamaterial-based microwave absorbers. However, the miniaturized unit cell dimensions of the metamaterial absorber appear to be a hindrance since the applications demands near total or perfect absorptivity at these dimensions. The numerous single, multi, and wideband absorbers are available [34-47], but the specific necessity for a near total absorption rate that, too, with ultrathin dimensions, is still a difficult preposition. The work on multiband absorbers is stretched with the design of two absorbers.

The first one is the absorber structure that has a combinational effect of three-square rings, and a square ring with a triangle annexed along sides acting as a central square ring is taken for analysis. The locational aspect of various patches with dimensional optimization provides high absorptivity levels of 99.14%, 98.29% at 6.08 GHz and 9.49 GHz, respectively, and above 95% absorption from 16.57 GHz to 16.83 GHz. The structure provides polarisation insensitivity up to 75^0 and has a wide angle of stability up to 60^0. The ultrathin dimensions and attainment of tri-band with high absorption make the structure fit for practical incorporation in various microwave applications

The second absorber is combination of three-ring resonators along with a symmetrical patch inside innermost ring. The locational dimensions of rings and inner patch provide a good degree of coupling due to inductance and hence play an instrumental role in attaining desired absorptivity at multiband. The almost perfect absorption peaks are realised after fine-tuning the shape parameters of the structure. The proposed absorber provides peak absorptivity of 99.96% at 4.75GHz, 99.98% at 9.47 GHz, and 99.62% at 14.40 GHz covering C-, X-, and Ku-band respectively. The identical TE and TM polarized waves are symmetric in nature with

good absorption rates thereby supporting the claim for practical utility. The structure exhibits up to 45^0 polarization-insensitive behaviour with angular stability is wide in nature. The commercially desired frequency of operation with ultrathin dimensions and perfect absorptivity in combination with polarisation insensitive behaviour till 45° justify the relevance of structure as practical catchy for various microwave applications.

3.2 Ultrathin Triple-Band Metamaterial Absorber

The work presents design and development of compact metamaterial-based microwave absorber having polarisation insensitivity, broad angle of incidence in microwave frequency range. The unit cell focuses to achieve maximum absorption at C-, X- and broad Ku- band. The structure is simulated and the results are analysed for different angle of polarization and angle of incidence. The dimension of proposed structure is ultrathin and compact having overall dimension as 8 mm × 8 mm × 0.8 mm. The three different peaks at three different bands are achieved with optimized dimensions thereby making the triple-band behaviour of metamaterial absorber possible. The structure is providing absorption of 99.14% absorption at 6.08 GHz (C-Band) while absorption of 98.29 % is achieved at 9.49 GHz (X-band) and 265 MHz bandwidth with above 95% absorption from 16.57 GHz to 16.83 GHz (Ku-Band) in microwave regime. The details analysis of the designed multi-band absorber is given in below sections.

3.2.1 Configuration of Triple-Band Absorber

The absorber configuration is a combination of square rings with one square split on all sides. The centralized square is annexed with triangles, while the outer square ring is appended with four rectangles on all sides to achieve desired triple band absorption. A unit cell that represents the proposed absorber comprises metallic layers, one being a complete metallic ground plane and the other with patches on top in between two layers that exist FR4 dielectric with a thickness of 0.8 mm. The top layer comprising resonating patch is etched on a substrate with copper having 0.017 mm thickness. Since, the complete metallic back-side maintained the transmission coefficient component as zero. The layers of proposed structure and configuration are shown in Fig. 3.1. Also, the detailed shape parameters of the triple-band absorber are mentioned in Table 3.1.

3.2.2 Results and Discussion

3.2.2.1 Design and Evolution of the Triple-Band Absorber

The structure is simulated using floquet boundary conditions for unit cells in Computer

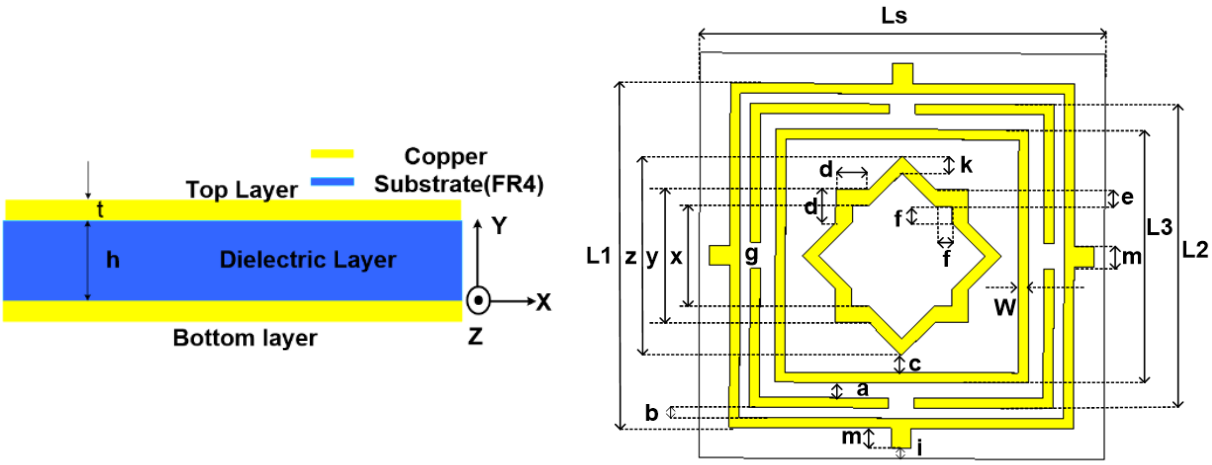

Fig. 3.1: Layers and configuration of the proposed absorber.

Table 3.1: Shape parameters of the triple-band metamaterial absorber.

S. No.	Parameters	Dimension (in mm)
1.	Ls	8
2.	L1	6.8
3.	L2	6
4.	L3	5
5.	x	2
6.	y	2.6
7.	z	3.92
8.	e	0.3
9.	k	0.32
10.	i	0.2
11.	m	0.4
12.	g	0.5
13.	a	0.3
14.	b	0.2
15.	c	0.34
16.	f	0.32
17.	d	0.65
18.	w	0.2
19.	h	0.8
20.	t	0.017

Simulation Technology Microwave Studio (CST MWS) incorporating finite integration technique. The electric and magnetic fields are polarized along the *x*- and *y*- directions as TE (0, 0) and TM (0,0), respectively. Fig. 3.2 and 3.3 gives information on the simulation setup and absorption level achieved for the proposed absorber in TE and TM mode, respectively. The simulation graph provides a clear indication of near-perfect absorption and the attained

absorption level that will surely be beneficial for all those applications that demand the incorporation of an absorber in its configuration setup.

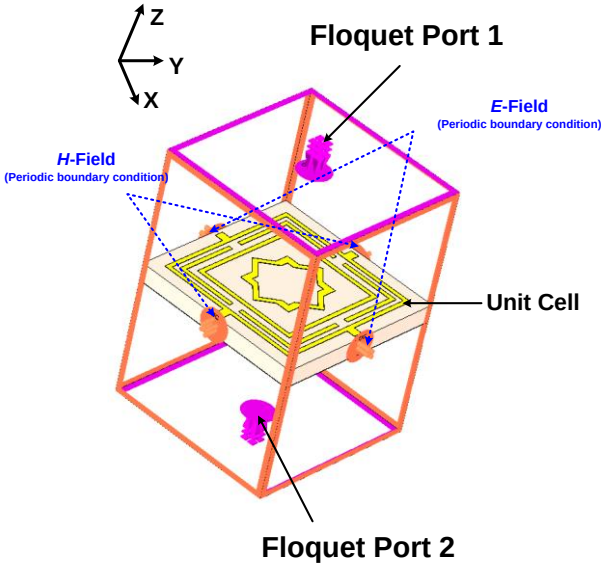

Fig. 3.2: Simulation setup for the design of absorber.

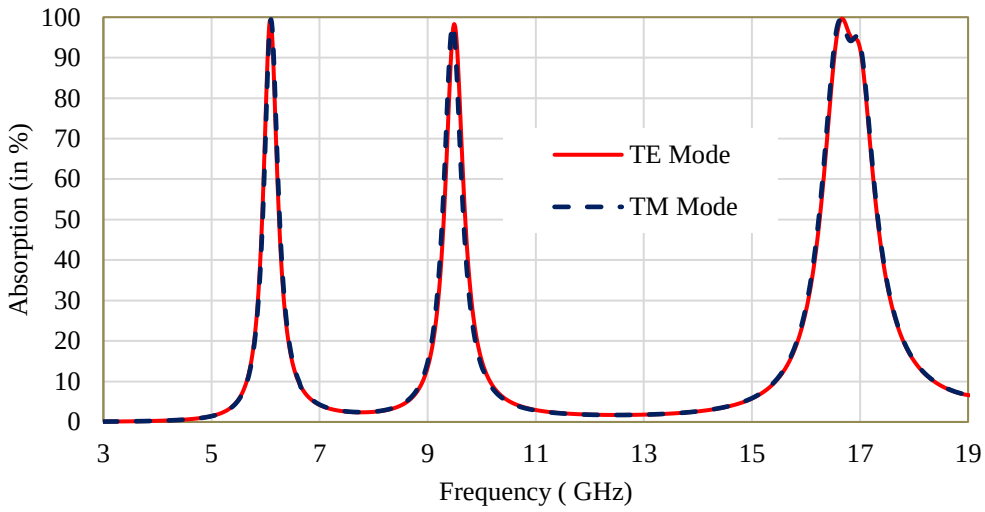

Fig. 3.3: Variation of absorptivity with frequency for TE and TM mode.

The basic mathematical equation taken for absorption of the unit cell metamaterial absorber [5] is;

$$A(\omega) = 1 - R(\omega) - T(\omega) \tag{3.1}$$

$$A(\omega) = 1 - |S_{11}(\omega)|^2 - |S_{21}(\omega)|^2 \tag{3.2}$$

where, absorption, reflectance, and transmittance are denoted by *A(ω), R(ω), and T(ω)*, respectively. Eq. (3.1) clearly indicates absorption $A(\omega)$ is dependent upon the S_{11} (reflection coefficient) and S_{21} (transmission coefficient).

Since, the ground geometry of the proposed absorber is completely metallic therefore, S_{21} (transmission coefficient) is reduced to zero, as given in Eq. (3.3) [5].

$$A(\omega) = 1 - |S_{11}(\omega)|^2 \tag{3.3}$$

The absorptivity achieved through the simulation of the desired structure is shown in Fig. 3.3. Further, the evolution process of proposed absorber started with an aim to produce tri-band in microwave regime is shown in Fig. 3.4 and corresponding absorption response is shown in Fig. 3.5. The Stage A of proposed absorber is square ring providing an absorption level of 81.73% at 13.38 GHz, the Stage B witness slight improvement in absorption characteristics by tilting the square ring and appending it with four triangles at each sides thereby witnessing 92.86% absorption at 17.10 GHz. The Stage C is a square ring engulfing proposed geometry of Stage A thereby providing a dual band at 9.38 GHz and 17.16 GHz with absorption level attained as 97.86% and 99.13%, respectively at dual frequencies. The stage D is an incorporation of another square ring thereby giving initial tri-band having resonance at 7.55 GHz, 9.578 GHz and 17.14 GHz with absorption level attained as 98.32 GHz, 9.578 GHz and 17.14 GHz, respectively. The Stage E is an incorporation of square ring and is preliminary step to widen the bandwidth with above 95% absorption level. The results attained through Stage E is 98.69% and 86.84% absorption at 6.36 GHz and 9.62 GHz while broad bandwidth of above 95% absorption is achieved from 17.05 GHz to 17.23 GHz providing a band of 180 MHz. The split ring is introduced in intermediate ring of group of three square rings influence the attainment an absorption levels of 98.97% and 97.34% at 6.36 GHz and 9.49 GHz further above 95% band is improved from 180 MHz to 280 MHz from 16.82 GHz to 17.10 GHz as shown in Fig. 3.5. The stage can be presumed as final stage but the absorption levels as 6.36 GHz and 9.49 GHz demands improvement. The quest for good absorption level and broad bandwidth is attained through final stage designated as Proposed Absorber, where the structure is witnessing absorption level of 99.14%, 98.29% as against 98.97% and 97.34% for previous stage for designated frequencies 6.08 GHz and 9.49 GHz, respectively. The attainment of broad band is reduced slightly from 280 MHz to 265 MHz (with above absorption 95% absorption) from 16.57 GHz to 16.83 GHz in microwave regime but this reduction in width is equally compensated by increase in absorption level at other frequencies thereby justifying the evolution step as final stage of Proposed Absorber. The evolution process culminates with the attainment of triple band comprising C-band, X-band and broad bandwidth of Ku-band.

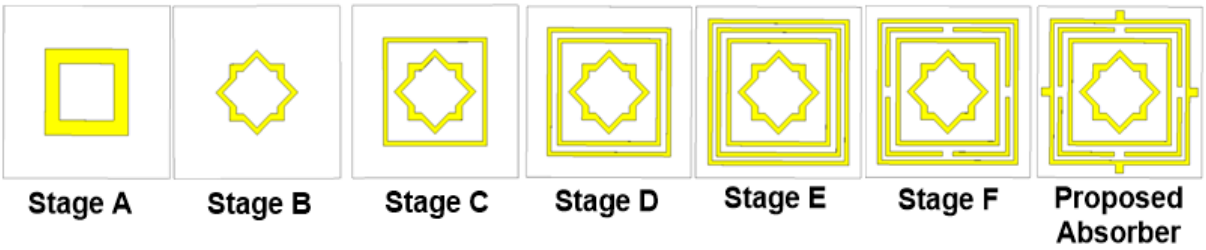

Fig. 3.4: Design evolution of the tri-band absorber.

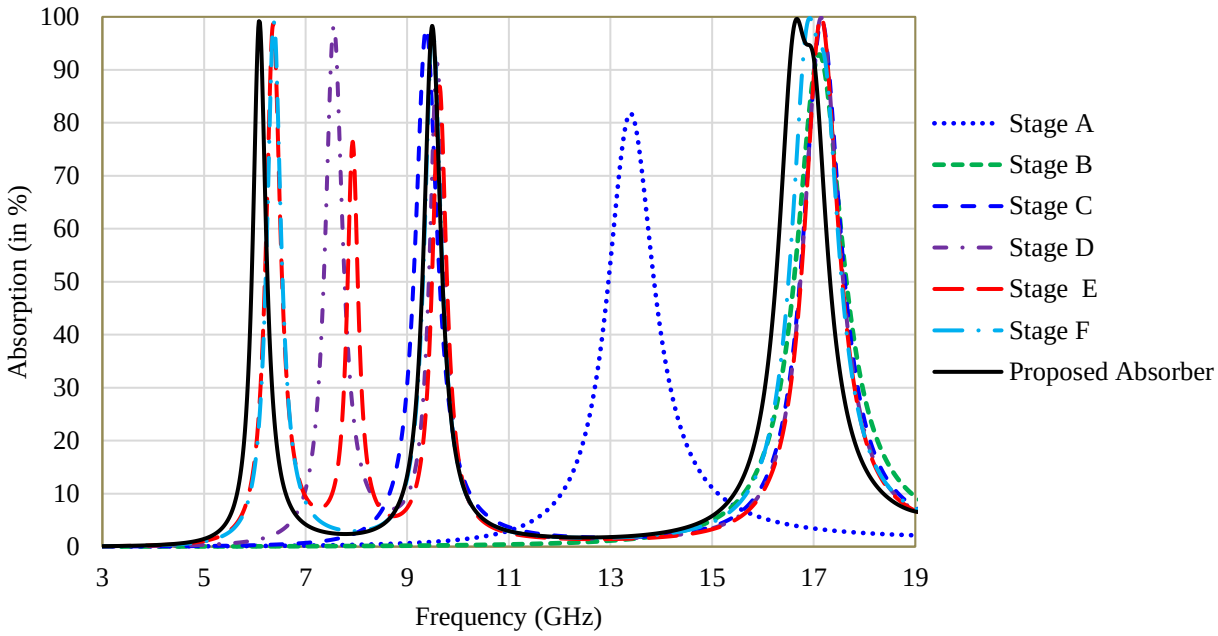

Fig. 3.5: Simulated absorption for a different configuration.

3.2.2.2 Constitutive Parameters

The exhibition of prefect absorption is attributed to electric and magnetic resonances. When the wave is incident on metamaterial electric field is coupled to top metallic structure and controls the electric permittivity (ε_{eff}). The current circulating on top and bottom ground layer is couples with magnetic field and thereby controlling magnetic permeability (μ_{eff}) of structure. Therefore, manipulating dimensions of different layers of structure it is possible that incident electric and magnetic field are absorbed [5]. According to transmission line theory when the wave is incident to absorber metallic layer, the reflection loss (RL) [189] for absorber structure with given thickness is given by Eq (3.4);

$$RL = -20log\left|\frac{Z_{in}-1}{Z_{in}+1}\right| \tag{3.4}$$

where, Z_{in} is normalized impedance of absorber and Z_{in} is described as Eq. (3.5) [189],

$$Z_{in} = \sqrt{\frac{\mu_r}{\varepsilon_r}}\, tanh\left[j\left(\frac{2\Pi ft}{c}\right)\sqrt{\mu_r \varepsilon_r}\right] \quad (3.5)$$

where, f is the frequency, t is thickness of absorber, c is velocity of light, μ_r and ε_r are complex permeability and permittivity of structure. The parameter μ_r and ε_r are linked to normalized input impedance and for complete absorption the Z_{in} =1 which can be achieved when $\mu_r = \varepsilon_r$ [189]. Thus by matching permittivity and permeability the impedance of structure is matched to free space impedance thereby providing maximum absorption and minimum reflectivity [5]. The material is characterized as metamaterial due to the exhibiting properties of negative permittivity and permeability. Fig. 3.6 provides an overview of permittivity, while Fig. 3.7 gives details of permeability. The normalized impedance of the proposed metamaterial absorber is shown in Fig. 3.8. From the graph, it is calculated that normalized impedance at 6.08 GHz, 9.49 GHz, and 16.57 GHz is 1.01 - *j*0.35 **Ω**, 1.01 + *j*0.00 **Ω** and 1.40 - *j*2.18 **Ω**, respectively. It is observed that real and imaginary values of normalized impedance show the values of one and zero, respectively. The attainment of the unity value of normalized impedance is a clear indication of perfect absorption on account of impedance matching of structure with free space impedance, thereby achieving high absorptivity. The designed absorber possesses low reflectance and perfect impedance resulting in perfect absorption in the microwave regime, thereby confirming the utility of the absorber in practical applications that require an absorber in its design configuration.

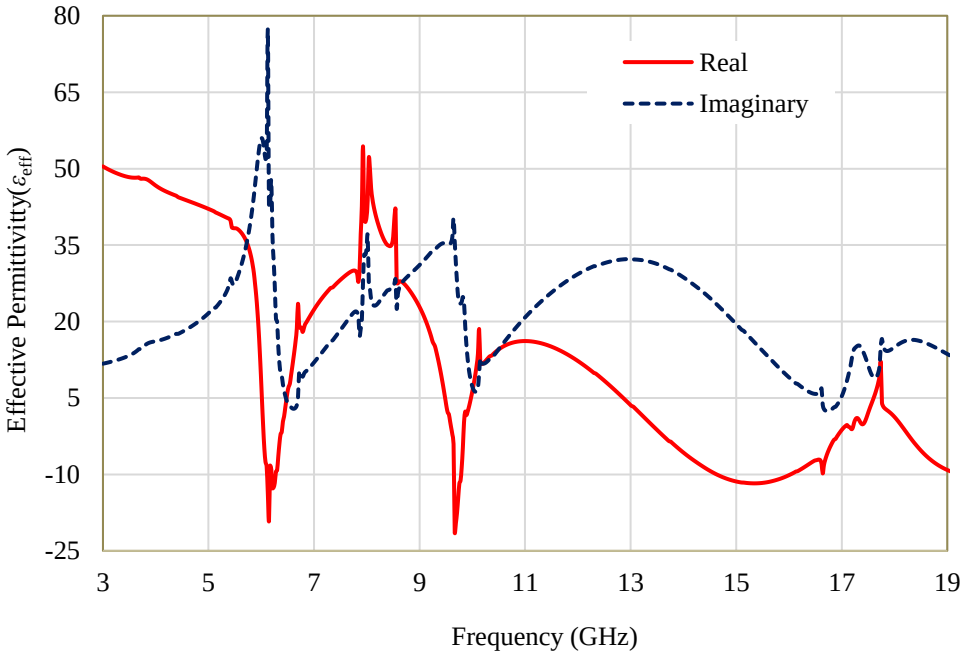

Fig. 3.6: Variation of permittivity with frequency

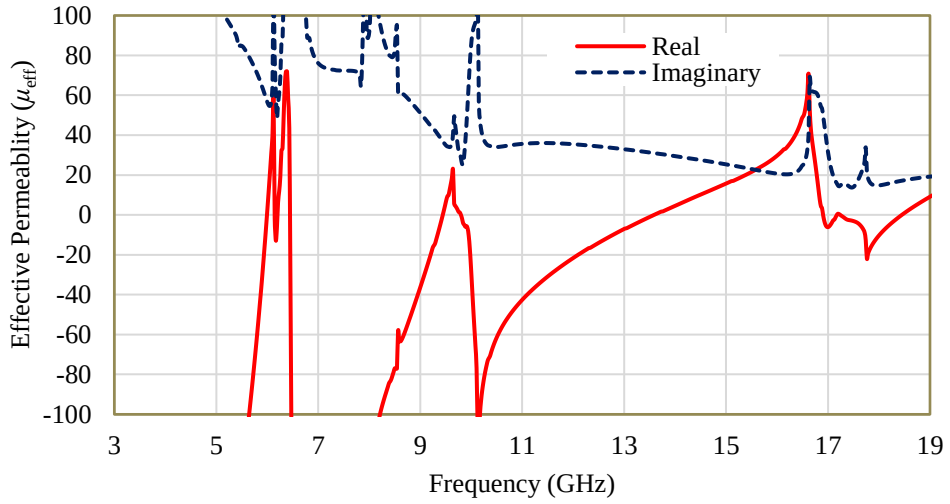

Fig. 3.7: Variation of permeability with frequency.

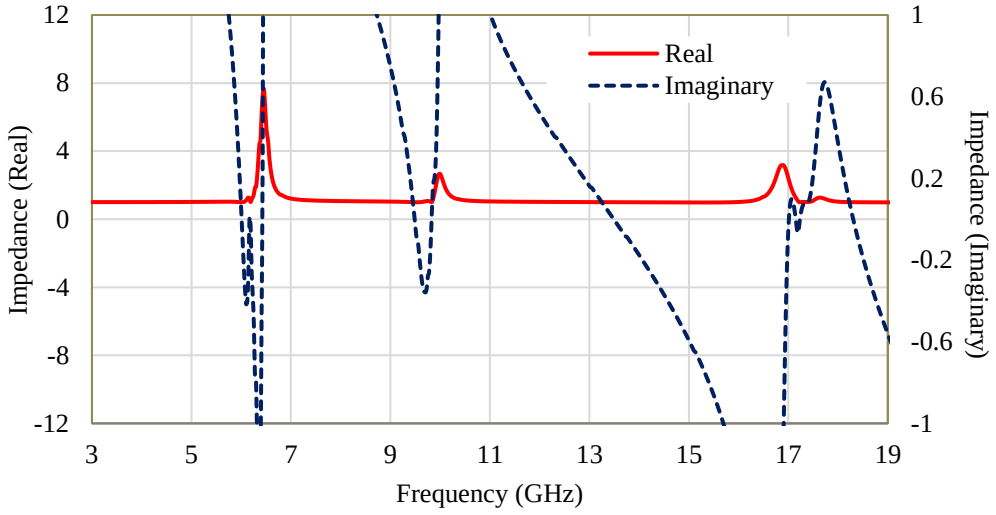

Fig. 3.8: Normalised impedance of the proposed absorber.

3.2.2.3 Parametric Analysis

The parametric study was performed for various parameters to ascertain the impact of dimensions on the absorptivity of the proposed absorber. The length of the innermost patch (p), the dimension of the substrate (Ls) and the gap (*g*) of the split are analyzed for optimized dimensions, and clearly, the inference from the analysis suggests the role of patches and dimensional geometry in absorption attainment. Fig. 3.9, 3.10, and Fig.3.11 provide insight into dimensional variation and its impact on absorptivity; the analysis was performed by the variation of one parameter and keeping other parameters constant. The dimension of parameter p varies from 4.5 mm to 5.5 mm, while the lower value of p, i.e., 4.5 mm, provides two relevant absorption peaks. In contrast, p = 5.5 mm absorption attained for the second peak is 91.32% at 8.362 GHz. Still, for the value of p = 5 mm, the desired

absorption level is attained, as shown in Fig. 3.9. The similar situation is witnessed at the dimension of the substrate where Ls = 8 mm provides a high absorption level in relative comparison to lower and higher values of relative dimension as shown in Fig. 3.10. The effect of gap (g) in second ring on absorptivity can be easily seen that with variation of parameter g when the value of g is 0.4 mm width of broadband for third peak is increased. Still, its absorption level at some points is reduced to below 90% value, while g = 0.6 mm provides a decrease in width for the desired level of absorption attained. The best response of absorptivity is attained at the value of g = 0.5 mm, where the attainment is of the broad band of 265 MHz (with above absorption 95% absorption) from 16.57 GHz to 16.83 GHz as shown in Fig. 3.11. The conclusion for parameterization is that for p = 5 mm, Ls = 8 mm g = 0.5 mm provide not only high absorptivity but are responsible for the attainment of triple-band behavior with broad Ku-band for the proposed absorber having high absorptivity levels of 99.14%, 98.29% at 6.08 GHz and 9.49 GHz, respectively, and above 95% absorption from 16.57 GHz to 16.83 GHz.

3.2.2.4 Surface current and Electric field Distribution

The behaviour of the absorber can be better understood with current vector distribution and electric field distribution in Fig. 3.12 (a-b). The current distribution clearly symbolizes that at 6.08 GHz, greater accumulation occurs at the outside ring. Whereas at 9.49 GHz, the maximum current distribution is along the innermost ring, while the central square patch has maximum current distribution at 16.62 GHz and shown in Fig. 3.12(a). The same phenomenon is witnessed through charge accumulation, as shown in Fig. 3.12(b). The current distribution

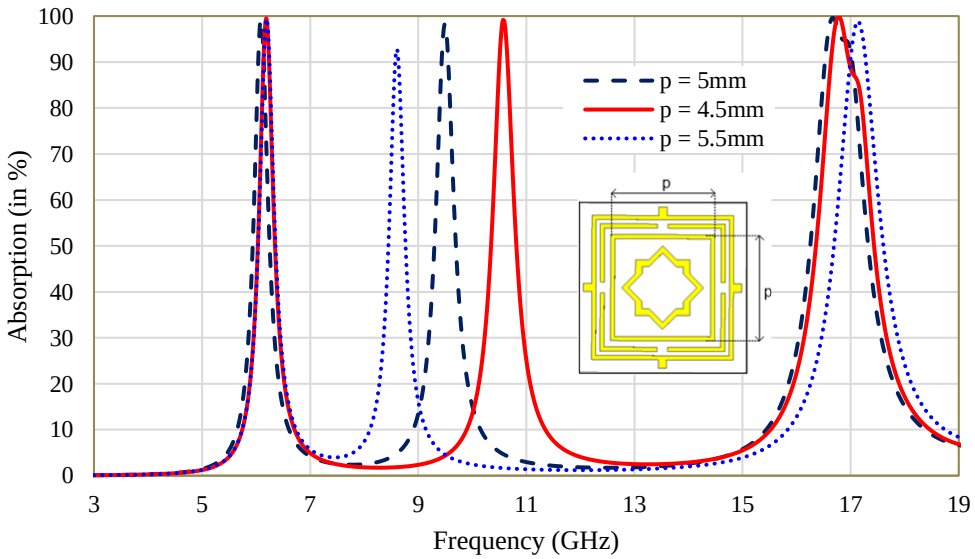

Fig. 3.9: Effect of the inner square ring (p).

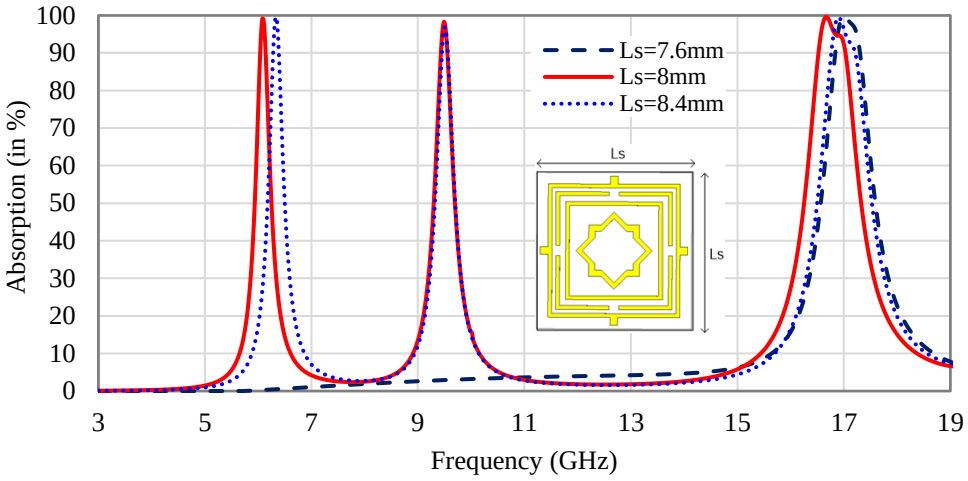

Fig. 3.10: Effect of the dimension of the substrate (Ls).

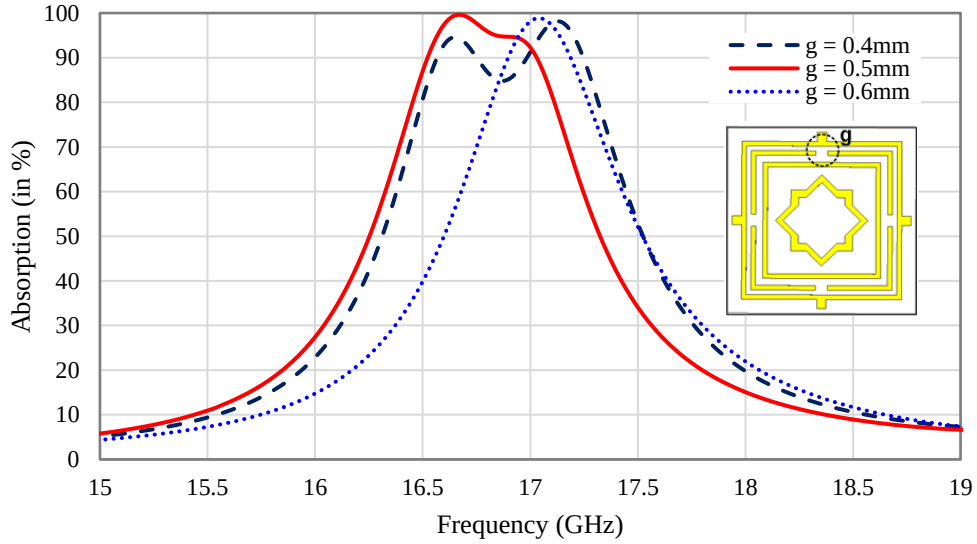

Fig. 3.11: Effect of gap (g) of the split ring.

analysis shown in Fig. 3.12 indicates current is predominantly present on the left and right sides of the ring. The analysis for designated frequencies 6.08 GHz, 9.49 GHz, and 16.62 GHz is taken on the behaviour of vector current distribution and electric field distribution.

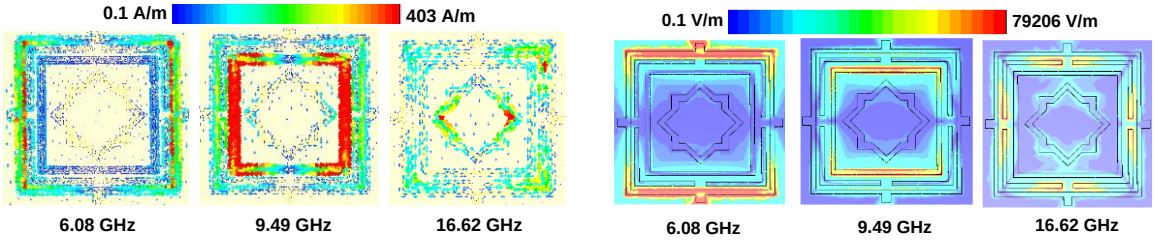

(a) (b)

Fig. 3.12: (a) Vector surface current distributions, and (b) Electric field distribution.

3.2.2.5 Experimental Characterization

The final analysis demands practical fabrication of the proposed absorber so that practical verification of results can be performed by comparison with the simulated one. The VNA E5063A, 100 kHz -18 GHz (Full two-port Keysight Network Analyser) with two wideband horn antenna and proposed absorber is taken for experimentation as shown in Fig. 3.13. The horn antennas and proposed absorber are maintained at a distance of 60 cm. Port-1 and Port-2 are connected to the transmitting and receiving horn antenna, respectively. The final analysis is drawn from measured results achieved from a practical setup and is compared with the simulated one in Fig. 3.14. The measured and simulated results are in close conformity, thereby justifying the claim for practical utility in the microwave regime. The results attained from measurement are 91.14%, 92.29% at 6.08 GHz and 9.49 GHz, respectively, and above 91% absorption from 16.94 GHz to 17.04 GHz. There is a mismatch between simulated and measured data is appearing which is mainly due to fabrication tolerances and measurement inaccuracy.

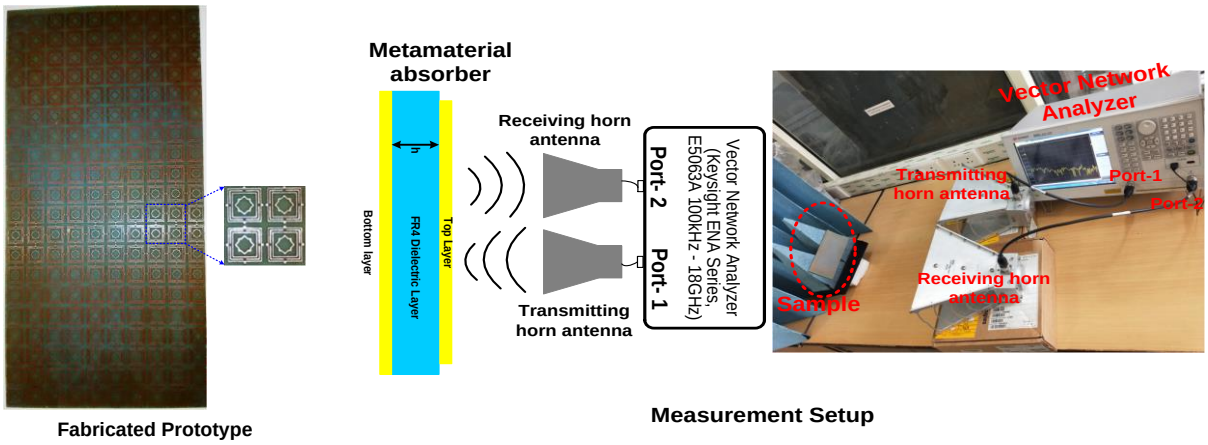

Fig. 3.13: Absorber measurement setup.

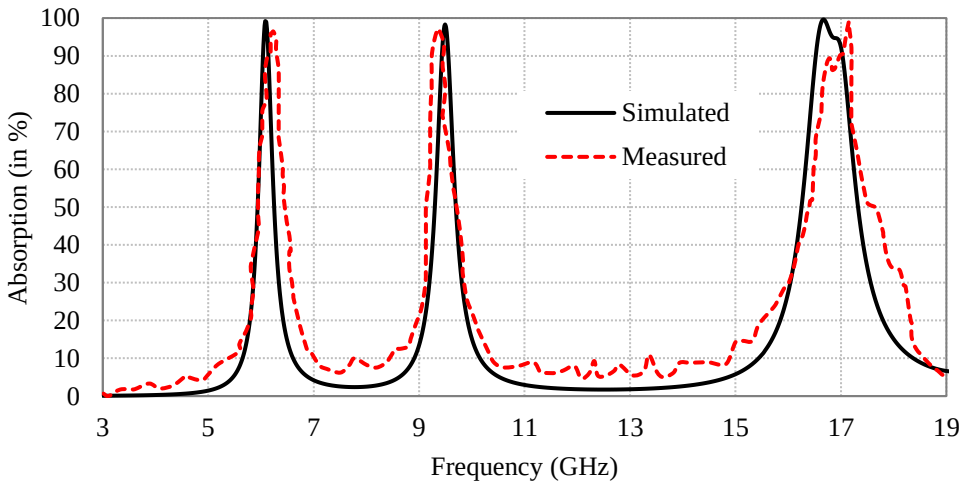

Fig. 3.14: Comparison of simulated and measured absorption of the proposed absorber.

Further, the nature of polarization is verified for the proposed absorber, and the angle (ϕ) is varied for the values of absorption attained. Fig. 3.15 provides the level of absorption attained for variation in the values of polarization angle (ϕ). From the analysis of the graph, the inference is drawn that more than 95% absorption level is retained on the variation of angle (ϕ) up to 45^0, thereby concluding the structure is polarization insensitive in behaviour up to 45°.

Moreover, the verification of the angle of incidence is done by the variation of angle (θ). The proposed absorber has a wide angle of operation, as is verified in Fig. 3.16 and 3.17(a) and (b). The analysis of graphs provides a clear indication that the proposed structure is stable to a wide angle up to 60^0. The polarisation insensitivity and wide angular stability is the requirement for all practical applications. The unwanted peaks are due to reflection and interference theory [190] and parasitic resonances [191] exhibiting their role at higher resonant frequencies.

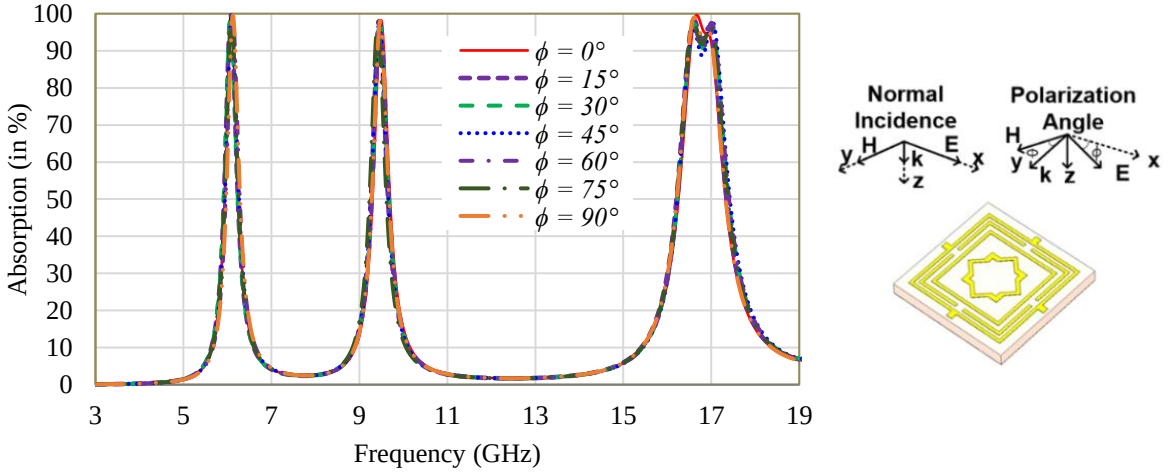

Fig. 3.15: Variation of absorption with polarization angle (ϕ)

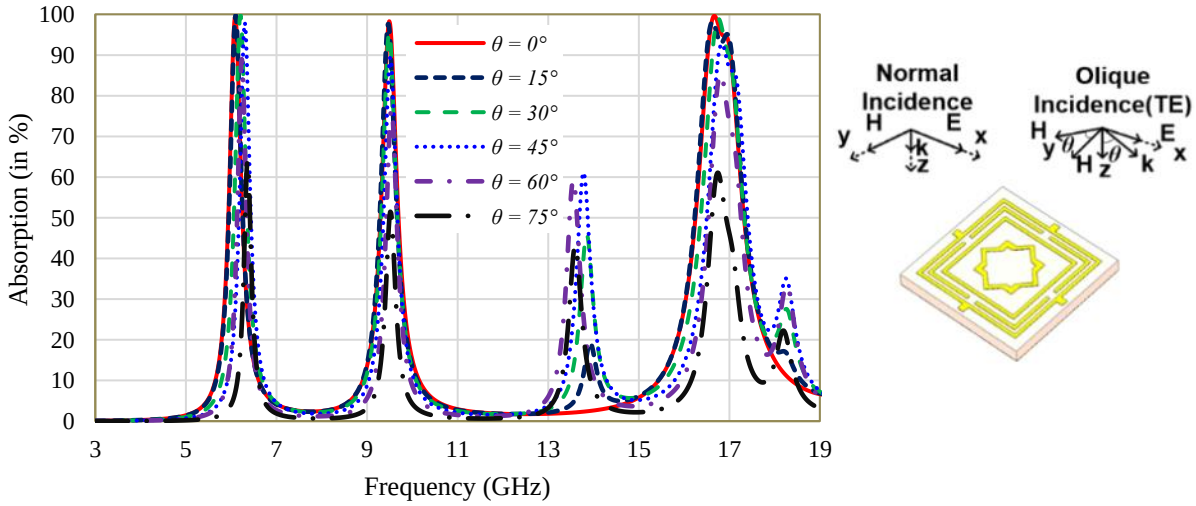

Fig. 3.16: Variation of absorption with oblique incidence (θ) for TE mode.

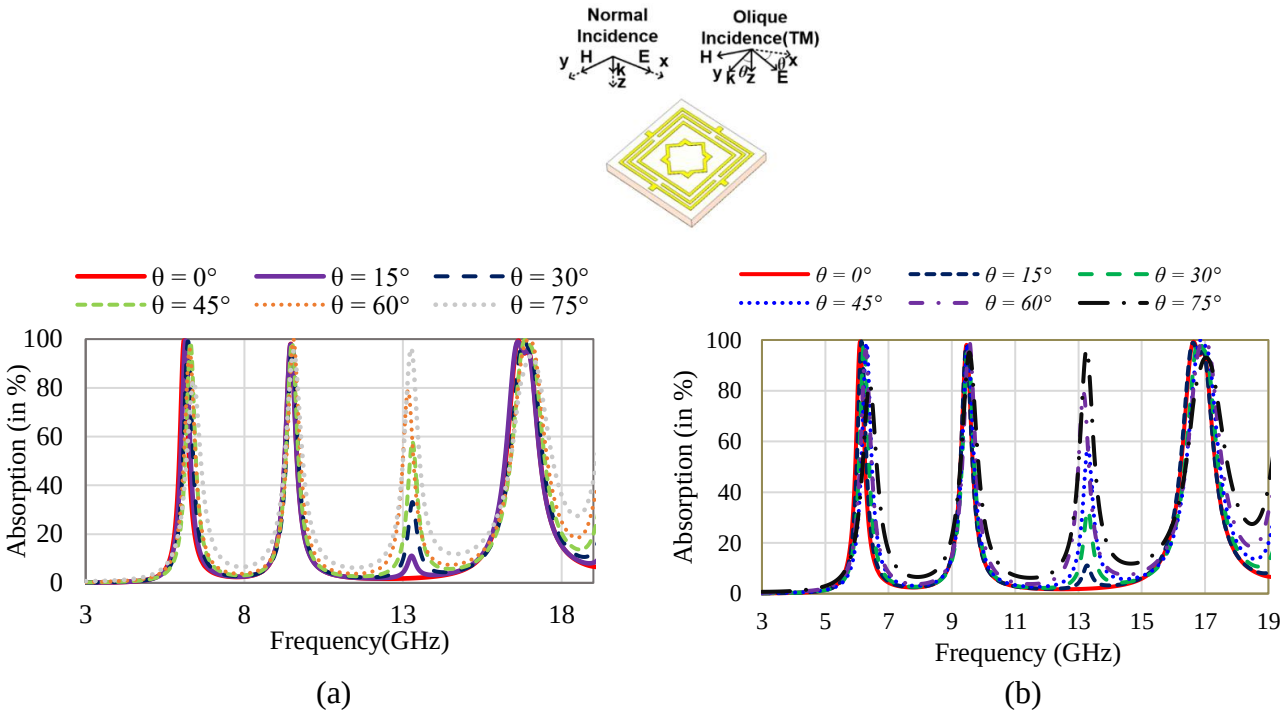

Fig. 3.17: (a) Simulated absorption, with oblique incidence (θ) for TM mode and (b) Measured absorption, with oblique incidence (θ) for TM mode

Thus, the angle of incidence is not the limiting force in the practical implementation of the proposed absorber, which further strengthens the relevance of the design.

3.3 Compact Ultrathin Triple-Band Metamaterial Absorber

This work is an attempt to explore possibility of ultra-thin dimension with attainment of highest form of absorption. The C-, X-, Ku- bands with absorption peaks results in triple band achievement with attainment of prefect absorption. The geometric dimension of structure is $7.2 \times 7.2 \times 0.8$ mm^3.The unit cell comprising patches provides 99.96%, 99.98% and 99.62% absorptivity at the 4.75GHz (C-band), 9.47GHz (X-band), and 14.40 GHz (Ku-band) respectively. The design of structure is compact and ultra-thin while the structure is polarization insensitive in behaviour till 45° and has an advantage of wide angular stability. The unit cell thickness is $0.012\lambda_{lowest}$ (where λ_{lowest} is at a lowest cut-off frequency).

3.3.1 Configuration of Compact triple-Band Absorber

The composition of proposed absorber three layers with the unit cell designed with metallic layers, encompassing a dielectric in layer formation. The side view and absorber configuration are shown in Fig. 3.18. The copper clad patch and ground conductor having a thickness of 0.017 mm. The top resonating structure is etched over a low-cost FR4 substrate and with thickness of 0.8 mm ($0.012\lambda_{lowest}$, where λ_{lowest} is at the lowest cut-off frequency).

The structure comprises symmetrical patch within the innermost ring and there is total of three ring resonators in the structure. The back structure is the complete metallic plate to make the transmission coefficient zero (S_{21} = 0) as shown in Fig. 3.18. The dimension of the unit cell is listed in Table 3.2.

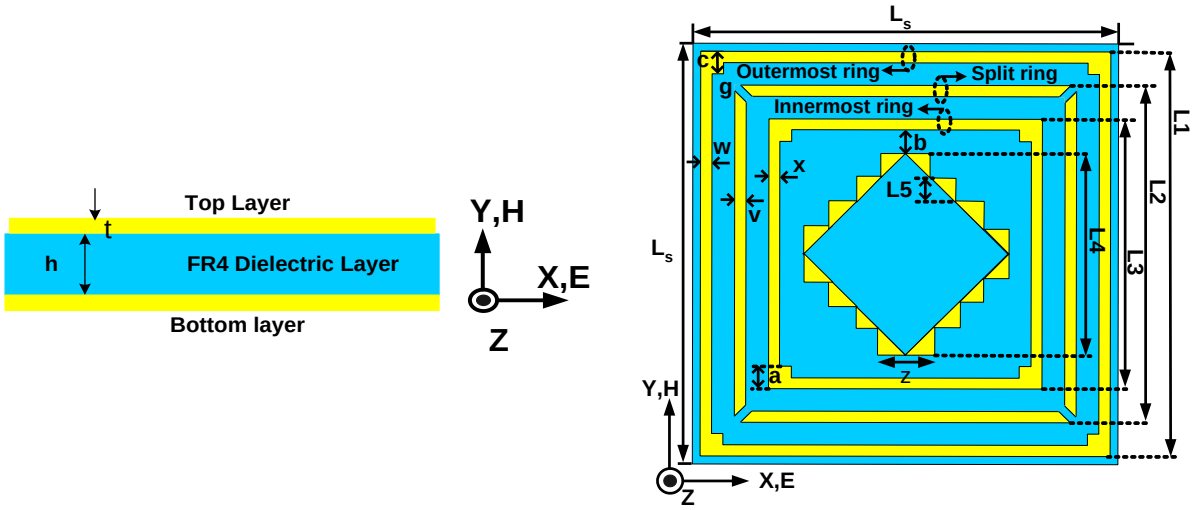

Fig. 3.18: Layers with the configuration of the proposed absorber.

Table 3.2: Shape parameters of the compact triple-band metamaterial absorber.

S. No.	Parameter	Dimension (in mm)
1.	Ls	7.2
2.	L1	7
3.	L2	6
4.	L3	5
5.	L4	4
6.	L5	0.5
7.	X	0.2
8.	v	0.2
9.	w	0.2
10.	g	0.2
11.	z	1
12.	a	0.5
13.	b	0.3
14.	c	0.3
15.	h	0.8
16.	t	0.017

3.3.2 Results and Discussion

3.3.2.1 Design and Evolution of the Compact Triple-Band Absorber

The proposed structure is simulated using methodology of finite integration technique-based Computer Simulation Technology Microwave Studio (CST MWS). The simulation setup is shown in Fig. 3.19. The methodology of floquet port excitation and Floquet port boundary

condition is used to understand the proposed metamaterial absorber. The *x*- and *y*-direction are used for TE (0, 0) and TM (0, 0) modes respectively for electric and magnetic fields. The simulated absorption of the proposed design for TE and TM mode is shown in Fig. 3.20. The absorption is achieved through expression given above by Eq. (3.1 to 3.3). For a condition with $\theta = 0°$ that is the case of the normal angle of incidence, the Eq. 3.1 reduces to Eq. 3.6;

$$A = 1 - R = 1 - \left|\frac{Z - Z_o}{Z + Z_o}\right|^2 = 1 - \left|\frac{\sqrt{\mu_r - \varepsilon_r}}{\sqrt{\mu_r + \varepsilon_r}}\right|^2 \tag{3.6}$$

where, $Z = \sqrt{\frac{\mu}{\varepsilon}}$ being impedance of structure and $Z_o = \sqrt{\frac{\mu_o}{\varepsilon_o}}$ Is the impedance of free space. The impedance matching is achieved by $Z = Z_0$ or $\mu_r = \varepsilon_r$, and it is referred to as the perfect condition for maximum absorption. The absorption achieved is nearly perfect, as shown in Fig. 3.20.

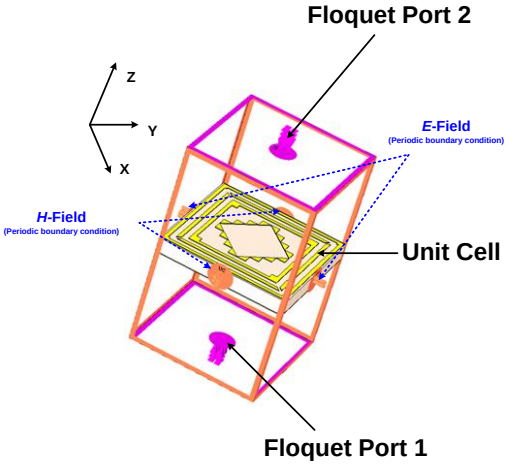

Fig. 3.19: Simulation setup for compact triple-band absorber.

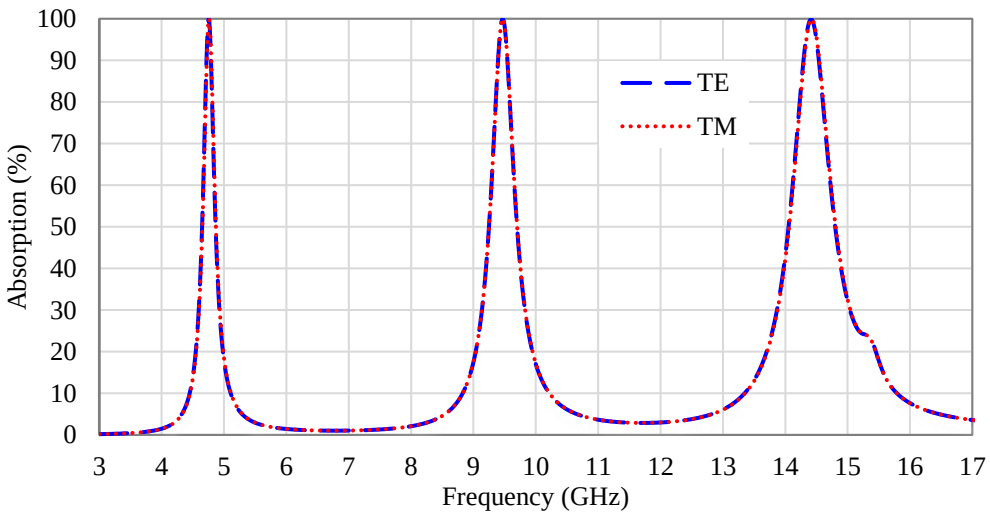

Fig. 3.20: Variation of absorptivity for TE and TM mode of compact triple-band absorber.

Further, the Stage 1 to Stage 4 evolution of structure is shown in Fig. 3.21. The Absorber A where outer CRR was designed and simulated the outer CRR is providing absorption of 99.5% at 4.694 GHz and is regarded as Stage 1. The Absorber B where outermost and one more CRR was simulated for results is taken as Stage 2. The results achieved were 98.9% and 99.8% at 4.694 GHz and 14.572 GHz, respectively. Further Stage 3 is Absorber C providing 98.9% absorptivity at 4.76 GHz and 9.6 GHz. The Proposed Absorber is final stage regarded as Stage 4 where CRRs with inner patch is simulated for results and absorptivity is 99.96%, 99.98% and 99.62% at 4.755 GHz, 9.468 GHz and 14.396 GHz, respectively. The inner patch with combination of CRR provide near total absorptivity at various bands of microwave regime thereby justify it as near total tri-band absorber. The simulated absorption characteristics of various stages are shown in Fig. 3.22.

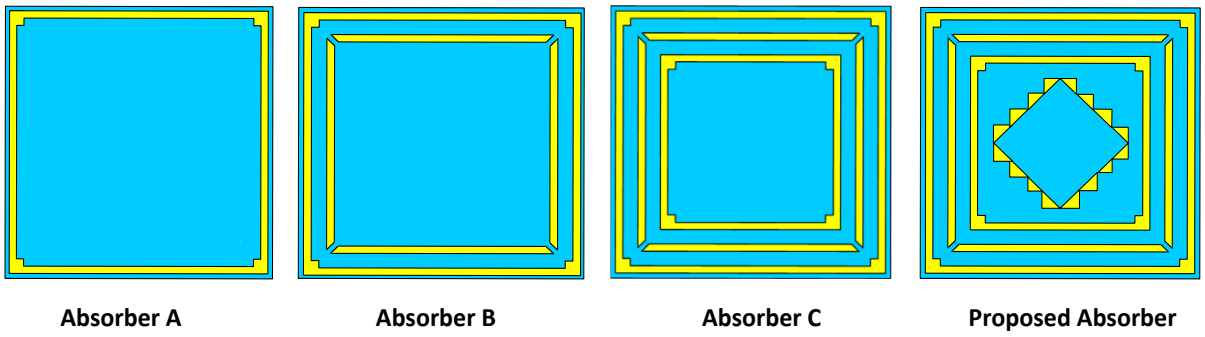

Fig. 3.21: Design evolution of the compact triple-band absorber.

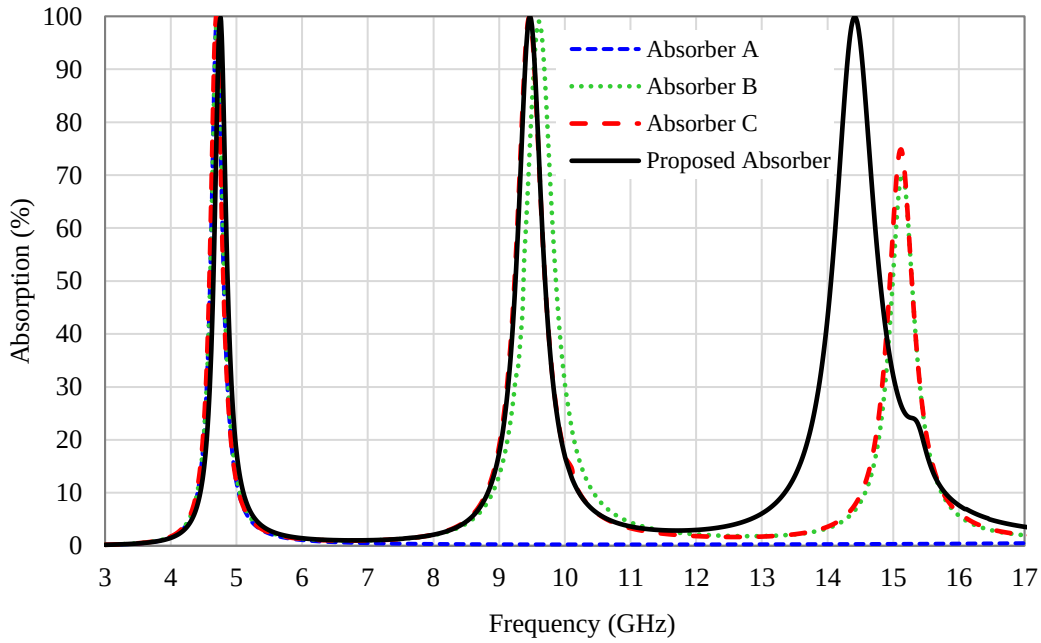

Fig. 3.22: Simulated absorption for various configuration.

3.3.2.2 Constitute Parameters

The negative permittivity and permeability of the proposed structure with normalized impedance are shown in Fig. 3.23, 3.24, and 3.25, respectively. The permittivity of the proposed structure is shown in Fig. 3.23 which is extracted using CST MWS. From the graph, it is clear that permittivity is negative at specific frequencies that are 4.76 GHz, 9.47 GHz, and 14.40 GHz. Fig. 3.24 gives an indication of negative permeability at 4.76 GHz, 9.47 GHz, and 14.40 GHz. Moreover, Fig. 3.28 is the calculation of normalized impedance against frequency for the designed triple-band absorber. From the figure, it is calculated that normalized impedance at 4.755 GHz, 9.468 GHz, and 14.396 GHz is 0.96 + j0.001, 0.98 + j0.01, and 1.08 - j0.09, respectively. It is observed that real and imaginary values of normalized impedance show the values of one and zero, respectively at the desired frequency.

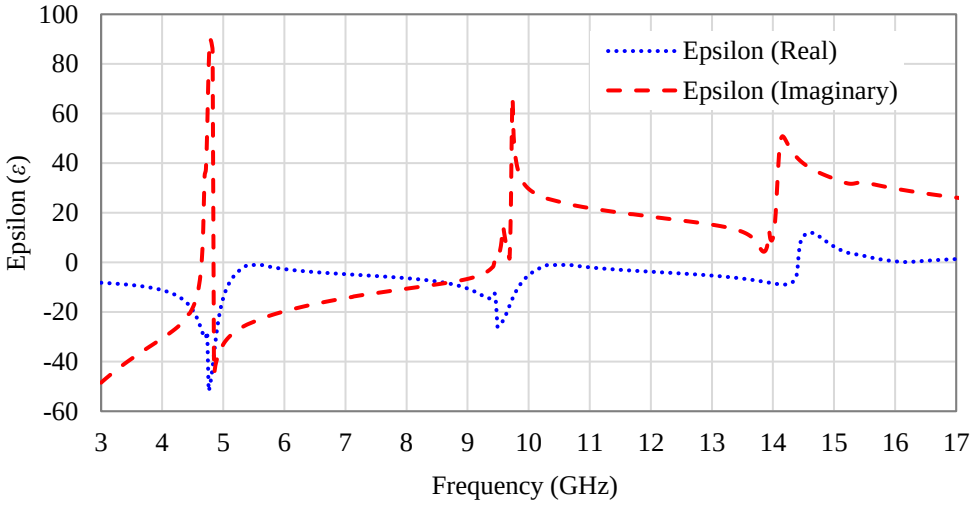

Fig. 3.23: Variation of permittivity with frequency.

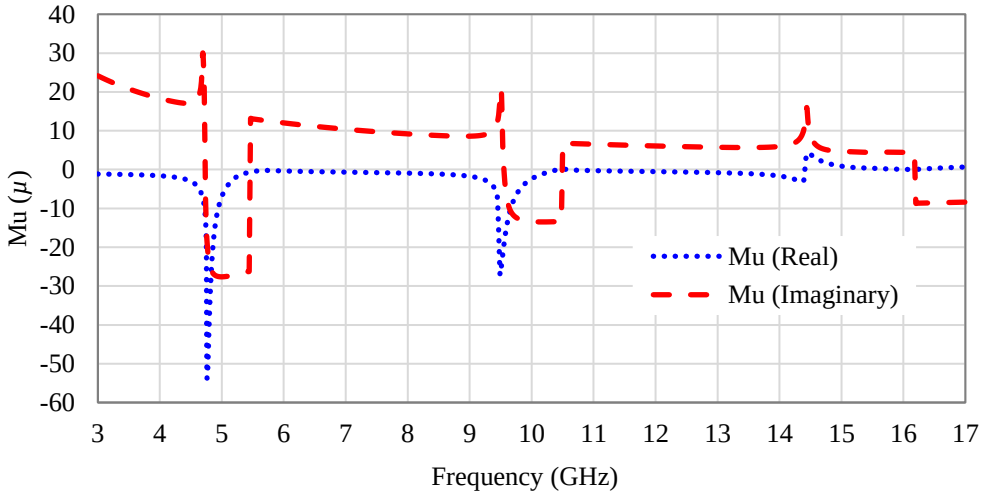

Fig. 3.24: Variation of permeability with frequency.

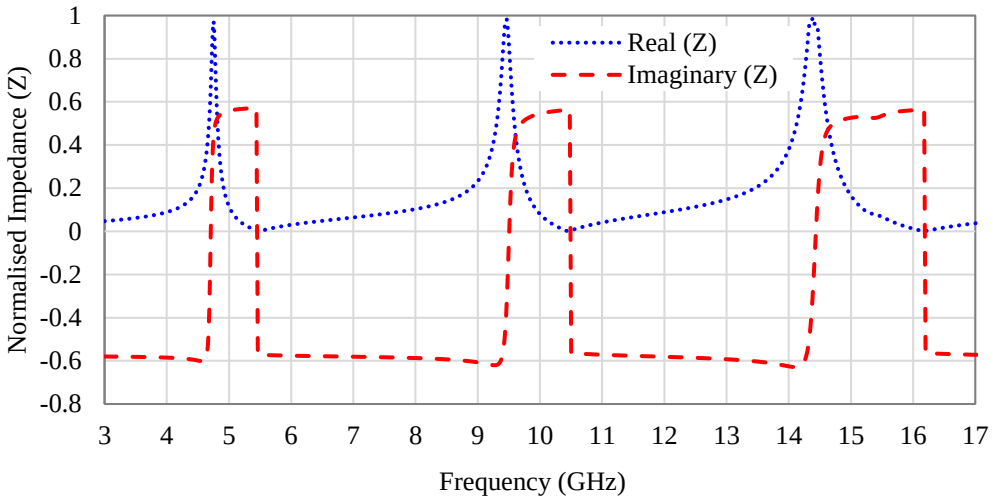

Fig. 3.25: The normalized impedance of the proposed absorber

The attainment of unity value of normalized impedance is a clear indication of perfect absorption on account of impedance matching of structure with free space impedance, thereby achieving near total absorptivity. The designed absorber possesses low reflectance and perfect impedance resulting in perfect absorption in the triple band microwave regime.

3.3.2.3 Parametric Analysis

The normal incidence criteria are taken for variation of dimensional parameters. The ‘w,’ ‘v,’ and ‘x,’ represent width of the outermost ring, split ring, and innermost ring respectively and that are varied to achieve optimum results. The analysis of dimension parameters is understood taking one parameter and keeping other parameters as constant. The parameter ‘w’ is varied in accordance with dimensional aspects, and it was seen that the optimized value is attained at w = 0.2 mm. The dimensions of ‘w’ are taken as 0.05 mm the absorption value achieved is 97.34% at 4.76 GHz, likewise attainment of 99.55% absorption at 9.424 GHz and 99.27% absorption at 14.374 GHz. When the dimension of w = 0.3, absorption of 98.97% is achieved 4.848 GHz while 99.10% is attained at 9.534 GHz and 99% absorption at 14.396 GHz, while the best values are attained at w = 0.2 mm, where the results achieved, are 99.96%, 99.98% and 99.62% at 4.755 GHz, 9.468 GHz and 14.396 GHz respectively. Clearly, it can be seen at when the value of ‘w’ is decreased from w = 0.2mm to lower dimensions, absorptivity of the first peak starts receding and when the dimension of ‘w’ is increased to higher dimension absorption attained is again reducing. Therefore, the best possible dimension by virtue of testing points at a lower and higher scale of the dimension of ‘w’ is w = 0.2 mm, as shown in Fig. 3.26.

The same hypothesis is taken for selecting the dimension of parameter 'v' by keeping another parameter in a constant state, and optimized parameter v = 0.2 mm is achieved. The value of v = 0.1 mm, the absorption attained is 97.25%, 99.25%, 98.59% at 4.76 GHz, 9.468 GHz and 14.396 GHz while when the dimension of v =0.3 mm, absorption achieved is 60.41%, 42.74%, and 99.98% at 4.76 GHz, 9.468 GHz, and 14.396 GHz, respectively. The optimized value is achieved at v = 0.2 mm with 99.96%, 99.98% and 99.62% at 4.755 GHz, 9.468 GHz, and 14.396 GHz, respectively. Clearly, it can be seen as dimensions of 'v' is reduced, absorption of 1st and 3rd peak is reduced while for v = 0.3 mm, absorption of 1st and 2nd peak is reduced as shown in Fig. 2.27. Thus, by above analysis it can be concluded that for attaining maximum absorption, the optimized dimension for v = 0.2 mm as other values of 'v' provide reduced absorption, and practical applications demand absorption of highest possible level.

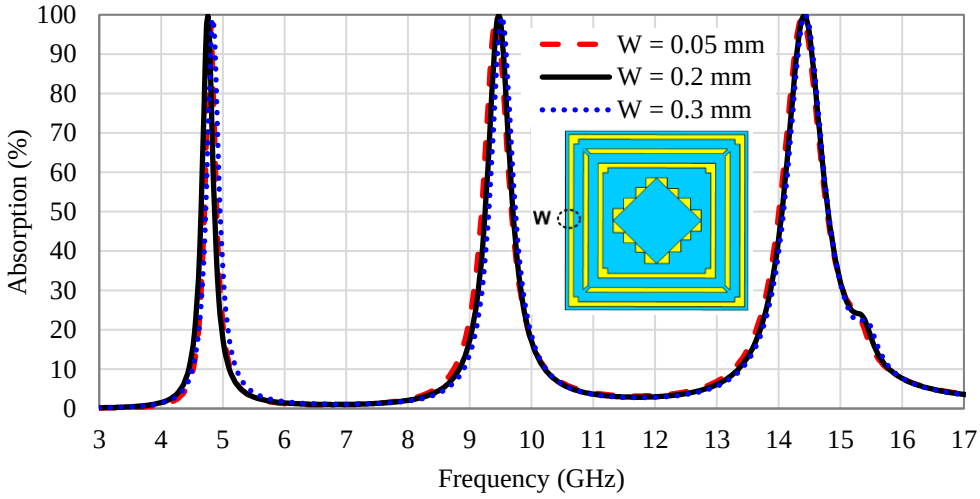

Fig. 3.26: The effect of width (w) of the outermost ring.

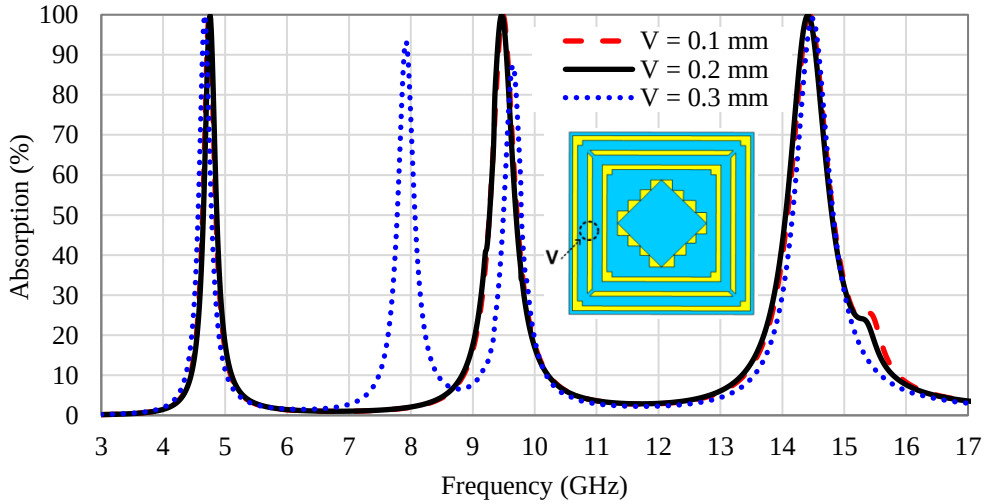

Fig. 3.27: Effect of width (v) of the split ring.

A similar approach is followed for deciding the dimensional aspect of parameter ‘X’, and it is seen that X = 0.2 mm provides optimum results in relative comparison to higher and lower values of ‘X’ in terms of dimensions. At X = 0.1 mm, absorption achieved is 94.74% and 95.81% at 9.424 GHz and 14.418 GHz while for x = 0.3 mm, absorption achieved is 97.69%, 97%, and 99.24% at 7.716 GHz, 9.644GHz and 14.374 GHz, respectively. From the relative comparison, it can be deduced that x = 0.2 mm provides optimum results in terms of absorption attained and therefore selected for further analysis purpose, as shown in Fig. 3.28. Thus, from the parameterization of structure, clearly it can be deduced that for w = 0.2 mm, v = 0.2 mm, and X = 0.2 mm, the unit cell comprising patches achieve almost perfect absorption (close to 100%) at C-, X-, and Ku-bands, thereby justifying the term perfect metamaterial absorber. The requirement of an absorber in any practical application is to provide the maximum possible level of absorption at the desired frequency of operation, and by virtue of parameterization, the final design achieved is successful in providing 99.96%, 99.98%, and 99.62% absorptivity at the 4.75 GHz (C-band), 9.47 GHz (X-band), and 14.40 GHz (Ku-band), respectively. The attainment of perfect absorption at different bands clearly justifies the triple-band utility in applications that demand the incorporation of the absorber in its operation.

3.3.2.4 Surface Current and Electric Field Distribution

In-depth analysis can be visualized for absorptivity by current distribution at various resonant peaks that are 4.75 GHz, 9.47 GHz, and 14.40 GHz, represented in Fig. 3.29 (a-b). The current distribution clearly symbolizes that at 14.40 GHz, greater accumulation occurs at the

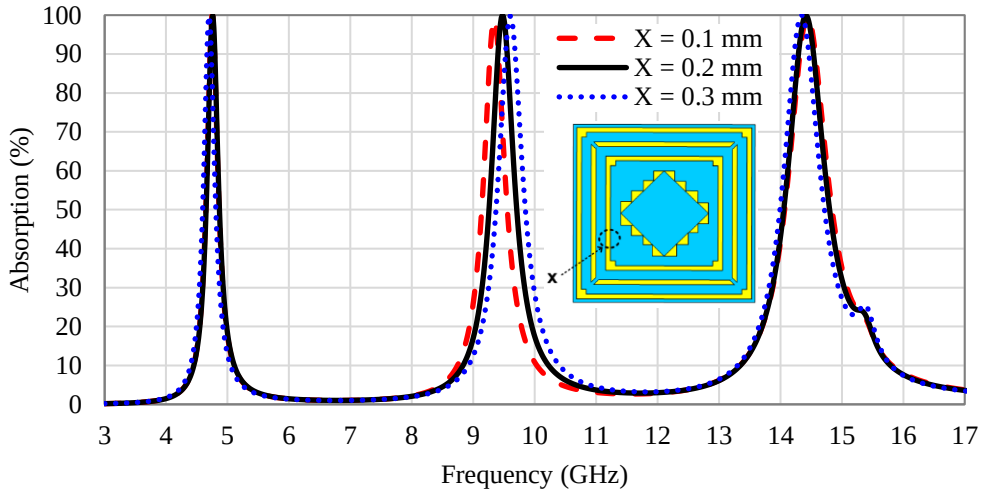

Fig. 3.28: Effect of width (X) of innermost ring.

innermost patch. Whereas at 9.47 GHz, mutual coupling occurs between the innermost and next CRR and the innermost patch with the innermost CRR. The current distribution indicates accumulation at outer CRR for 4.75 GHz as shown in Fig. 3.29 (a). Therefore, the conclusion arrives that the Inner patch and innermost CRR are responsible for absorption peaks at 14.40 GHz and 9.47 GHz while outermost CRR and mutual coupling of inner CRR is responsible for absorption peak at 4.75 GHz. Thus, the proposed structure comprising CRR and the inner patch is responsible for achieving near total absorptivity at designated frequencies, thus justifying its claim for a triple-band metamaterial absorber. Similarly, electric field distribution analysis in Fig. 3.29 (b) signifies charge accumulation on top and bottom for 4.75 GHz along the outermost ring, while the three rings show charge accumulation along top and bottom while for 14.40 GHz, maximum charge accumulation is witnessed along the inner square patch. The current and field distribution provides insight into absorption levels attained at designated frequencies. Clearly, the design of the absorber is as such that its absorption is visible in surface current and electric field distribution.

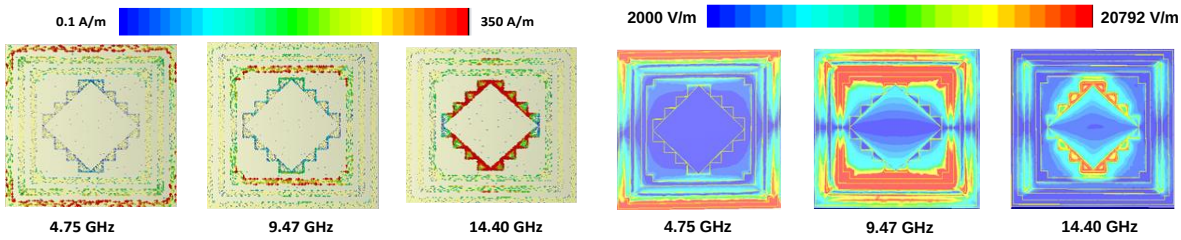

(a) (b)

Fig. 3.29: (a) Vector surface current distributions and (b) Electric Field Distribution.

3.3.2.5 Experimental Characterization

The last step is fabrication part of optimized design for measurement. The space wave measurement setup with fabricated prototype and the is shown in Fig. 3.30. The composition of experimental setup is wideband horn antennas two in number, VNA E5063A with a range of 100KHz-18GHz (full two-port Keysight Network Analyser), and a fabricated prototype for experimentation. The transmitting horn antenna (operating over a range of 2 GHz to 20 GHz) is connected to Port-1 of the VNA, and receiving horn antenna (operating over a range of 2 GHz to 20 GHz) is connected to Port-2 of the VNA. A 60 cm distance is maintained between the fabricated structure and horn antennas. The behaviour of the proposed absorber is understood by analysing simulated and experimental values as exhibited in Fig. 3.31. The results are found in agreement for simulated and experimental values, the slight variation is attributed to the substrate non-conformity and free space measurement.

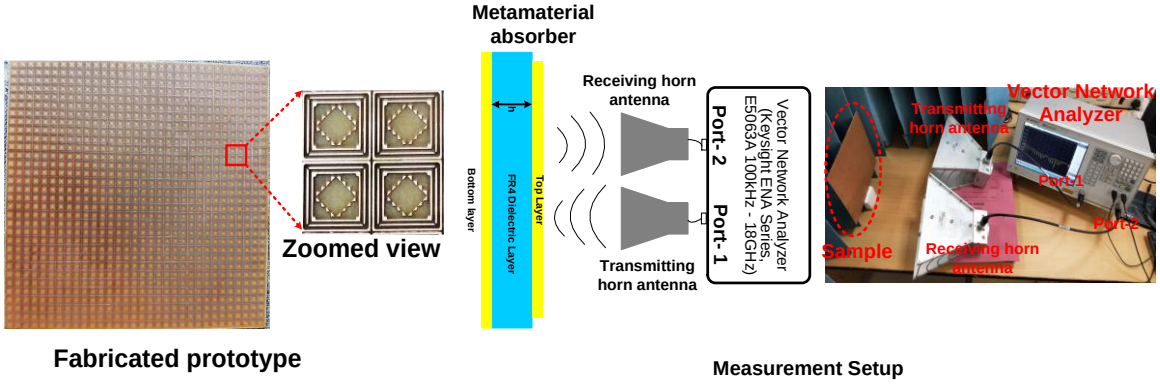

Fig. 3.30: Fabricated prototype and experimental setup.

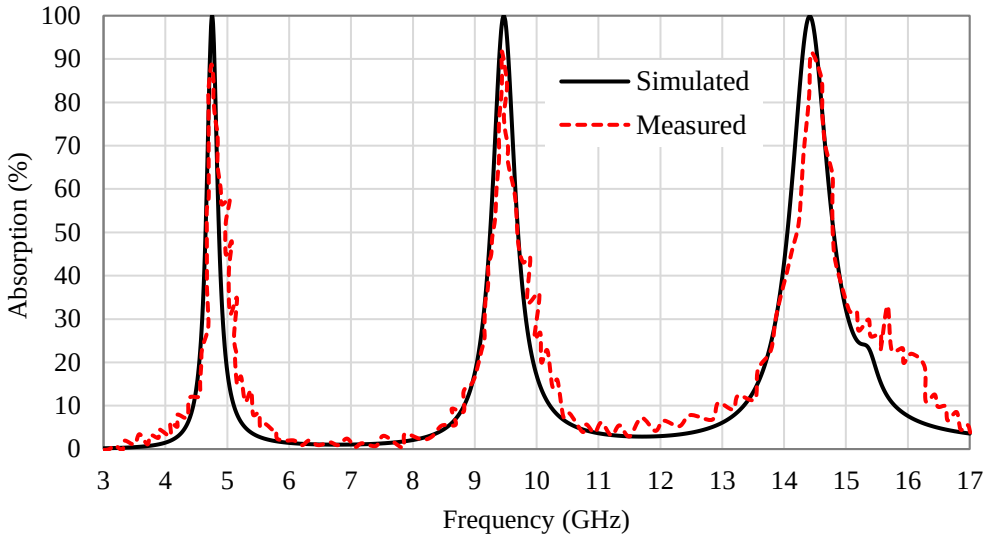

Fig. 3.31: Comparison of simulated and measured absorption of the proposed absorber.

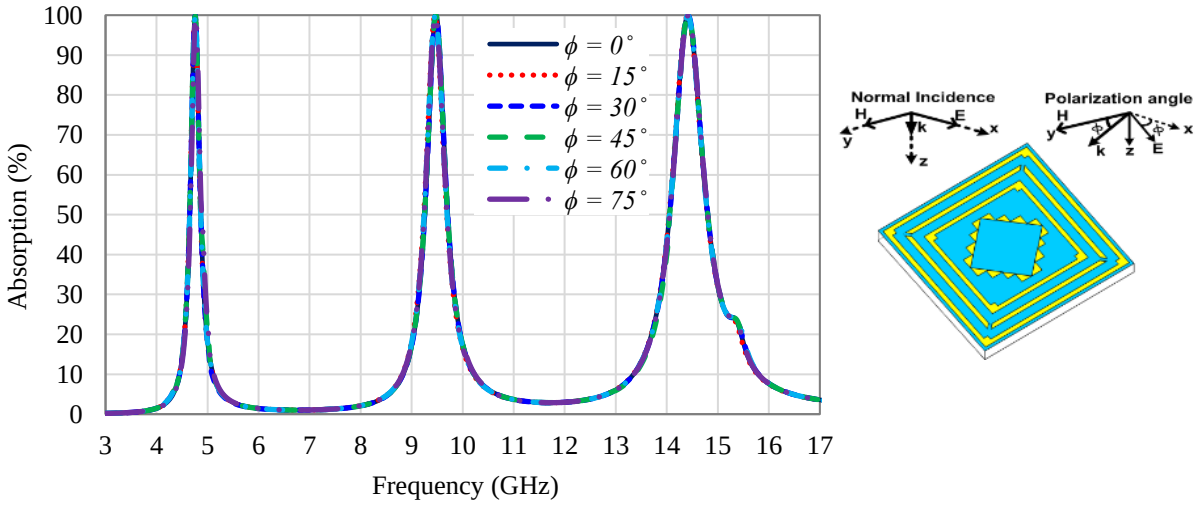

Fig. 3.32: Variation of absorption with polarization angle (ϕ).

Further, the variation from 0^0 to 75^0 is taken for polarization angle (ϕ) to visualise polarization sensitivity. The Fig. 3.32 provides information on results of the polarization angle with absorptivity. From the analysis, it is clearly seen that the structure exhibit polarization insensitivity and, therefore, is useful for incorporation in microwave-based engineering applications.

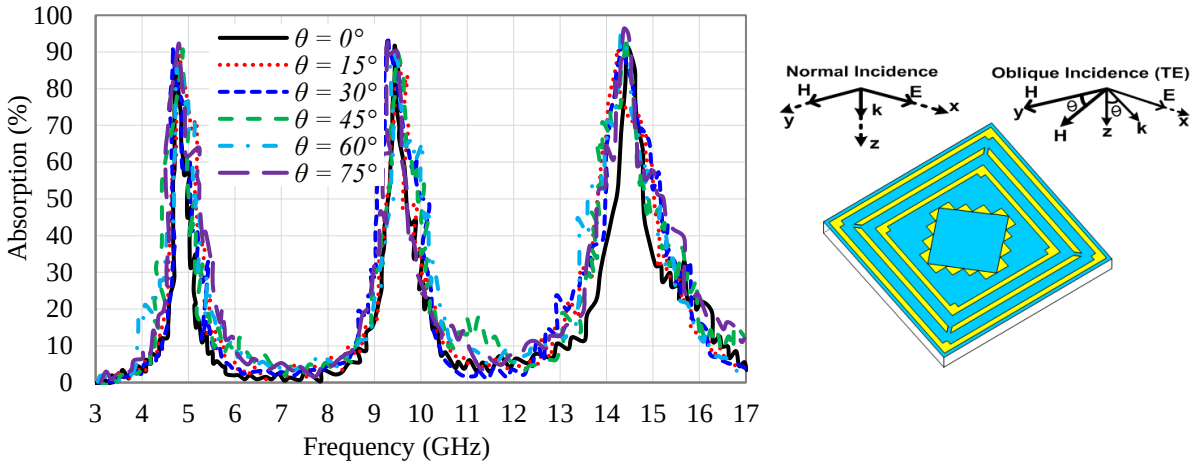

Fig. 3.33: Variation of measured absorption with oblique incidence (θ) for TE mode

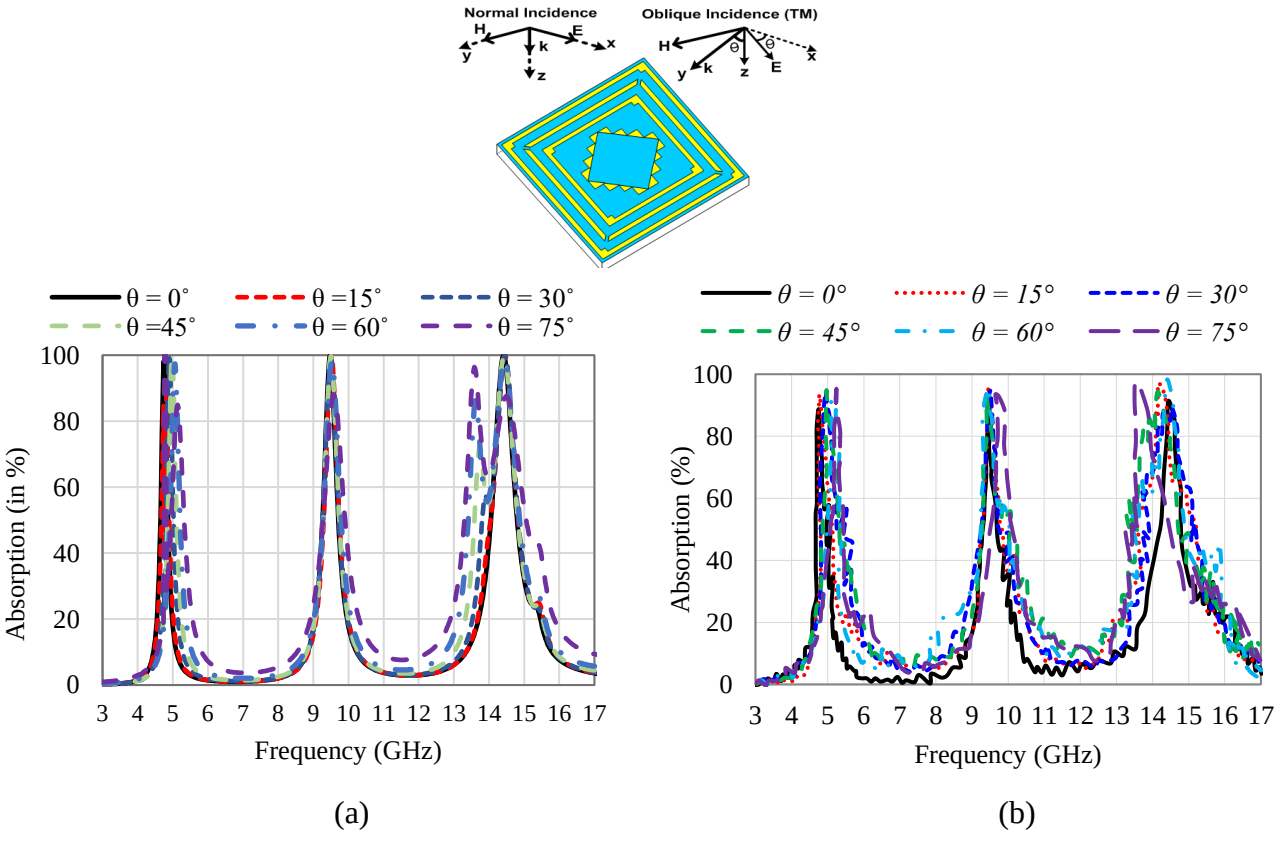

Fig. 3.34: (a) Simulated absorption, with oblique incidence (θ) for TM mode and (b) Measured absorption, with oblique incidence (θ) for TM mode

Moreover, the variation of absorptivity at various incidence angles (θ) under TE mode and TM mode are plotted in Fig. 3.33 and Fig. 3.34(a) and(b). The experimentally verified values clearly indicate that the structure exhibit stable for a wide incident angle up to 45^0 for both TE and TM mode. The practical applications demand wide angle stability to oblique incidence angles, and the unit cell size leads to practical angularly stable designs. In Fig. 3.33 and Fig. 3.34(a) and(b), additional peaks appear at higher resonance frequency which is due to reflection and interference theory [190] and deviation in absorption curves is linked to parasitic resonances [191] and fabrication tolerances.

3.4 Conclusion

The experimentally verified metamaterial absorber is discussed for practical implementation in applications pertaining to the triple-band microwave regime. The design of first structure is verified through surface current and electric field distribution over designated frequencies. The attainment of 99.14% and 98.29% absorption at 6.08 GHz and 9.49 GHz, respectively and a band of 265 MHz from 16.57 GHz to 16.83 GHz having a continuous absorption level of above 95% is achieved. The first multi-band structure is practically fabricated as a finite absorber having 20 × 10 unit cells. The structure is verified for polarisation insensitivity and angle of incidence operation. The comparisons of measured and simulated results conform to and testify to the practical utility of the proposed absorber in applications pertaining to the C-, X-, and Ku-band of microwave frequency regimes.

In the next design, a compact triple-band with perfect absorption is designed and verified through experimentation. The different resonant frequencies, 4.75 GHz, 9.47 GHz, and 14.40 GHz providing absorption of 99.96 %, 99.98 %, and 99.86 %, respectively is signified through surface current distribution. The 32 × 32-unit cells are used for finite proposed absorber which is practically fabricated and tested. There is conformity in practical and simulated results. Finally, insensitive behaviour for polarization parameter till 45° and wide angle of stability is analysed at the microwave regime, and overall conclusion is that proposed structure finds capability in incorporation for engineering designs. The transition of technology from 4G to 5G requires absorbers as isolators in multi-antenna systems. In this context, both the multiband absorbers having miniaturized dimensions and compact design will be a viable solution for solving the isolation problem in the MIMO setup and radar cross section issues in stealth application.

CHAPTER 4 DESIGN, OPTIMIZATION AND DEVELOPMENT OF WIDEBAND ABSORBER

4.1 Introduction

The research domain in metamaterial-based absorbers is witnessing rapid advancement from single-band absorbers to multi-band absorbers [34-42]. The research aims to develop a wideband [43-47] absorber with a prime focus on attaining the highest form of absorption for the continuous band in the microwave regime. The goal of near-perfect absorption is achieved in single and multi-band absorbers but achieving the highest state of absorption in the continuous band, and that too with polarization insensitivity and wide incident angle of operation is difficult. The methodology of lumped elements and multilayer structure result in fabrication constraints, thereby restricting the practical implementation of metamaterial-based absorbers on account of complexity in design. The level of attaining polarisation insensitive (up to 45°) near-perfect absorption with a wide incident angle is a dream to be realized.

The work's prime objective is to design and develop a simple wideband absorber witnessing near-perfect absorption and to suffice absorption is polarization insensitivity and wide incident angle of operation justifying the practical prospect of the absorber in microwave applications. The work attempts to attain polarization insensitive broadband absorber till 45°. by incorporating conductive ink. The patch prepared through conductive ink comprises a square ring appended with a triangle at all sides of the square to appear as a consolidated structure. The compact design is etched with T-shaped geometry along four sides (at the triangular part) to attain the desired form of absorption. The patch adjustment with dimensional aspects is achieved through evolutionary methodology and parameterization. The proposed absorber is achieving more than 99% absorption from 11.17 GHz to 19.40 GHz with the attainment of an ultra-wideband bandwidth of 8.23 GHz.

4.2 Configuration of Wideband Absorber

The layout of the proposed structure comprises three layers with the ground as a metallic layer of copper with a thickness of 0.017 mm and having finite conductivity of 5.8×10^7 S/m, while the top layer is a consolidated shape of a square ring appended with triangles patterned with conductive silver ink. The conductive ink composition is of nano-silver and carbon filler, with surface resistance of the conductive ink of 50 Ω/sq. The top and bottom layers are separated by substrate, acting as the dielectric. The material composition of dielectric is of Rogers RT5880 having dielectric constant (ε_r) = 2.2 and loss tangent (tan δ) = 0.0009. The

bottom structure is entirely metallic in the design, thereby providing a zero value of transmission coefficient (S_{21} = 0). The side view and absorber configuration are shown in Fig. 4.1. The dimension of the unit cell used for the design of structure is listed in Table 4.1.

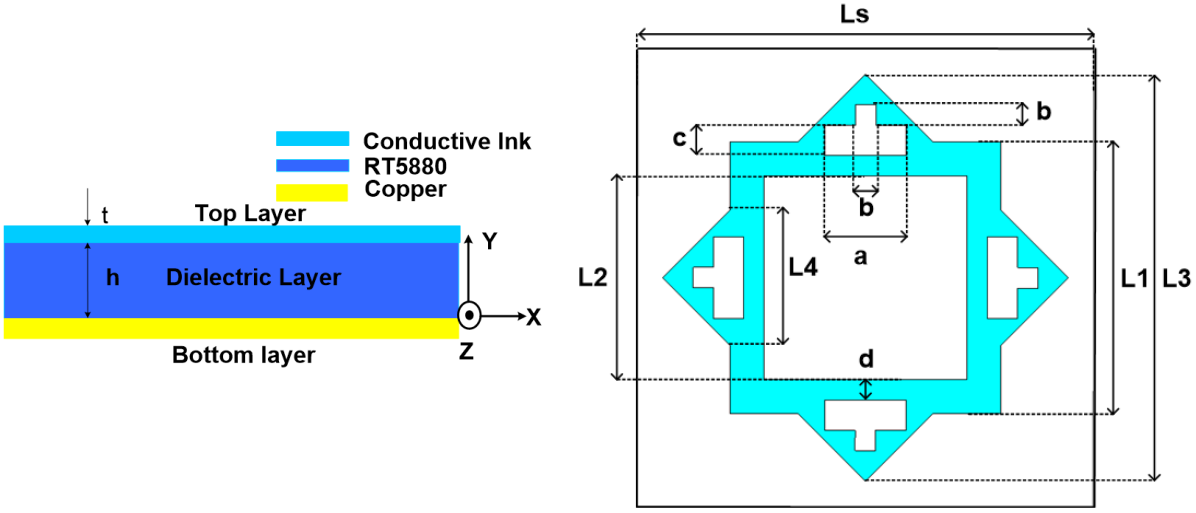

Fig. 4.1: Layers with the configuration of the absorber.

Table 4.1: Shape parameters of the wideband absorber.

S. No.	Parameters	Dimension (in mm)
1.	Ls	9.00
2.	L1	5.34
3.	L2	4.00
4.	L3	8.00
5.	L4	2.66
6.	a	1.60
7.	b	0.40
8.	c	0.60
9.	d	0.40
10.	h	3.2
11.	t	0.017

4.3 Results and Discussion

4.3.1 Design and Evolution of the Wideband Absorber

The finite integration technique (FIT) based EM solver, i.e., Computer Simulation Technology Microwave Studio (CST MWS), is used for simulation by using floquet port excitation and floquet port boundary condition. The simulation setup (floquet port excitation and floquet port boundary condition) used to analyze the proposed wideband metamaterial absorber is shown in Fig. 4.2. The TE (0, 0) and TM (0, 0) modes for electric and magnetic

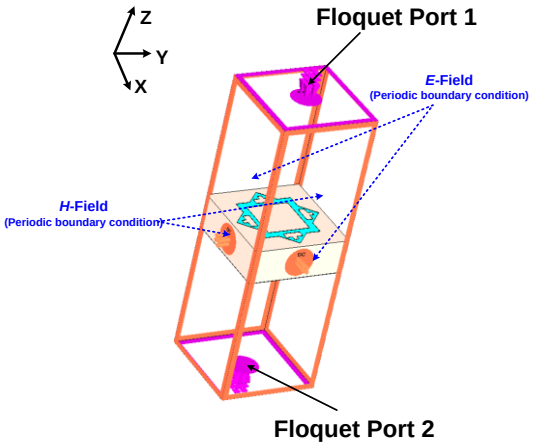

Fig. 4.2: Simulation setup for wideband absorber.

fields are polarized along *x*- and *y*- direction, respectively. The absorption level of the proposed absorber in TE and TM mode is shown in Fig. 4.3. The mathematical expression for defining absorption is as follows [5];

$$A(\omega) = 1 - R(\omega) - T(\omega) \tag{4.1}$$

$$A(\omega) = 1 - |S_{11}(\omega)|^2 - |S_{21}(\omega)|^2 \tag{4.2}$$

where, absorption, reflectance, and transmittance are represented by $A(\omega)$, $R(\omega)$, and $T(\omega)$, respectively. From Eq. (4.1), it is evident that the parameter absorption [$A(\omega)$] is linked to the parameter reflection coefficient (S_{11}) and transmission coefficient (S_{21}). In the methodology of using a complete metallic bottom layer as the ground plane, the value transmission coefficient (S_{21}) or $T(\omega)$ becomes zero and taking the value of S_{21} or $T(\omega) = 0$, the Eq. (4.1) is modified as;

$$A(\omega) = 1 - |S_{11}(\omega)|^2 \tag{4.3}$$

The matching of effective permeability $\mu(\omega)$ and effective permittivity $\varepsilon(\omega)$ results in the reduction of transmission parameter. The frequency range for which the value of $R(\omega)$ is minimized through matching of free space impedance to normalized impedance, consequently enhancing the absorption parameter. The normalized input impedance is calculated using Eq. (4.4) [5];

$$z = \pm\sqrt{\frac{(1+S_{11})^2 - S_{21}^2}{(1-S_{11})^2 - S_{21}^2}} \tag{4.4}$$

The proposed absorber is a completely metallic ground plane, thereby making the value of $|S_{21}|^2 = 0$ on substituting the $S_{21} = 0$, then Eq. (4.4) reduces to;

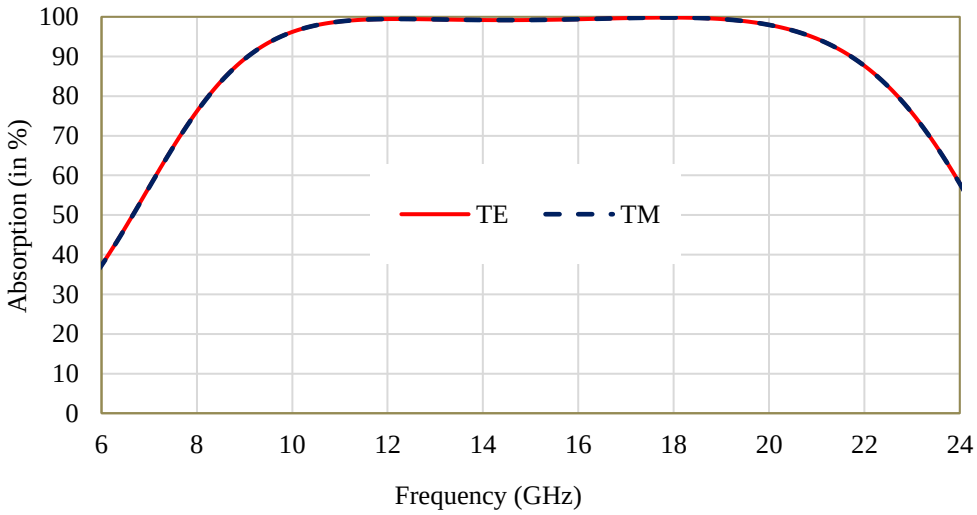

Fig. 4.3: Variation of absorptivity for TE and TM mode.

$$z = \pm\frac{1+S_{11}}{1-S_{11}} \tag{4.5}$$

Further, the wideband absorber evolved from various stages marked for Stage A and culminated at the final stage designated as Proposed Absorber for design purposes, as shown in Fig. 4.4. The response to the evolution process in the form of absorption level attained for various stages is also shown in Fig. 4.5. The evolution process starts at Stage A, where a square-shaped design is used to analyze the behaviour of the 1.55 GHz band from 10.92 GHz to 12.475 GHz with 59% absorption. Still, neither the absorption achieved nor the band is widening enough to suffice the requirement of a wideband absorber. The second stage is the square ring, where the middle portion is etched from the square, thereby relinquishing the shape of the square ring. The band achieved is 6.48 GHz from 12.27 GHz to 18.75 GHz having 99% absorption. The absorption level achieved is good, but the desire to further enhance the band led to the transition from Stage B to Stage C. In Stage C, the square ring is appended with four triangles at four sides of square ring. The two wide bands provide with more than 99% absorption of 1.95 GHz and 2.08 GHz from 9.92 GHz to 11.87 GHz and 18.27 GHz to 20.35 GHz, respectively.

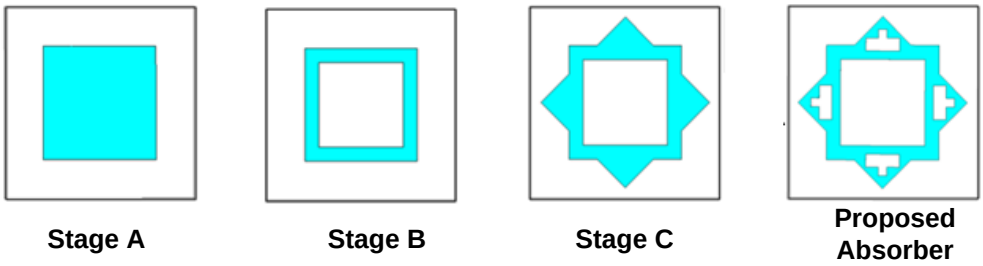

Fig. 4.4: The design evolution of the wideband absorber.

The clue from this stage is two bands, but one consolidated band is yet to be attained, which led to the transition from Stage C to Proposed Absorber. The desire for a complete wideband with more than 99% absorption was realized through the final stage designated as the Proposed Absorber, where a T-shaped slot is created from the main square-shaped ring (square ring with triangles at the sides) as shown in Fig. 4.4. The result from this step provides attainment of wideband from 11.17 GHz to 19.40 GHz of 8.23 GHz and the attainment of the near total highest form of absorption above 99%, as shown in Fig. 4.5.

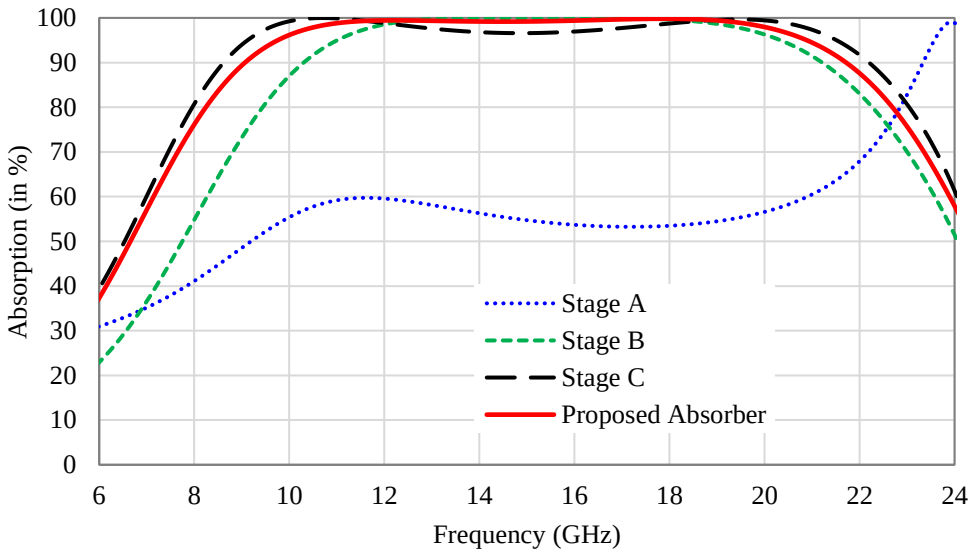

Fig. 4.5: Simulated absorption for a different configuration.

4.3.2 Constitutive Parameters

The proposed structure is characterized by metamaterial properties, as shown in Fig. 4.6 and 4.7. The material constituent properties are retrieved from *S*-parameters [reflection coefficient (S_{11}) and transmission coefficient (S_{21})] [14]. From the graphs, it is verified that the proposed absorber is attaining negative values of effective permittivity (ε_{eff}) and effective permeability (μ_{eff}), indicating the characteristics of the proposed absorber as metamaterial in behaviour. The value of normalized impedance for proposed absorber $Z = 1$ matches with free space impedance. From Fig. 4.8, the proposed absorber achieves a value of unity and zero for the real and imaginary part of the normalized impedance, absorption (more than 99%), with a broad band of 8.23 GHz from 11.17 GHz to 19.40 GHz.

The absorber's performance is linked to proper substrate selection for the design of the proposed absorber. The selection of substrate material is based on the dielectric constant (ε_r), which affects the performance of the proposed absorber. The Fig. 4.9 provides a detailed picture on the behaviour of various substrate materials on absorption characteristics. The

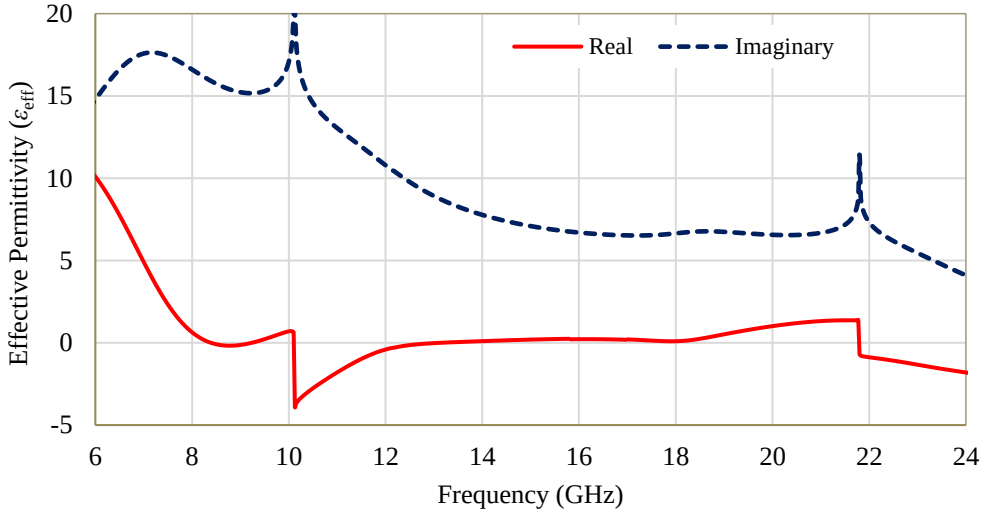

Fig. 4.6: Variation of permittivity with frequency.

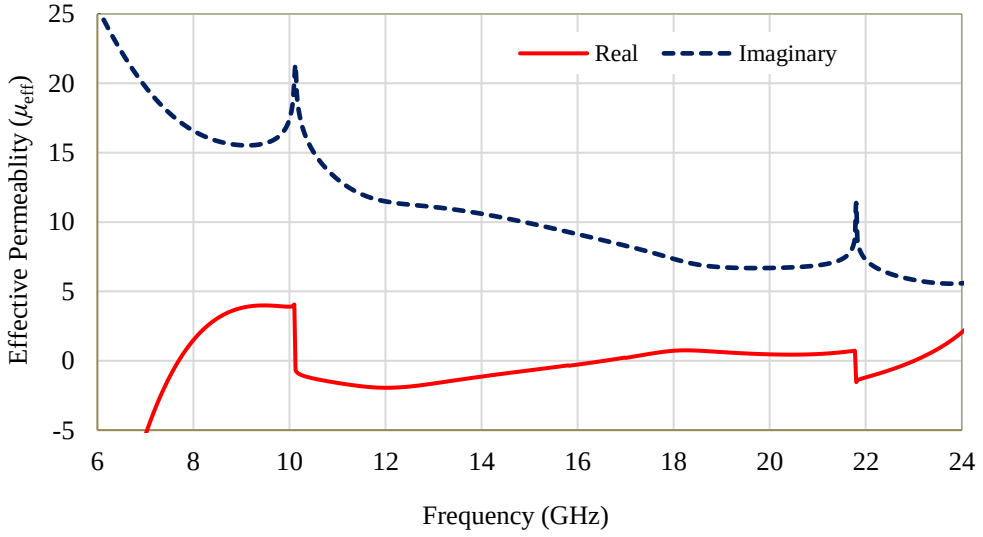

Fig. 4.7: Variation of permeability with frequency.

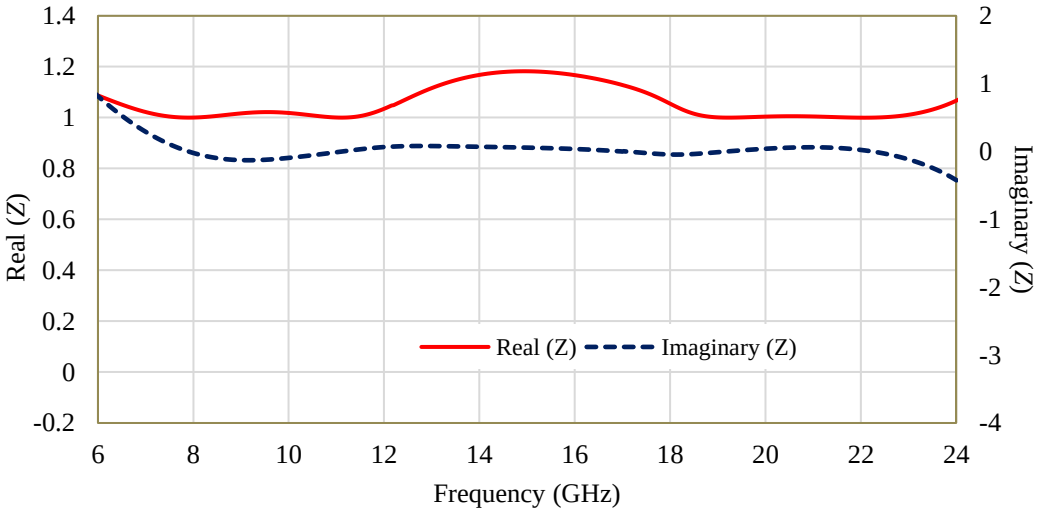

Fig. 4.8: The normalized impedance of the proposed absorber

various substrate material included for comparison are FR-4 with dielectric constant (ε_r) = 4.3, Rogers RO4350B with dielectric constant (ε_r) = 3.61, Rogers RO3003 with dielectric constant (ε_r) = 3, Rogers RT6002 with dielectric constant (ε_r) = 2.94, Rogers RT5880 with dielectric constant (ε_r) = 2.2 and Rogers RT5880LZ with dielectric constant (ε_r) = 1.96. The criteria for absorption are set to be above 99% for analysis purposes. The net outcome for comparison is that FR4 (ε_r = 4.3) provides 0.7 GHz bandwidth from 10.05 GHz to 10.75 GHz, Rogers RO4350B (ε_r =3.61) provides 2.73 GHz bandwidth from 10.27 GHz to 13 GHz. The Rogers RO3003 (ε_r =3) provides a bandwidth of 4.52 GHz from 10.55 GHz to 15.07 GHz, while a bandwidth of 4.52 GHz from 10.55 GHz to 15.07 GHz is achieved from Rogers RT 6002 (ε_r = 3). The outcome from Rogers RT6002 (ε_r = 2.94) is a wideband of 4.85 GHz from 10.44 GHz to 15.40 GHz, and the outcome from Rogers RT5880 (ε_r = 2.2) is a wideband of 8.23 GHz from 11.17 GHz to 19.40 GHz, Rogers RT5880LZ (ε_r = 1.96) is a wideband of 3 GHz from 11.47 GHz to 14.47 GHz. It is clearly noted that the Rogers RT5880 provides a wideband with a determined absorption level of 99% taken for comparison. The dielectric constant (ε_r) in the range of 2 to 3 provides a good absorption level in the wideband perspective. With the further reduction of the dielectric constant (ε_r) below 2, the width of the wideband is substantially decreased. The dielectric constant (ε_r) plays a pivotal role in the absorption level attained and deciding factor for the bandwidth of the proposed wideband absorber.

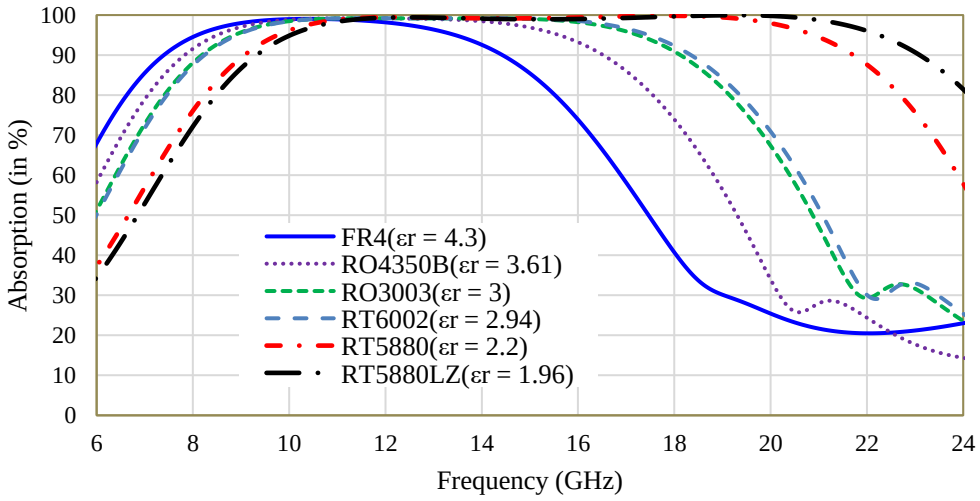

Fig. 4.9: Variation of absorption with change in material properties.

4.3.3 Parametric Analysis

The parametric analysis is performed to provide optimized dimensions to attain the desired objective of near total absorption with wide bandwidth. The parametric analysis is performed

with normal incidence under the condition of $\theta = 0^0$ and $\phi = 0^0$. The parameters taken for optimization are length (Ls), substrate height (h), and proper selection of surface resistance for conductive ink. The parameter Ls is studied for Ls = 8 mm, Ls = 9 mm, and Ls = 10 mm, as shown in Fig. 4.10, with the pre-requisite condition of near-total absorption with wideband achievement. The Ls = 8 mm and Ls = 10 mm reduce wideband achievement in comparison to Ls = 9 mm, where the best bandwidth of 8.23 GHz is achieved.

Similarly, from optimization, the best result was achieved for the substrate height (h) = 3.2 mm with a bandwidth of 8.23 GHz and more than 99% absorption, as shown in Fig. 4.11. The resistance per square provided by conductive ink is studied for optimum results through parameterization, as shown in Fig. 4.12. The resistance value of 40 ohm/sq. provides two bands of 1.8 GHz and 2.25 GHz from 10 GHz to 11.8 GHz and 18.35 GHz to 20.6 GHz, respectively. The resistance value of 45 ohm/sq. provides two bands of 2.1 GHz and 2.82 GHz from 10.47 GHz to 12.58 GHz and 17.18 GHz to 20 GHz, respectively. The 50 ohm/sq. provides a wideband from 11.17 GHz to 19.4 GHz with a bandwidth of 8.23 GHz, clearly providing an increase in the width of the band with more than 99% absorption.

The analysis part extended intending to establish the effect of a further increase in resistance/sq. but with the Selection of resistance of 55 ohm/sq. The width of the wideband decreased from 8.23 GHz to 6.9 GHz in a range of 11.97 GHz to 18.87 GHz. The effect was further confirmed with a further increase in resistance to 60 ohm/sq. clearly providing a further decrease in width from 6.9 GHz achieved in the case of 55 ohm/sq. to 5.45 GHz in case of 60 ohm/sq. from 12.67 GHz to 18.12 GHz. The inference drawn from the resistance parameterization per square indicates that 50 ohm/sq. resistance of conductive ink is best suited for the design of the proposed absorber to attain optimum results.

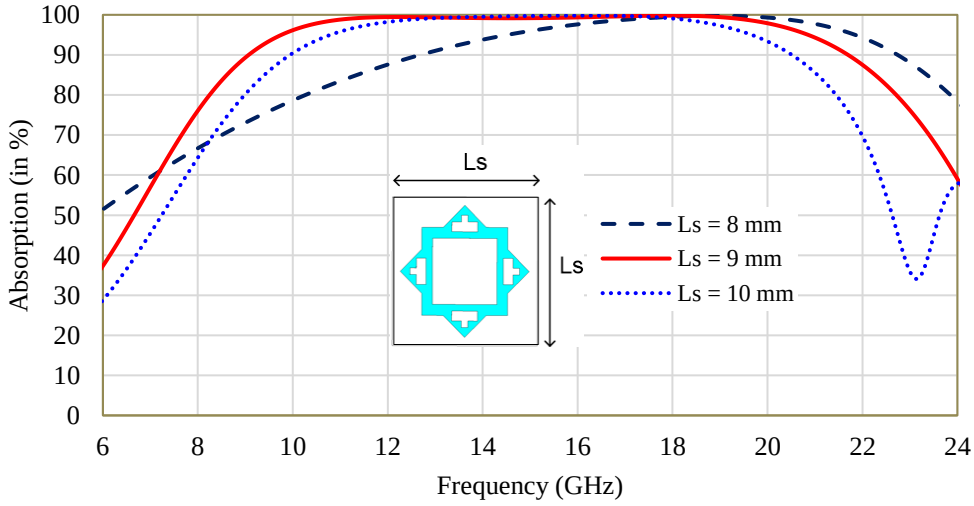

Fig. 4.10: Variation of absorption with parameter 'Ls'.

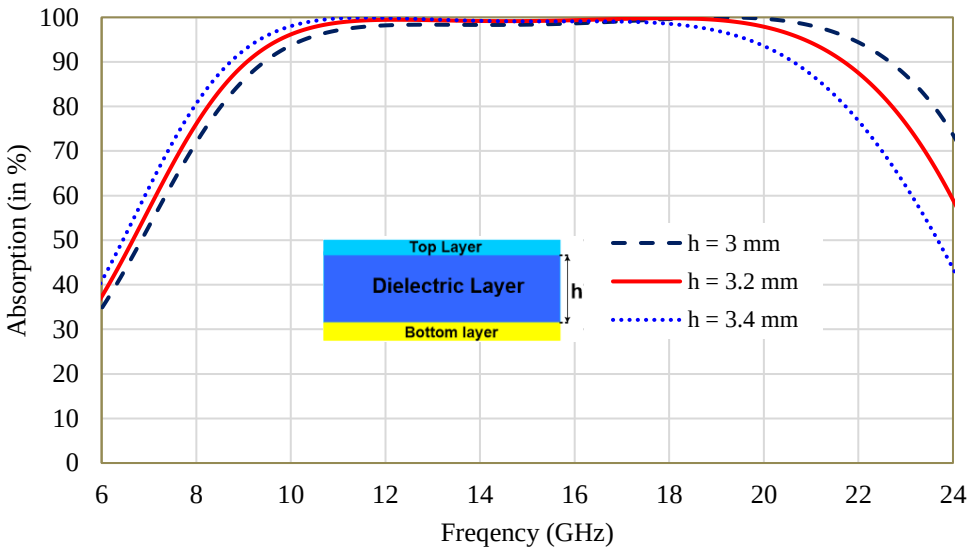

Fig. 4.11: Variation of absorption with parameter 'h'.

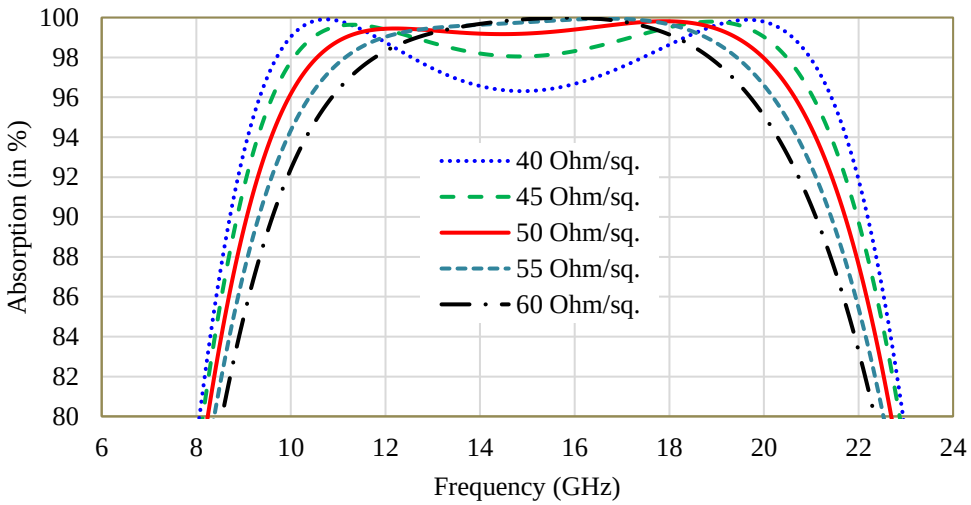

Fig. 4.12: Variation of absorption with surface resistance of conductive ink.

4.3.4 Surface Current and Electric Field Distribution

The field and current distribution are also analyzed to provide more insight into the behaviour of geometrical shape on absorption levels, as shown in Fig. 4.13. Three frequencies, i.e., 12.14 GHz, 15 GHz, and 20 GHz, are taken to understand the absorption behaviour in the proposed wideband absorber. From Fig. 4.13(b), it is seen that the electric field is dominant along the top and bottom of the geometrical shape of the proposed absorber. At the same time, the current distribution is more prevalent along the sides as shown in Fig. 13 (a). Thus, the structure is responsible for achieving near total absorptivity at designated frequencies, thus justifying its claim for a wideband metamaterial absorber.

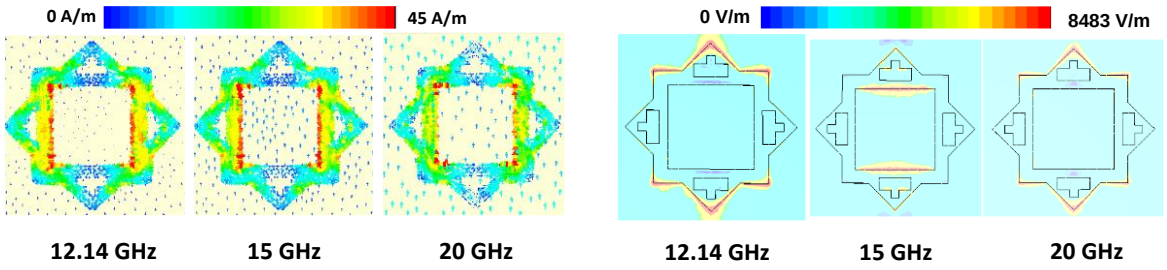

(a) (b)

Fig. 4.13: (a) Vector surface current distribution and (b) Electric field distribution.

4.3.5 Experimental Characterization

The measurement setup for establishing experimental verification of results is done through space wave measurement. The requirements for space wave measurement are a fabricated prototype of the proposed absorber, wideband Horn antennas two in number (with operating range from 2 GHz to 20 GHz), and a two-port Keysight Network Analyser (E5063A, 100 kHz - 18 GHz). The initial step is a measurement of the reflectance of the bottom side of the proposed absorber with an utterly metallic ground plane. The methodology incorporated is Port-1 of VNA is connected to the transmitting antenna and Port-2 is connected to receiving antenna (both being Horn antennas), and the 60 cm distance is set as a separation between antennas (Transmitting and Receiving Horn antenna) and fabricated prototype. The final step involves measuring the front side with a patch placed 60 cm from Horn antennas, as shown in Fig. 4.14. The results achieved through experimentation are up to 18 GHz; after that, a prediction based on results achieved up to 18 GHz and simulated results are taken for reference (due to unavailability of the VNA beyond 18 GHz in the department). The experimentally verified results conform to simulated results with attainment of more than 90% absorption, as shown in Fig. 4.15, thereby confirming the significance of the proposed absorber as a wideband absorber with near-perfect absorption of more than 99% absorption value. The minimum variation in results is attributed to measurement in free space and the non-conformity of the substrate. The proposed absorber is evaluated on the polarization angle parameter. The absorption parameter for the proposed absorber is studied for variation of polarization angle from 0° to 90° under normal incidence by taking electric and magnetic fields along *x*-direction and *y*-direction, respectively.

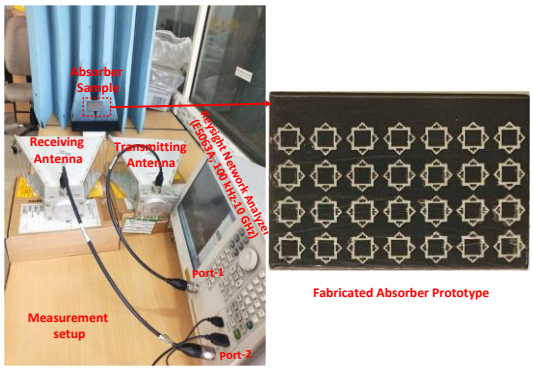

Fig. 4.14: Fabricated prototype and measurement setup.

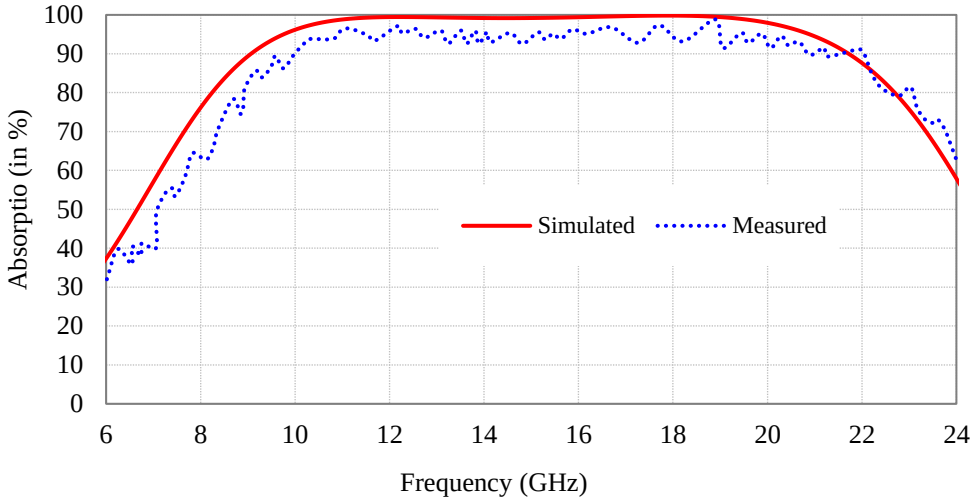

Fig. 4.15: Comparison of simulated and measured absorption of the proposed absorber.

The measurement is done using the same setup as shown in Fig. 4.14. The measured behaviour of the proposed absorber is insensitive to polarization angle variation till 45°, as shown in Fig. 4.16. The highest form of absorption is achieved for broad bandwidth in a range varying from angle ϕ = 0° to 90°, thereby confirming the polarization insensitive of the proposed absorber till 45°.

The performance of the proposed absorber is also measured on the angle of incidence for oblique incidence under the condition of TE and TM mode. The behaviour under TE mode is taken by the variation of magnetic field component and wave propagation in tandem by an angle (θ) with respect to *y*- and *z*-direction. The direction of the electric field is along the *x*-direction. Similarly, the TM mode is taken by keeping the direction of the magnetic field along the *y*-direction and variation of the electric field and wave propagation component simultaneously by an angle (θ) with respect to *y*- and *z*-direction. The measured performance of the proposed absorber in TE mode is stable for an angle θ = 0° to 45°, and after that absorption, the level decreases to 80%, as shown in Fig. 4.17(a) and (b). A similar pattern is

exhibited in TM mode, as shown in Fig. 4.18 (a) and (b). The unwanted peaks in the analysis of theta variation are attributed to reflection and interference theory [189].

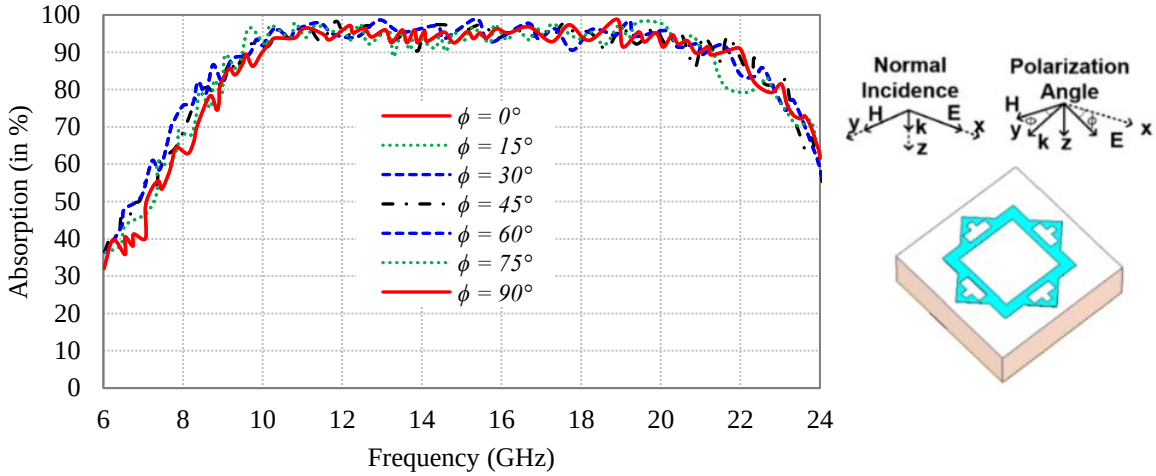

Fig. 4.16: Variation of absorption with polarization angles (ϕ).

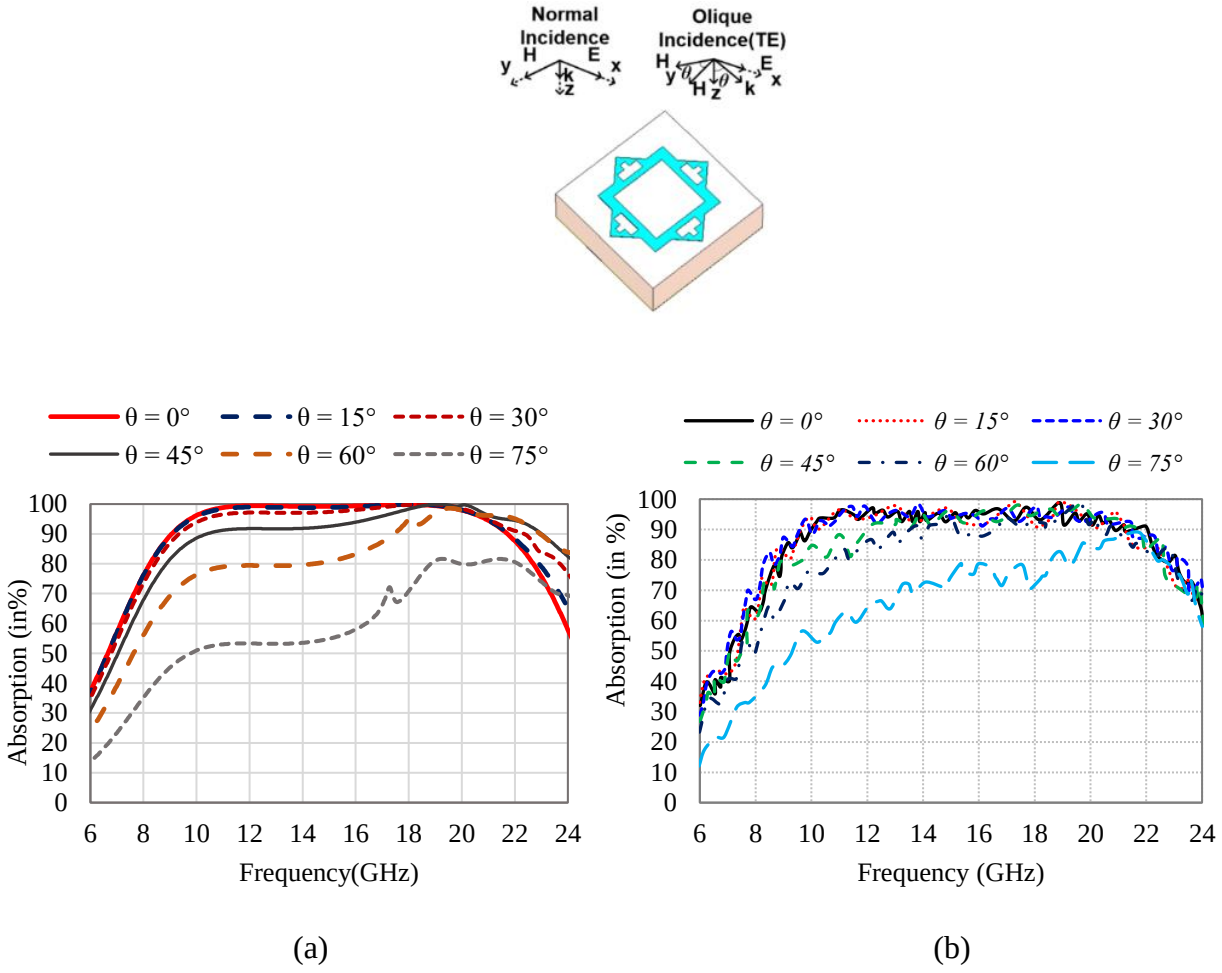

Fig. 4.17: (a) Simulated absorption, with oblique incidence (θ) for TE mode and (b) Measured absorption, with oblique incidence (θ) for TE mode

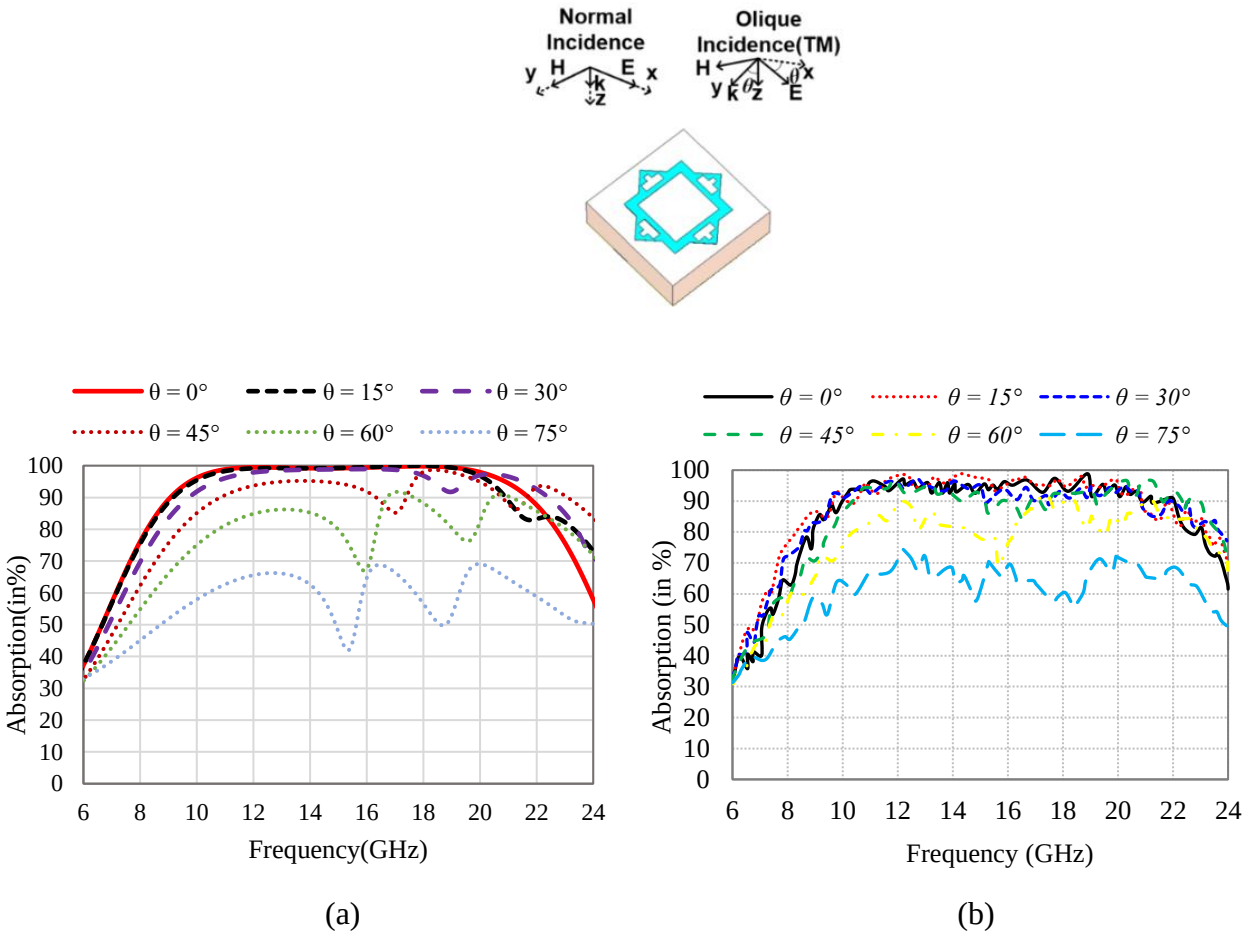

Fig. 4.18: (a) Simulated absorption, with oblique incidence (θ) for TM mode and (b) Measured absorption, with oblique incidence (θ) for TM mode

4.4 Conclusion

This chapter proposes a metamaterial-based wideband absorber with near-perfect absorption for practical applications in microwave regimes. The absorption level attained is more than 99%, from 11.17 GHz to 19.40 GHz, and the bandwidth is 8.23 GHz. The attainment level and width of the proposed absorber are verified experimentally. The experimental verification is performed with a fabricated proposed absorber having finite dimensions comprising 7 × 7 unit cells. The results achieved match the results obtained through the simulation process, and the minor contrast is observed ascribed to fabrication and measurement inaccuracy. The practicability of the proposed absorber is verified by polarization insensitive behaviour and wide incident angle of operation till 45°. The article claims the proposed structure will be a viable solution for wideband mutual coupling problems in practical design implementation for microwave applications.

CHAPTER 5 APPLICATION OF METAMATERIAL ABSORBER TO IMPROVE ISOLATION FOR MIMO CONFIGURATION

5.1 Introduction

The mobile systems are exhibiting ever-rising demand due to surge in customer base and enormous user-based daily applications. The intent of researchers is an attempt to provide services with highest form of quality to subscribers, and in this attempt for quality-based services, Multiple-Input Multiple-Output (MIMO) configuration is incorporated in practical antenna systems by the researchers with extremely demanding features of high data rate and reliability [48-49]. The availability of limited space is a hindrance in exploitation of MIMO setup in communication arena. The limited area incorporation of the MIMO setup will surely increase the capacity of the system, but isolation problem will be the disadvantageous part. The strong case of mutual coupling exists between antenna elements in the experimental setup so isolation parameter will be compromised, meaning thereby overall performance deterioration of performance [50]. The gain in channel capacity will be marred by correlated signals, and hence the prime focus shall be to improve performance by neutralizing strong mutual coupling. The -15 dB reference level for isolation is considered as reference level for practical applications involving MIMO systems [51]. However, the demanding proposition shall be high isolation level in practical applications, and the focus of the work is to provide optimum isolation for enhanced performance in the MIMO setup. The practical applications used for design consideration are realised with compact size and dimension. The overall performance and practical applicability of the communication setup are interlinked to many parameters like antenna size, isolation technique, isolator placement, MIMO performance, and antenna configuration that provide a limitation to the feasibility of the MIMO antenna for wireless applications.

The prime focus of work is aimed in high isolation levels through elevated metasurface-based absorber in height conformity to planar inverted F-antenna (PIFA) which is designed, simulated, and practically verified for results. The inference from results achieved is an indication that the practically designed MIMO configuration holds good for applications. The achievement part is high isolation level below -23 dB, thereby realising complete isolation between elements of the MIMO setup. The simple structure, high isolation, low envelope correlation coefficient will be the advantageous aspect for the proposed PIFA antenna having metasurface absorber.

5.2 Design and Configuration of Antenna and Isolator

The design of MIMO configuration setup is composed of two antenna elements and the resonant frequency of 4.712 GHz is taken for realising PIFA [51] antenna elements. The side view and dimension of the individual element for overall MIMO configuration, is shown in Fig. 5.1. The Eq. (5.1)is used for the design of PIFA;

$$f = \frac{c}{4\times(L+W)} \tag{5.1}$$

where, 'c' is free space velocity, 'L' and 'W' represent dimensions of radiating element having a value of L = f (corresponding to proposed design) = 5 mm and W = b (corresponding to proposed design) = 10 mm, respectively, for the design of PIFA.

The two antenna elements of MIMO configuration are exact mirror images of each other and are geometrically maintained at extreme edges of the FR4 substrate having material properties of ε_r = 4.4 and tan δ = 0.02, the geometrical dimension is 100 × 50 × 0.8 mm^3. The copper clad ground plane is completely metallic with a thickness of 0.035 mm and is used on the other side of the substrate as ground plane. The antenna element PIFA structure is radiating and a height of 4.2 mm is maintained from the printed circuit board (PCB) surface in the design. The pattern diversity is witnessed in Antenna-1 and Antenna-2 of MIMO setup. A 50Ω coaxial cable is used to fed each antenna element and the feed location is optimized in relation to shorting strip in order to achieve perfect impedance matching for maximization of results. The geometrical dimensions of the single element in MIMO configuration are discussed in Table 5.1, and its arrangement are shown in Fig. 5.2.

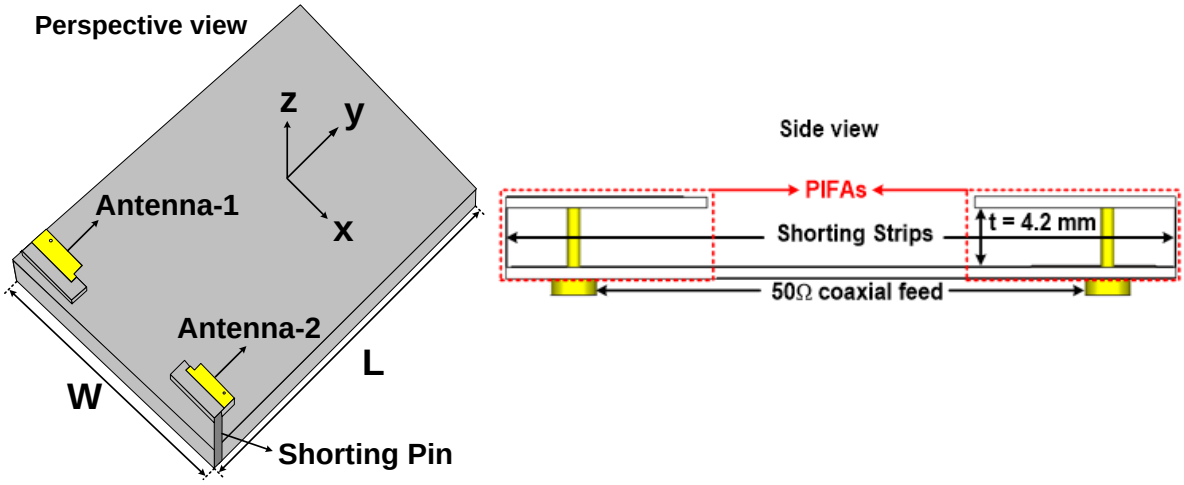

Fig. 5.1: The different views of MIMO antenna without isolator.

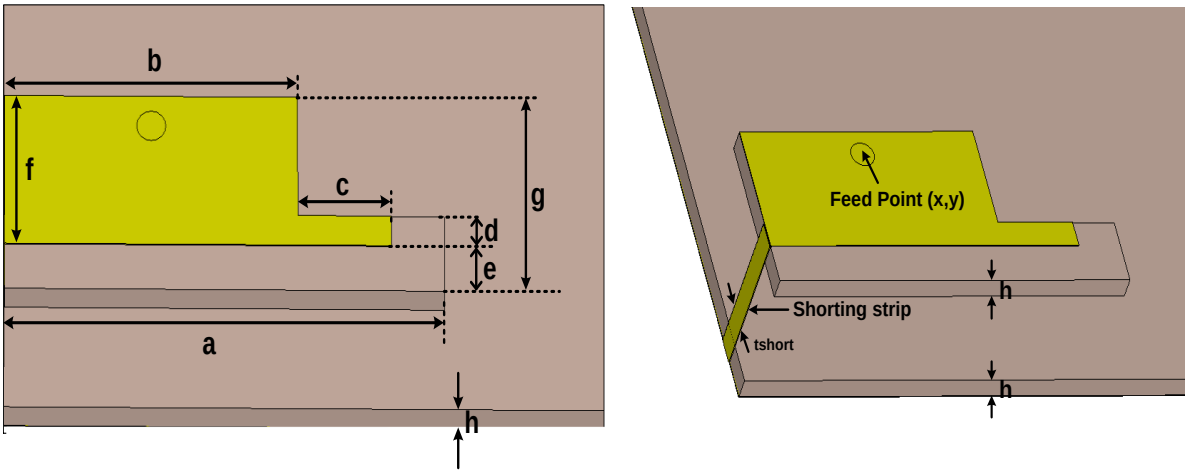

Fig. 5.2: Details of the single antenna element.

Table 5.1: Dimensions of single antenna element.

S. No.	Parameter	Dimension (in mm)
1.	L	100
2.	W	50
3.	a	15
4.	b	10
5.	c	3.2
6.	d	1
7.	e	1.5
8.	f	5
9.	g	6.5
10.	x	5.5
11.	y	5
12.	tshort	1
13.	h	0.8
14.	t	4.2

The unit cell used as an isolator is already designed and analyzed in Chapter 3 under Section 3.2. The structure and dimensional configuration is shown in Fig. 5.3. The absorber is a composition of three layers and is a unit cell comprising two metallic layers, and a dielectric in between the top and bottom layer. The thickness of 0.017 mm is maintained for patch and ground conductor which is made of copper. The top resonating structure is etched over a low-cost FR4 substrate with and thickness of 0.8 mm. The complete metallic back structure is used to make the transmission coefficient zero (Complete analysis given in Section 3.2).

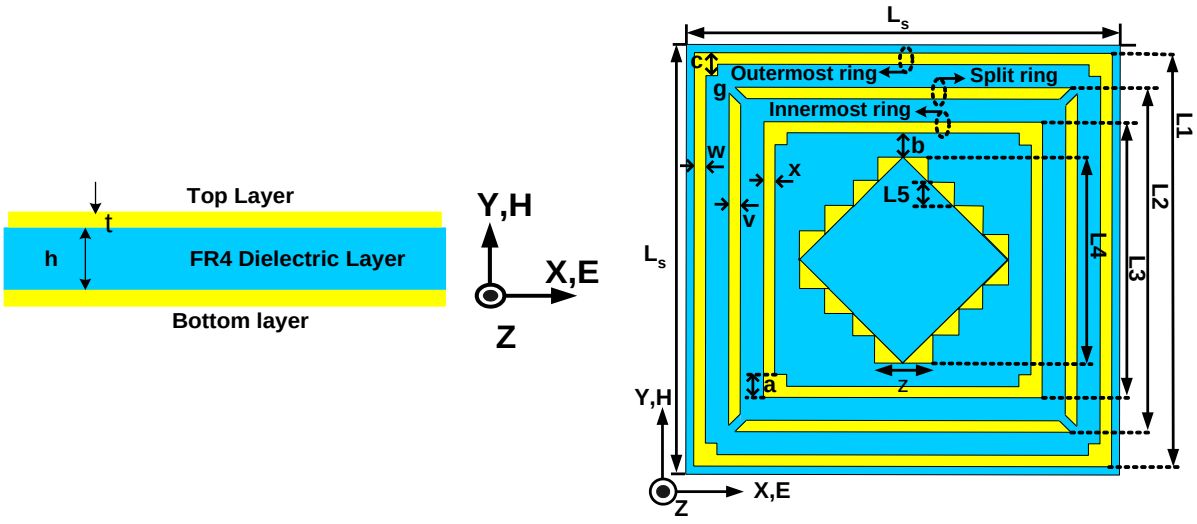

Fig. 5.3: Layers and configuration of unit cell.

5.3 Results and Discussion

The design, simulation, and optimization have been carried out using finite integration numerical technique based Computer Simulation Technology Microwave Studio (CST MWS). The discussion of the finding is given below.

5.3.1 Design Evolution

The evolution is divided into two important segments, the first being the evolution of the antenna structure. The antenna element of MIMO is taken for simulation as shown in Fig. 5.4. It comprises of completely covered patch on the substrate at the upper layer of the PIFA antenna and its characteristics in terms of S_{11} and S_{21} parameters denoted for various stages. Also, variation of *S*-parameters of the various stages is visualised in Fig. 5.5. From the graph, it is seen that value of S_{11} and S_{21} achieved is -5.21 dB and -13.78 dB, respectively which clearly indicates the designed antenna unable to cover the WLAN frequency band also showing poor isolation. Then, a modification of the patch is done with the removal of the partial portion from the complete covering metallic patch named as Stage B given in Fig. 5.4. The results achieved are not encouraging and failed to cover the desired operating frequency band (WLAN) as shown in Fig. 5.5. The evolution process is further extended to L-shaped patch which termed as Stage C for proper impedance matching. The result attained, in this case, is covering the operating frequency band from 4.1 GHz to 5.2 GHz with -34 dB impedance matching level based on -10 dB reflection coefficient. The level of isolation achieve through this stage is -12 dB. Then, process of evolution is completed with the removal of the extra substrate portion where non-metallic portion lies thereby giving the

Final Stage to the antenna element. Through design, impedance bandwidth and isolation is significantly improved. The result achieved in this case is the improvement of S_{11} to cover from 4.2 GHz to 5.5 GHz based on -10 dB reflection coefficients with -13 dB isolation level as shown in Fig. 5.5. Also, the evolution process of the second segment is a unit cell of the absorber which is already discussed in depth in Chapter-3 (Section 3.2.2), where the design evolution of absorbers from stage A to the Final stage was discussed with the attainment of the highest form of absorption is shown in Fig. 5.6.

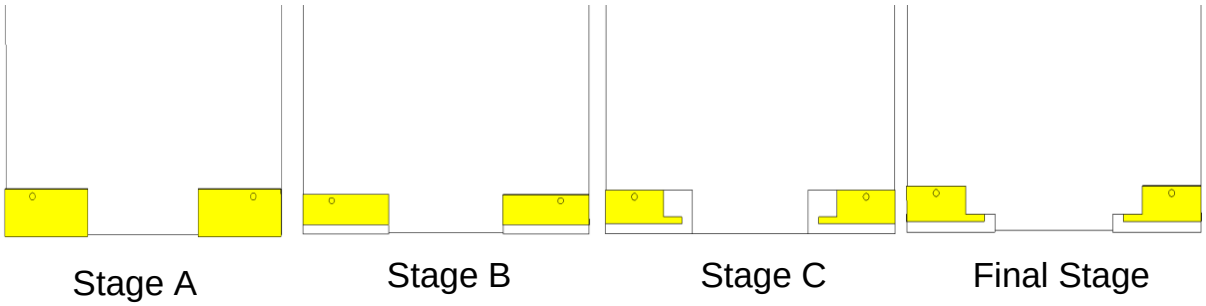

Fig. 5.4: The design evolution of antenna element.

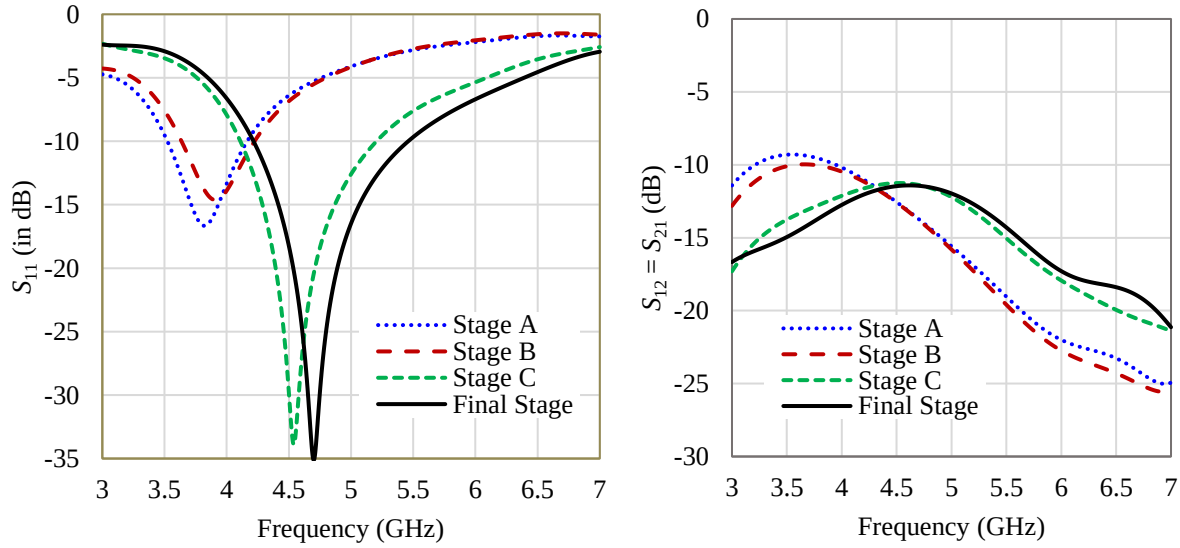

Fig. 5.5: *S*-parameters for various stages.

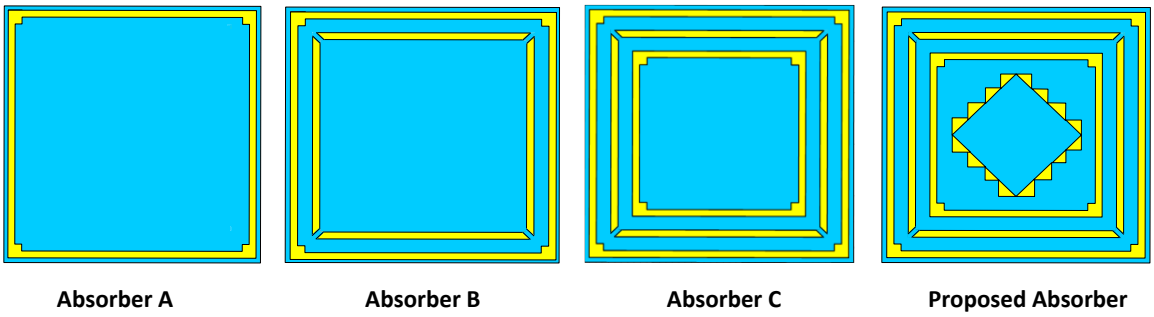

Fig. 5.6: The design evolution of unit absorber

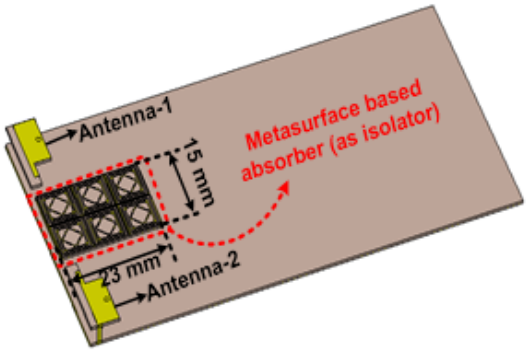

Fig. 5.7. Proposed MIMO configuration with metamaterial absorber (as an isolator).

The evolution process is moved to the combination of two segments, one with the finally evolved antenna element and the second being the absorber attained through the evolution of the metamaterial-based unit cell. The combination is such that in between the two antenna elements of MIMO configuration, the absorber unit is placed as shown in Fig. 5.7. The aim of placing the absorber (as an isolator) between antenna elements is to reduce mutual coupling between the two elements. The placement and number of a unit cell of metasurface absorber (as isolator) are optimized to increase the isolation of MIMO configuration. The 3 × 2 unit cell of the absorber is placed within the area of 15 × 23 mm^2 between multiple antenna elements to improve the isolation, as shown in Fig. 5.7.

5.3.2 Effect of Isolator

The elements of the MIMO antenna is symmetrically approached in design such that Antenna-1 and Antenna-2 of MIMO configuration mirror image; therefore, the scattering parameters $S_{11} = S_{22}$ and $S_{21} = S_{12}$ express reciprocity. The Fig. 5.8 is behaviour of *S*-parameters without isolation. As 1.4 GHz bandwidth is achieved from 4.04 GHz to 5.48 GHz and the reflection coefficient attained with respect to a -10 dB, while the resonant peak value is achieved at 4.712 GHz. The strong coupling exists between antenna elements as shown in Fig. 5.8, and is signified by a value of S_{21} achieved equal to -11.44 dB, which under normal circumstances should be less than -15 dB, thus the inference drawn is performance degradation in MIMO configuration, and when practically fabricated, it will have further deterioration thereby resulting in unsuitable for practical applications. The field radiated by the driven antenna element coupled to adjacent antenna elements, as well as there exist common ground planes is prime source of deterioration. To achieve suitability in applicability the situation demands incorporation of an isolator which in turn will turn the design practically viable.

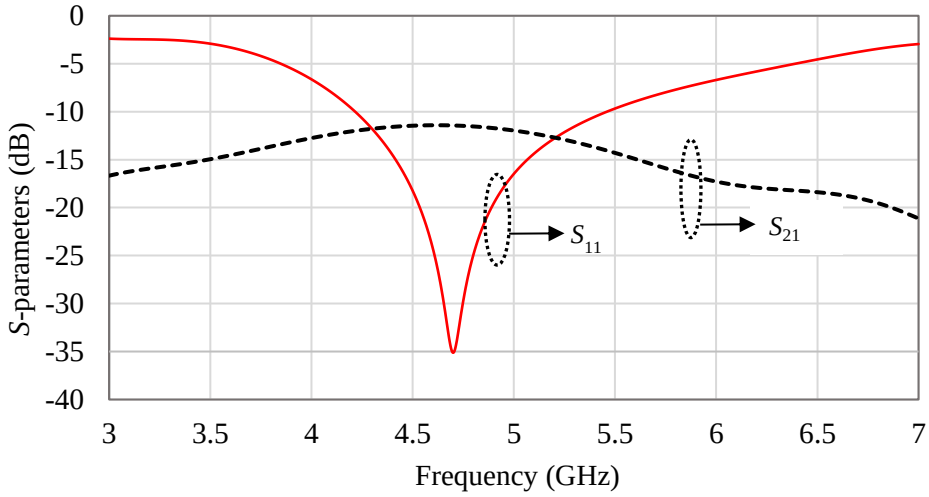

Fig. 5.8: Variation of *S*-parameters without isolator.

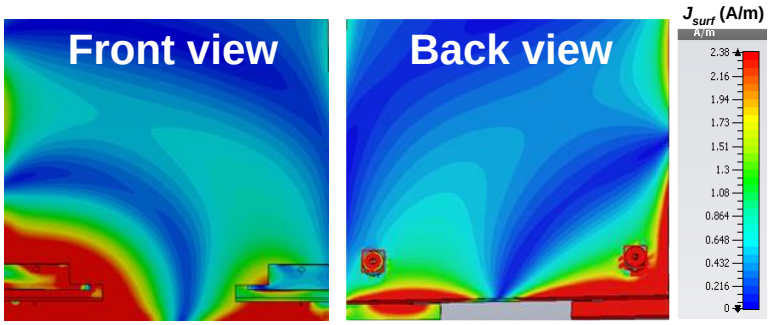

Without metasurface absorber (Isolator)

Fig. 5.9: Surface current distribution at 4.8 GHz without metasurface absorber (isolator).

The effectiveness of the proposed absorber is analysed to further support the claim for high isolation using the aid of surface current distribution (plotted at 4.8 GHz), as shown in Fig. 5.9. The condition without absorber is demonstrating surface current distribution having strong mutual coupling in PIFA antennas. The reason being the radiated field from a driven element inducing field on a nearby antenna and the other reason is common ground due to which strong coupling exists between PIFA elements. The Antenna-1is kept in excited mode while the other one is terminated with 50Ω matching impedance for preparing plots. The visualisation can be inferred as Antenna-2 is coupled to Antenna-1. The analogous procedure is repeated, keeping other antenna Antenna-2 in excited mode while 50Ω matching impedance is used for Antenna-1 termination.

Then, an isolator with the optimized metamaterial absorber is incorporated geometrically such that it is in between two PIFA antennas, and the *S*-parameter characteristics due to incorporation of the isolator on are shown in Fig. 5.10. The result attained justify the placement of isolator with attainment of maximum possible isolation in MIMO configuration.

The analysis of the metasurface absorber in close proximity to the PIFA antenna clearly gives the indication that resonant values are affected due to the placement of the absorber in close vicinity of the PIFA antenna. This result obtained through reflection coefficient can be properly interpreted by the placement of isolator, the reflection coefficient deteriorated due to the placement of the absorber in close proximity however, the desired operating band (WLAN) is achieved and it is observed that -10dB level is achieved for S_{11} and S_{22} shown in Fig. 5.10 thereby signifying the practical utility of MIMO configuration. The analysis of transmission coefficient is taken for in depth analysis for metasurface isolator in MIMO configuration and it is seen that from Fig. 5.10, that a drastically improved isolation is witnessed with rise from -11.44 dB to -23.42 dB (approximately 12 dB isolation improvements), thereby concluding that the practical relevance of proposed MIMO PIFA configuration in mobile applications.

The negligible coupling on account of both radiated field and common ground is witnessed in surface current distribution for the proposed MIMO configuration (antenna along with isolator) and from the absorber analysis, it can be clearly seen that high absorptivity levels of the absorber is instrumental for providing good isolation shown in Fig. 5.11.

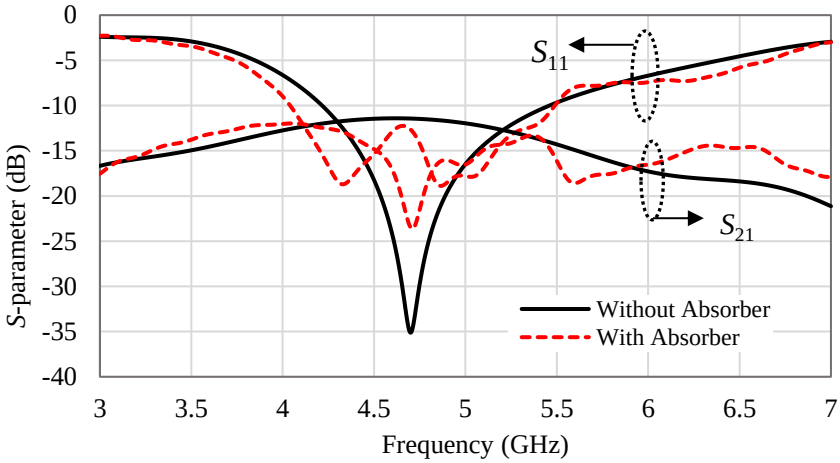

Fig. 5.10: *S*-parameters variation (with and without isolator).

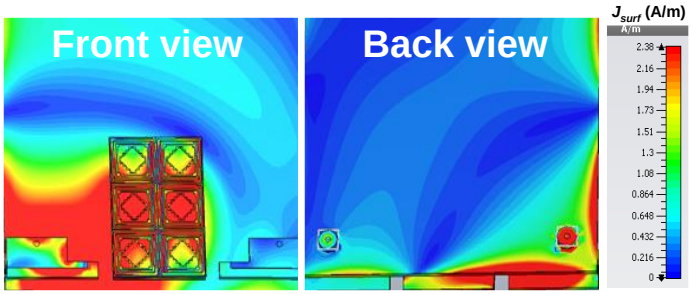

With metasurface absorber (Isolator)

Fig. 5.11: Surface current distribution at 4.8 GHz with metasurface absorber (isolator).

The special behaviour due to presence of a metasurface-based absorber is responsible for coupling current becoming antiparallel to metasurface based absorber current, which is instrumental for magnetic resonance and therefore absorbing a considerable portion of coupling wave and the flow of current through ground plane is blocked the leftover coupled field is reflected perpendicular in response to the polarization to incident angle behaviour thereby enhancing the decoupling effect. The decoupling mechanism is responsible for high rate of isolation in the proposed MIMO configuration, thereby justifying its practical incorporation on account of highest form of isolation attained. The reflection coefficient less than a -10 dB (in the desired band of operation) is achieved for MIMO configurations (with and without absorber).

Thereafter, the parametric analysis is done by verifying the impact of the number of unit cells on the isolation characteristics of the MIMO setup. The number of unit cells between antenna elements is varied to understand the behavioural properties of the increase in the number of unit cells on the isolation level. The coupling is analysed with the incorporation of 3 × 1 metamaterial unit cell as an isolator, as shown in Fig. 5.12, and S_{21} (with 3 × 1 unit cell) is shown in Fig. 5.13. The result achieved reflects an increase in the Isolation level with a slight drop in S_{21} from -11.44 dB to -15.64 dB. The parametric analysis is further extended with an increase in number from 3 × 1 to 2 × 2, and the drop of S_{21} is from -11.44 dB to -11.61 dB with a shift in the band. The investigation is strengthened by increasing the number from 2 × 2 to 3 × 2 and the result achieved is quite encouraging, with decreasing in S_{21} from -11.44 dB to -23.62 dB to confirm the behaviour and decide the final outcome. We increased the number to 4 × 2 by keeping the symmetric approach of the setup into account, but there was again a rise in coupling with the increase in the number of unit cells due to the loading effect as the S_{21} parameter increased from an earlier stage of -23.62 dB to -12.24 dB as shown in Fig. 5.13. Thus, from the parametric study of isolator in MIMO setup, it is evident that when the number of unit cells is 3 × 2 for isolation purposes, the desired optimized result is achieved, so 3 × 2 unit cells are chosen for the design of MIMO setup with isolator.

5.3.3 Experimental Validation

The fabrication of metasurface absorber (as isolator) is done to determine the relevance of the work, the proposed MIMO antenna configuration with absorber is measured using VNA E5063A (Full two-port Keysight Network Analyser) having range from100 kHz – 18 GHz. The Fig. 5.14 provide insight to network parameter and radiation pattern measurement setup as shown in Fig. 5.14. The practically achieved reflection coefficient are found to be in

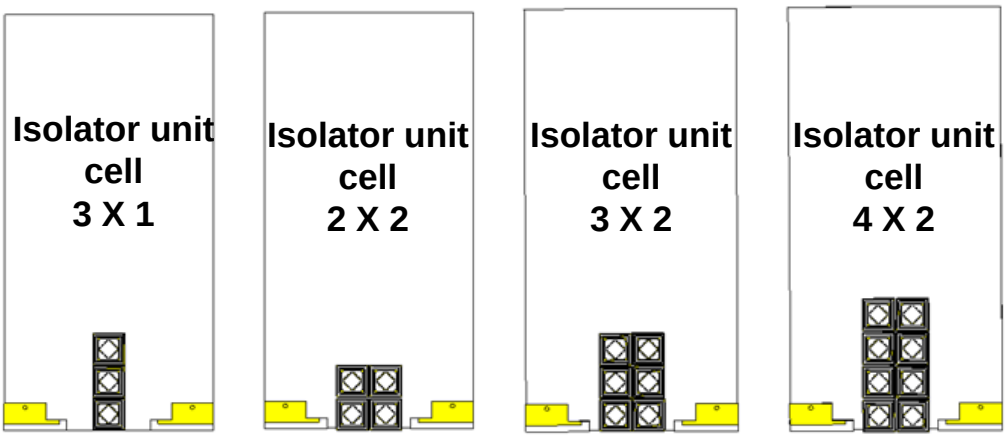

Fig. 5.12: Configuration of various number of unit cell as an isolator for MIMO setup.

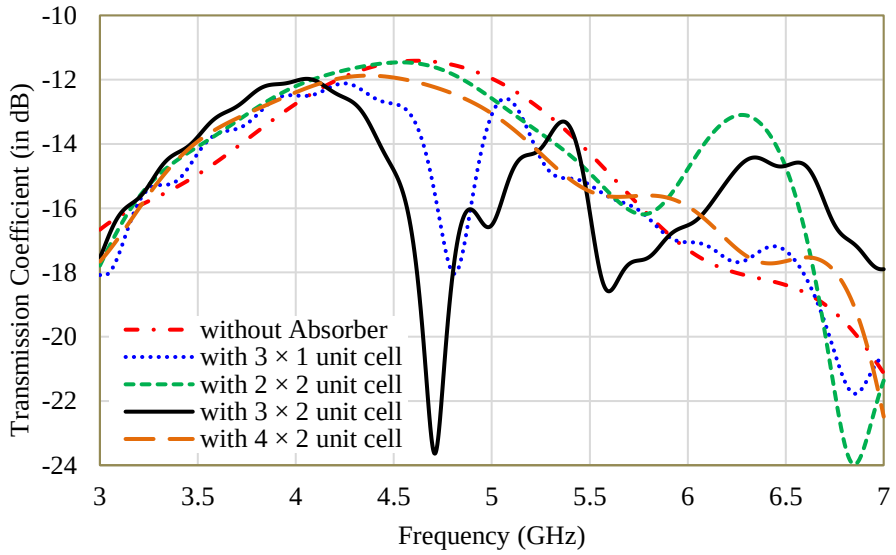

Fig. 5.13: Impact of various number of unit cell on S_{21} parameter.

agreement with the simulated one, as shown in Fig. 5.15 and 5.16. The desired band of operation for both configurations (with and without an Isolator) for proposed setup is witnessing less than -10 dB value for reflection coefficient. The comparison in experimental and simulated values is inferred with the conclusion that the results achieved are in close agreement, thereby approving the claim for incorporation in mobile phone applications. Further, the radiation pattern behaviour of the MIMO antenna provide visualisation to deep fading environment that can be observed at the designated resonant frequency. The calculated reflection coefficient parameter provides insight into the behaviour of MIMO setup as any demanding application based on isolation will strive for the achievement of minimum values of coupling between antenna elements of MIMO setup.

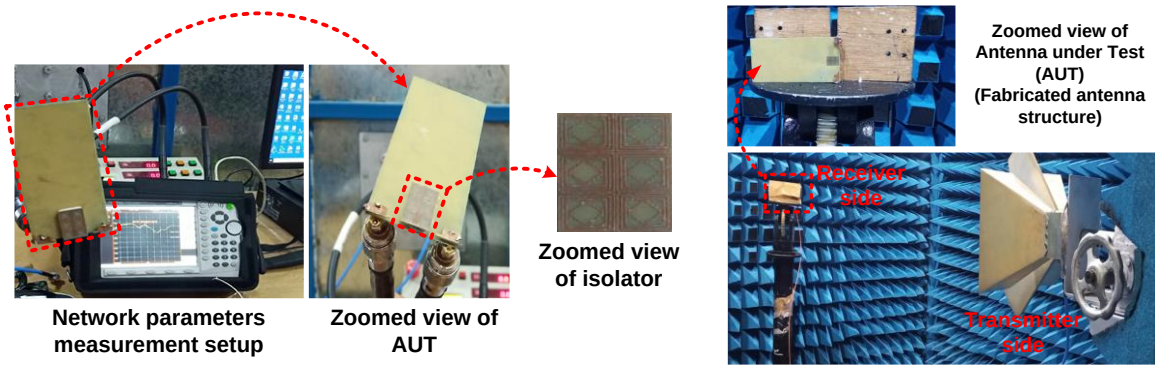

Fig. 5.14: Measurement setup along with fabricated prototype.

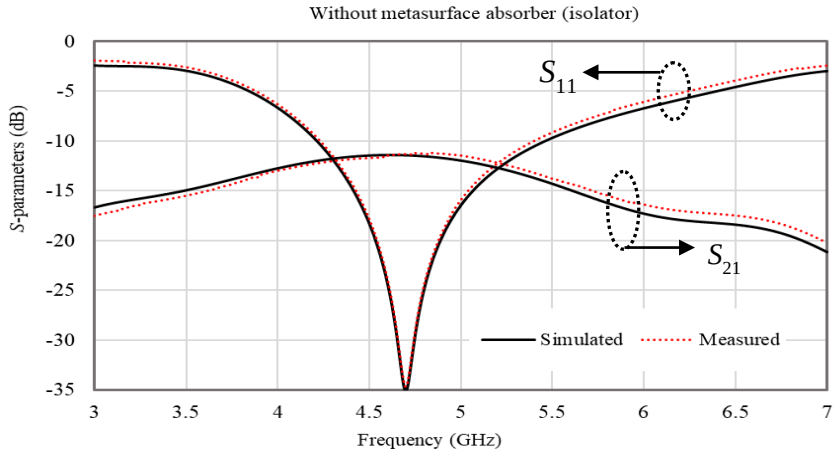

Fig. 5.15: Comparison of simulated and measured *S*-parameters without isolator.

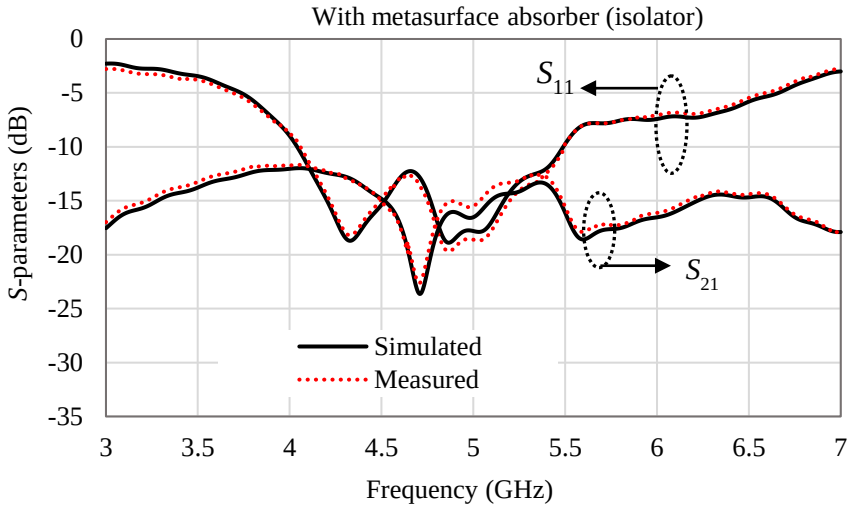

Fig. 5.16: Comparison of simulated and measured *S*-parameters with isolator.

5.3.4 Radiation Performances

5.3.4.1 Radiation Patterns

The Fig. 5.17 provide information on 3D radiation pattern which is clearly showing that pattern diversity. The combating of multipath fading in actual scenario is aided with

complimentary radiation pattern in space clearly indicating that the proposed MIMO configuration is further supporting the claim for practical implementation in real mobile environment. To verify the 3D pattern diversity, the comparison of simulated and measured 2D radiation patterns is also carried out, as shown in Fig. 5.18 and the results for simulated and measured radiation patterns are in close agreement. However, fabrication and measurement inaccuracy are responsible for insignificant deviation observed in the measured results. Further, at a designated resonant frequency the deep fading environment is witnessed that is clearly visualized from the radiation pattern behaviour of the MIMO antenna.

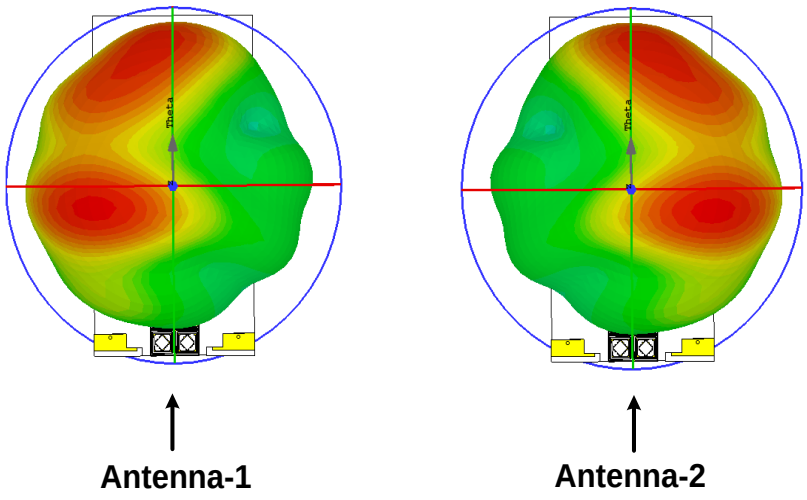

Fig. 5.17: 3D radiation patterns at 4.8 GHz (Simulated).

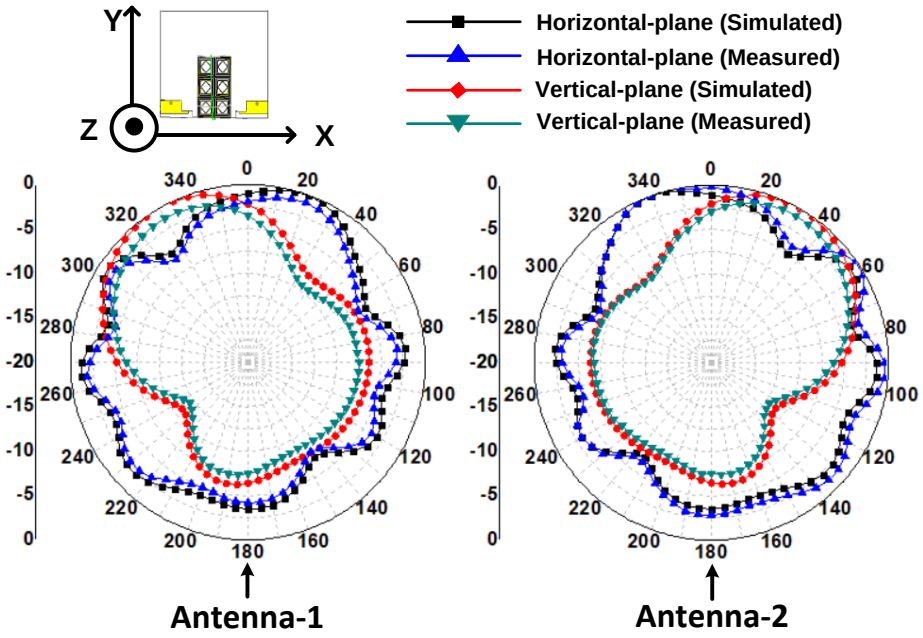

Fig. 5.18: Comparison of simulated and measured 2D radiation patterns at 4.8 GHz.

5.3.4.2 Gain and Efficiency

To determine the radiation performance of the proposed design the peak realized gain and the total antenna efficiency of the proposed MIMO configuration are calculated. The Fig. 5.19 provide calculated values of the peak realized gain and total antenna efficiency. The simulated and measured peak realized gain are compared and the calculated total antenna efficiency is shown in Fig. 5.19. The variation from 3.41 dBi to 3.61 dBi over the operating frequency band is achieved for parameter realized gain. The comparison of measured gain with the simulated one, provide an inference of excellent matching between simulated and measured realized gain. However, measurement and fabrication tolerances are responsible for small deviations (within acceptable limit) that are observed. The Fig. 5.19 provide information that the numerically calculated values of total radiation efficiency varying from 72.14% to 84.85 % over desired operating bands. The calculation for total antenna efficiency is done after taking all losses into account [192]. Thus, it is noticed that total antenna efficiency greater than 80% (proposed MIMO antenna) is maintained throughout the operating frequency band, which signifies its practical utility in practical mobile applications. The minimal complexity in design of proposed MIMO configuration is additional advantage, thereby clearing all decks in practical incorporation at microwave frequency regime.

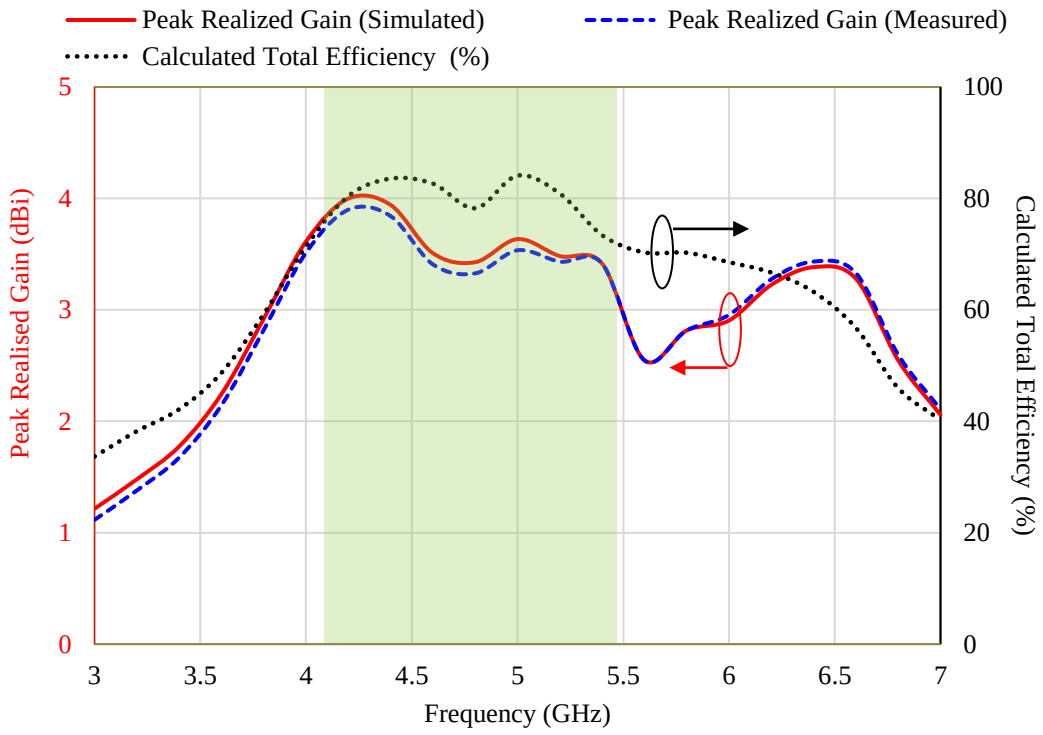

Fig. 5.19: Peak realized gain (simulated and measured) and total antenna efficiency.

5.3.4.3 Total Active Reflection Coefficient (TARC)

The ratio of the square root of total reflected power to the square root of total incident power using equation Eq. (5.2) [180] is defined as TARC for the N-port antenna. The minimum and maximum range of TARC value is between 0 and 1, while the maximum radiation is signified by 0 value, and the value of 1 represent maximum reflection parameter. The inference from attainment of near 0 value of TARC is that the maximum power is radiated or moved to adjoining ports.

$$\Gamma = \frac{\sqrt{\left(\sum_{i=1}^{N}|b_i|^2\right)}}{\sqrt{\sum_{i=1}^{N}|a_i|^2}} \tag{5.2}$$

where, b_i and a_i are reflected and incident power, respectively. The proposed antenna is achieving a value of 0.128 for TARC parameter as shown in Fig. 5.20.

5.3.5 Diversity Performance

The characterisation of MIMO is done through the calculation of various important parameters to establish the practical usability of the designed setup. The following parameters were taken to understand the practical aspects of the designed structure;

5.3.5.1 Envelope Correlation Coefficient (ECC)

The value ECC is calculated from Eq. (5.3) [51] using different pairs of antennas. The value of ECC achieved is 0.5 as shown in Fig. 5.21, thereby justifying its practical usability on account of very low cross correlation between two antenna elements

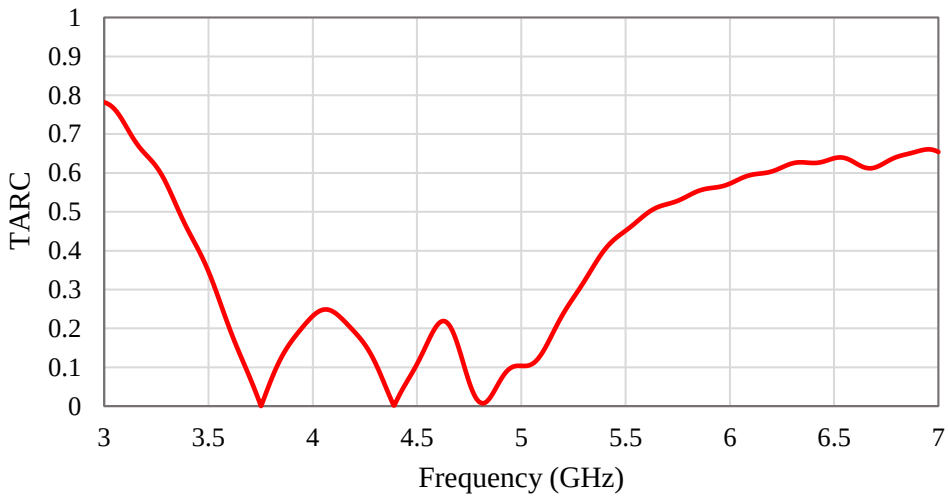

Fig. 5.20: Variation of TARC with frequency.

From the Fig. 5.21, it is seen that the simulated and measured ECC are in close agreement. The achievement of low correlation is attributed to incorporation of metasurface-based absorber (as isolator), resulting in achievement of decoupling for antenna port.

$$\rho_e(i,j) = \frac{\left|\sum_{n=1}^{N} S_{i,n}^{*}\ S_{n,j}\right|^2}{(1-\sum_{n=1}^{N} S_{i,n}^{*}\ S_{n,i})(1-\sum_{n=1}^{N} S_{j,n}^{*}\ S_{n,j})} \tag{5.3}$$

Where, the *N* represents the number of ports in MIMO configuration, whereas alphabets *i* and *j* are a number of elements in MIMO configuration.

5.3.5.2 Effective Diversity Gain (EDG)

To demonstrate the capability of the MIMO system in a fading environment the diversity gain (DG) is one of the key parameters and is calculated by using Eq. (5.4) [53], and the results achieved for DG are plotted in Fig. 5.22. From the results it is seen that the DG are nearly 10 dB for calculated values of overall operating frequency band ranging from 4.04 GHz to 5.48 GHz. Hence, a clear inference can be drawn that the of proposed MIMO configuration is providing good diversity performance which is prerequisite for practical applications.

$$\textit{Diversity Gain (DG)} = 10\ \sqrt{1-|ECC|^2} \tag{5.4}$$

The effectiveness in diversity capability is through inclusion of total radiation efficiency as in case of apparent diversity gain, 1% distribution level is without consideration of total antenna efficiency. The total antenna efficiency provide realistic judgement therefore calculation of effective diversity gain (EDG) is attained by multiplication of apparent diversity gain (DG) with total antenna efficiency calculated Eq. (5.5) [53], and from the graph plotted in Fig. 5.23 it is observed that there is a variation of EDG from 7.14 dB to 8.40 dB in the range from 4 GHz to 5.5 GHz. The calculation of total antenna efficiency is by considering all the losses [192].

$$\text{Effective Diversity gain (EDG)} = \text{DG} \times \text{Total Antenna Efficiency} \tag{5.5}$$

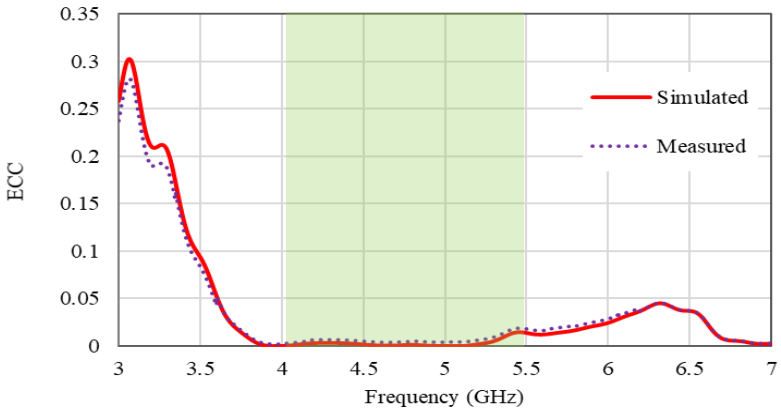

Fig. 5.21: Variation of ECC with frequency

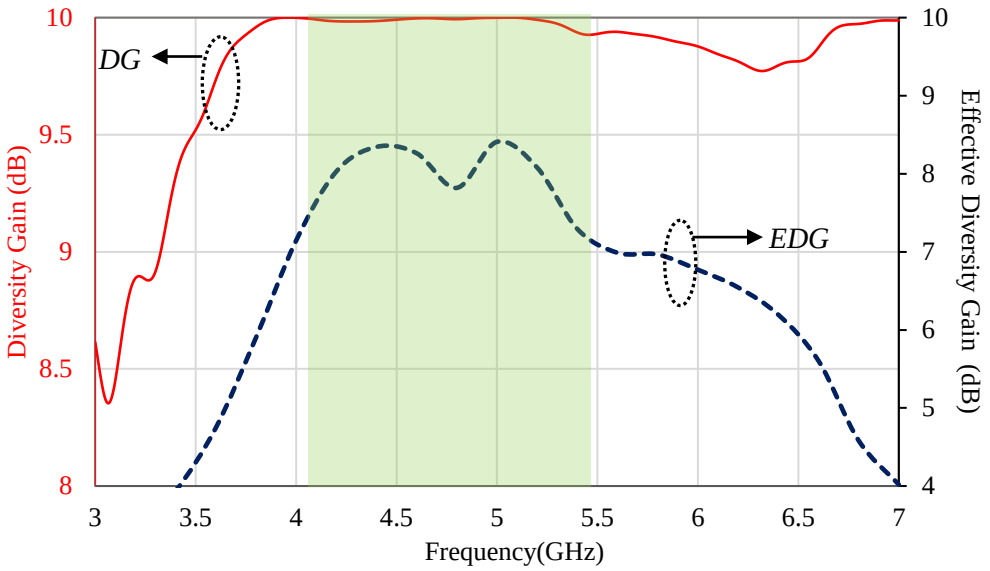

Fig. 5.22: Variation of DG and EDG with frequency.

5.3.5.3 Mean Effective Gain (MEG)

The random route calculation for ratio of mean received power of antennas, and at antenna elements total received mean incident power is defined as mean effective gain (MEG). The MEG for the designed configuration is calculated through following expression [53]

$$MEG = \int_0^{2\pi}\int_0^{\pi}\left[\frac{XPR}{1+XPR}\,G_\theta(\theta,\phi)P_\theta(\theta,\phi) + \frac{1}{1+XPR}G_\theta(\theta,\phi)P_\theta(\theta,\phi)\right] sin\theta d\theta d\phi \qquad (5.6)$$

where, XPR represent cross-polarization ratio when polarization of transmitted radio waves is horizontal to reciprocal of cross-polarization when polarization of transmitted wave is vertical. The G_θ, G_ϕ are power gain pattern while P_θ and P_ϕ are angular density function of θ- and ϕ- components of incident power. The value of MEG is calculated for different XPR [53] at frequency of reference. The MEG is calculated by various values of XPR [53] and shown in tabular form as Table 5.2. It is visualised that the ratio of MEG1/MEG2 is equal to one thereby justifying the equality criteria for antenna elements used in MIMO setup.

Table 5.2 Evaluation of MEG in free space.

Frequency at 4.712 GHz	Indoor (XPR = 5dB)		Outdoor (XPR = 1dB)		Isotropic (XPR = 0dB)	
	MEG1	MEG2	MEG1	MEG2	MEG1	MEG2
	-3.451	-3.451	-3.3002	-3.3002	-3.0103	-3.0103
MEG Ratio	MEG1 / MEG2 = 1		MEG1 / MEG2 = 1		MEG1 / MEG2 = 1	

5.3.6 Performance in Mobile Phone Proximity

The practical mobile environment provides better understanding to implementation in real environment. The mobile setup comprising an LCD touch screen, battery, speaker, camera, connector, microphone, and the outside mobile covering is used for analysis and MIMO setup with metasurface absorber is placed in mobile setup. The dimensions of the LCD touch screen are 70 mm × 50 mm × 2 mm, the battery dimension is fixed as 6.4mm × 46 mm × 3 mm, the camera dimension is a circle with a diameter of 12mm, and with a thickness of 6.5 mm, the microphone has dimensions of 3 mm × 10 mm × 1.8 mm, the dimensions of connectors are 2 mm × 5 mm × 1 mm, the speaker has a dimension of 4 mm × 2 mm × 1 mm. The perfect electric conductors (PEC) is used for mobile components mentioned above and are taken as for simulation purposes. The battery and LCD touch screen is maintained at a 1mm distance from the main PCB. The outer covering is Mobile cover that encompasses all mobile components with a 1mm thick plastic box having electric conductivity of 0.02S/m and dielectric constant of 3.4. The Fig. 5.23 provides insight into the mobile environment, the comparison of result in the form *S*-Parameters under two conditions that are with and without a mobile environment is shown in Fig. 5.24. The inference from the analysis of the graph is attainment of -19.48dB value for S_{11} parameter and -15.57dB attainment for S_{21} parameter for MIMO configuration (with isolator) in mobile environment, so operating band of WLAN is covered in the real environment of mobile phone which indicates that the metasurface absorber in MIMO setup is suitable for practical implementation.

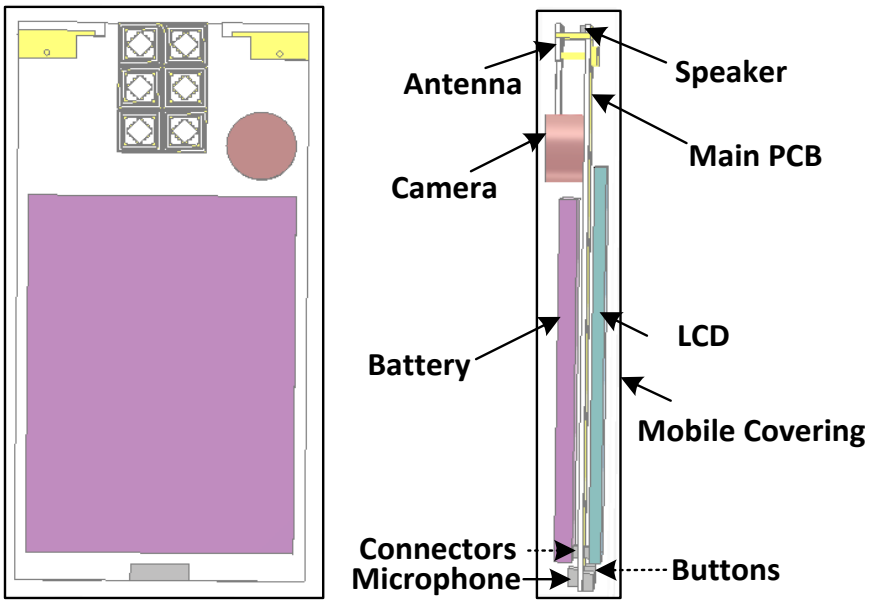

Fig. 5.23: The mobile environment with designed antenna.

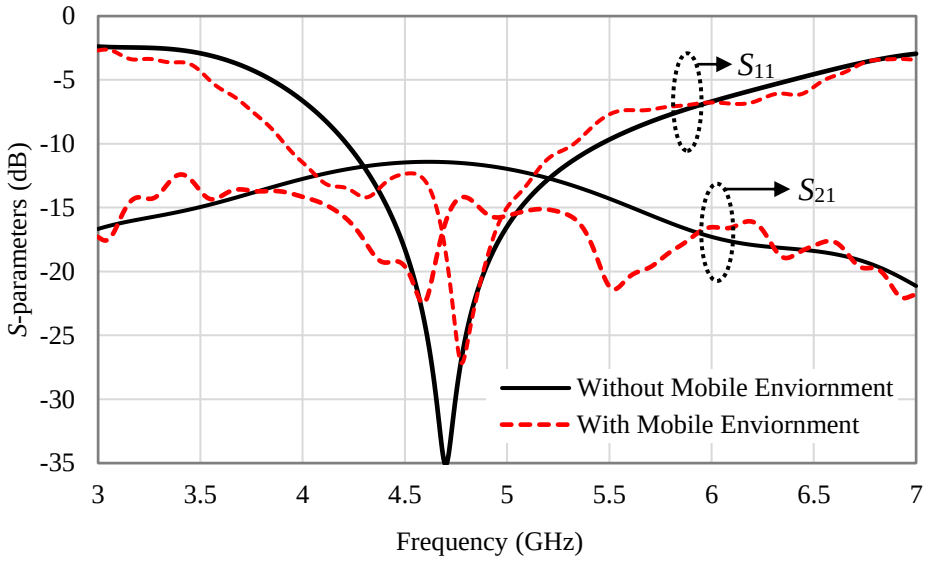

Fig. 5.24: *S*-Parameters behaviour with the mobile environment.

5.4 Conclusion

The attainment of results for designed MIMO setup is providing good isolation on account of implementation of metamaterial absorber thereby justifying the practical usability and implementation in applications at microwave regime. The diversity in pattern further supplements the practical implementation scenario for mitigating multipath fading in real scenarios. The surface current visualisation provide insight to utility of optimally placed absorber in reducing mutual coupling among antenna elements. The achieved value of envelope correlation coefficient is below the standard value of 0.5 which further suffice the claim for practical implementation. The results attained for peak realized gain and total radiation efficiency are good enough to propose MIMO configuration with metasurface absorber for practical mobile based applications.

6.1 Overall Conclusion of the Thesis

The thesis work was cantered on the attainment of two objectives, the first being design, development, and characterization of the multi-band and wideband absorber and the second one is the application part involving the designed absorber in attaining isolation for MIMO configuration. The work starts from the realization of design in terms of desired parameters and then the development of a prototype as a part of fabrication with a comparison of experimentally established results with results achieved through simulation. The work was focused not only on design and fabrication but on establishing technical usability and applicability of work in practical applications that fall under the microwave regime. The design of various structures in a multi and wideband category is processed through a systematic evolutionary approach followed by parameterization of important parameters of design to attain the best possible result through geometric alteration, thereby focussing on optimization of geometrical aspects of structure in relation to the level of absorption achieved. The outcome of evolutionary and parameterization is the attainment of two important destinations, one being the highest form of absorption, which is near unity in most cases, and the other being minimization of geometrical dimensions, which is attained geometrical dimensions of fabricated designs. The absorption phenomenon was further investigated through surface current and electric field distribution in the design of multi-band and wideband absorbers. The work is further tested through polarization and incident angle criteria to conform its performance in the practical arena, and it was found that structures fabricated are polarization insensitive in nature till 45° and have a wide incident angle of operation, which is concluded in various portions of the work under design development and fabrication of both multi-band and wideband absorber.

The design of the multiband section is enriched with the investigation of two multi-band absorbers. The first structure focussed on the attainment of multi-band absorption focuses on the design and development of a metamaterial-based microwave absorber having polarisation insensitivity, broad angle of incidence, low profile, and compactness in the microwave frequency range. The unit cell focuses on achieving maximum absorption at C-, X-, and broad Ku-band. The dimension of the proposed structure is ultrathin and compact, having an overall dimension of 8 mm × 8 mm × 0.8 mm. The dimensions are optimized in such a fashion to achieve three different peaks at three different bands, thereby making the triple-band

behaviour of the metamaterial absorber. The structure provides absorption of 99.14% absorption at 6.08 GHz (C-Band), while absorption of 98.29 % is achieved at 9.49 GHz (X-band) and 265 MHz bandwidth with above 95% absorption from 16.57 GHz to 16.83 GHz (Ku-Band) in the microwave regime. The structure is experimentally verified for results and is found to be in close agreement with simulated ones establishing its utility in practical applications.

The second structure focuses on absorption achievement in C-, X-, and Ku-bands from design of super compact ultrathin absorber having polarization insensitive response till 45° with wide angular stability to be called as triple-band metamaterial absorber. The perfect absorption (close to 100%) is achieved through unit cell comprising patches thereby justifying the term perfect metamaterial absorber. The structure provides 99.96% at 4.75 GHz in C-band, 99.98% at 9.47 GHz in X-band, and 99.62% absorptivity at 14.40 GHz in Ku-band, respectively. The dimension of $7.2 \times 7.2 \times 0.8$ mm^3 make the structure super compact having ultrathin profile. The unit cell thickness is $0.012\lambda_{lowest}$ (where, λ_{lowest} is at a lowest cut-off frequency). The composition of proposed absorber is an outermost ring, split ring, innermost ring, and square line with triangle patches at the boundary. The rings and internal patches are instrumental in providing close to perfect absorption at designated frequencies. The transverse electric, and transverse magnetic polarized waves analysis shows that absorptivity remains insensitive till 45° and exhibits matched absorption. Moreover, the practical utility of structure is signified by stability of the proposed design which validated with the different incident (for TE and TM modes) angles. Finally, the close agreement is witnessed in behaviour of simulated results and measured results.

The objective of a wideband absorber is attained through a systematic approach to designing and developing a metamaterial-based ultra-wideband absorber with a prime focus on attaining more than 99% absorption for ultra-wideband covering a bandwidth of 8.23 GHz from 11.17 GHz to 19.40 GHz. However, the proposed absorber achieves more than 95% absorption from 9.77 GHz to 20.87 GHz, covering a bandwidth of 11.10 GHz. The structure provides a full-width half maximum (FWHM) of 17.68 GHz from 6.67 GHz to 24.35 GHz. The proposed absorber demonstrating polarisation insensitive behaviour till 45° and broad incident angle stability affirm that the proposed absorber stands up for incorporation in practical applications. The attainment of the highest form of absorption with minimized dimension is instrumental in its usability in those engineering applications having dimensional constraints and requiring absorption in its working, and one such application is a practical MIMO (multiple-input and

multiple output) setup that demands both dimensional aspect and highest form of absorption in subduing coupling among various antenna elements in practical MIMO configuration. The work succeeded in incorporating a designed absorber in a practical MIMO setup with the attainment of good isolation. The work with practical relevance in communication is presented through a design of isolation improved MIMO antenna having two elements working in 4.04 GHz to 5.48 GHz operating band. The two antenna elements MIMO configuration is designed so that elements are maintained at two extreme edges of a substrate having the dimension of 100 × 50 × 0.8 mm^3. The incorporation of a metasurface-based isolator between MIMO antenna elements provides exceptional isolation (< -23dB) for practical mobile and wireless applications. The major deterrent to exploiting the optimum performance of the MIMO antenna is factors involving mutual coupling of unwanted fields between MIMO antenna elements. The work is an attempt to design and develop MIMO elements with a metasurface-based isolator (acting as absorber) clearly with an intention to provide high order optimum isolation levels between two antenna elements. The insight to the high isolation level is signified through surface current distribution by visualising impact of metasurface-based isolator in MIMO configuration. The technical parameters like spatial/pattern diversity and envelope correlation coefficient clearly testify the suitability for MIMO based mobile application in microwave regime and thereby concluding the work with the attainment of the goal for which the work was carried upon.

6.2 Future Scope of the Work

The work can further be extended with equivalent circuit modelling. The survival of the human race is possible through the ability of human race to continuously evolve for betterment in different circumstances and for the betterment of the human race researchers and scientists always strive for achieving better results. The work on metamaterial area extended with its incorporation in various engineering applications which started with single and dual band and then extended to multi-band and from multi-band to wideband.

The future scope of work in multi-band absorber section will be to realize mobile equipment with layer composition designed in such a fashion so as to provide complete absorption in specific bands thereby providing not only the highest form of isolation but provide protection of human intervention in an undesired radiation environment. The work can be extended to the realization of smart absorbers, which can change their normalized impedance in real-time based on feedback received in accordance with radiations.

The wideband section can extend to the attainment of perfect absorption in the infinite band, ideally providing all band absorption (especially in communication spectrum). The concept is an extension of the realization of a dynamically controlled fabricated device in response to an infinite band of incoming radiation, thereby completely isolating the reference area under observation. The human race will be benefited with the realization of space that is totally isolated from impact from radiations of the ideally infinite band. The impact of radiation on the human race is a subject of research, and a completely isolated reference section will aid a true comparative analysis of the impact of radiation on the human race, which can only be realized when the impact of any form of radiation is somehow isolated. The study will surely be a guiding force for the future and survival of the human race.

[1] N. Engheta, and R. Ziolkowski, *Metamaterials: Physics and engineering explorations*. John Wiley and Sons, 2006.

[2] K. Y. Kane, "Numerical Solution of Initial Boundary Value Problems Involving maxwell's Equations in Isotropic media," *IEEE Transactions on Antennas Propaga*tion, vol. 14, no.3, pp. 302-307, 1966.

[3] N. Engheta, "Thin absorbing screens using metamaterial surfaces," *IEEE Antennas and Propagation* Society International Symposium, vol. 2, pp. 392-395, 2002.

[4] I. A. Buriak, V. O. Zhurba, G. S. Vorobjov, V. R. Kulizhko, O. K. Kononov, and O. Rybalko, "Metamaterials: theory, classification and application strategies," *Journal of Electronics and Nano Physics*, vol. 8, pp. 11, 2016.

[5] N. I. Landy, S. Sajuyigbe, J. J. Mock, D. R. Smith, and W. J. Padilla, "A perfect metamaterial absorber," *Physical Review Letters*, vol. 100, pp. 207402-10, 2008.

[6] A. Ali, A. Mitra, and B. Aissa, "Metamaterials and Metasurfaces: A Review from the Perspectives of Materials, Mechanisms and Advanced Metadevices," *Nanomaterials*, vol. 12, no. 6, pp. 1-32, 2022.

[7] V. G. Veselago and P. N. Labedev, "The electrodynamics of substances with simultaneously negative values of ε and μ," *Soviet Physics Uspekhi*, vol. 10, no. 4, pp. 509-514, 1968.

[8] H. Tao, N. I. Landy, C. M. Bingham, X. Zhang, R. D. Averitt, and W. J. Padilla, "A metamaterial absorber for the terahertz regime: Design, fabrication and characterization," *Optics Express*, vol. 16, pp. 7181–7188, 2008.

[9] Y. Avitzour, Y. A. Urzhumov, and G. Shvets, "Wide-angle infrared absorber based on a negative- index plasmonic metamaterial," *Physical Review B*, vol. 79, pp. 0451311-7, 2009.

[10] R. Mahajan, and V. Vyas, "Verification, enhancement and mathematical analysis of EBG structure using complex geomsetrical shapes and eigenmode analysis approach," *SN Appl. Sci.*, vol. 2, no. 30, pp. 1-8, 2019.

[11] Kazemzadeh, and A. Karlsson, "Capacitive circuit method for fast and efficient design of wideband radar absorber," *IEEE Transactions on Antennas and Propagation*, vol. 57, no. 8, pp. 2307–2314, 2009.

[12] F. Costa, S. Genovesi, and A. Monorchio, “A frequency selective absorbing ground plane for low-RCS microstrip antenna arrays,” *Progress In Electromagnetics Research*, vol. 126, pp. 317–332, 2012.

[13] F. Costa, and A. Monorchio, “A frequency selective radome with wideband absorbing properties,” *IEEE Transactions on Antennas Propagation*, vol. 60, no. 6, pp. 2740–2747, 2012.

[14] S. Yagitani, K. Katsuda, M. Nojima, Y. Yoshimura, and H. Sugiura, “Imaging radio-frequency power distributions by an EBG absorber,” *IEICE Transactions Communications*, vol. E94-B, no. 8, pp. 2306–2315, 2011.

[15] E. Rephaeli, and S. Fan, “Absorber and emitter for solar thermo photovoltaic systems to achieve efficiency exceeding the shockley-queisser limit,” *Optics Express*, vol. 17, pp. 15145–151, 2009.

[16] H. T. Chen, W. J. Padilla, M. J. Cich, A. K. Azad, R. D. Averitt, and A. J. Taylor, “A metamaterial solid state terahertz phase modulator,” *Nature Photon*, vol. 3, pp. 148–151, 2009.

[17] T. Maier, and H. Bruckl, “Wavelength-tunable microbolometers with metamaterial absorbers,” *Optics Letters*, vol. 34, no. 19, pp. 3012, 2009.

[18] X. Liu, T. Tyler, T. Starr, A. F. Starr, N. M. Jokerst, and W. J. Padilla, “Taming the blackbody with infrared metamaterials as selective thermal emitters,” *Physical Review Letters*, vol. 107, no. 4, pp. 045901, 2011.

[19] W. W. Salisbury, “Absorbant body for electromagnetic waves,” US Patent, 2599944, filed 11 May 1943, granted June 10, 1952.

[20] B. A. Munk, P. Munk, and J. Pryor, “On Designing Jaumann and Circuit Analog Absorbers (CA Absorbers) for Oblique Angle of Incidence,” *IEEE Transactions on Antennas and Propagation*, vol. 55, pp. 186-193, 2007.

[21] B. Chambers, and A. Tennant, “Active Dallenbach radar absorber,” in *Proc. IEEE Antennas Propag. Soc. Int. Symp.*, Albuquerque, NM USA, 2006, pp. 381-384.

[22] E. Popov, D. Maystre, R. C. McPhedran, M. Neviere, M. C. Hutley, and G.H. Derrick, “Total absorption of unpolarized light by crossed gratings,” *Optics Express*, vol. 16, pp. 6146-6155, 2008.

[23] D. Sjoberg, “Analysis of wave propagation in stratified structures using circuit analog, with application to electromagnetic absorbers,” *European Journal of Physics*, vol. 29, pp. 721–734, 2008.

[24] G. T. Ruck, D. E. Barrick, and W. D. Stuart, *Radar cross section Handbook*, vol. 2, Plenum Press, New York 1970.

[25] S. Kuznetsov, A. Paulish, A. Gelfand, P. Lazorskiy, and V. Fedorinin, "Bolometric THz-to-IR converter for terahertz imaging," *Applied Physics Letters*, vol. 99, pp. 023501-07, 2011.

[26] H. Mosallaei, and K. Sarabandi, "A one-layer ultra-thin meta-surface absorber," *IEEE Antennas and Propagation Society International Symposium*, 2005, pp. 615-618.

[27] S. Simms, and V. Fusco, "Tunable thin radar absorber using artificial magnetic ground plane with variable backplane," *Electronic Letters*, vol. 42, no. 21, pp. 1197–1198, 2006.

[28] C. Mias, and J. H. Yap, "A varactor-tunable high-impedance surface with a resistive-lumped-element biasing grid," *IEEE Transactions on Antennas and Propagation*, vol. 55, no. 7, pp. 1955– 1962, 2007.

[29] A. Noor, Z. Hu, H. H. Ouslimani, and A. Priou, "Wideband thin resistive metamaterial radar absorbing screen," *IEEE International Symposium on Antennas and Propagation*, pp. 1–5, 2009.

[30] B. A. Munk, *Frequency Selective Surfaces*. John Wiley & Sons, New York 2000.

[31] W. H. Emerson, "Electromagnetic wave absorbers and anechoic chambers through the years," *IEEE Transactions on Antennas and Propagation*, vol. 21, no.4, pp. 484–490, 1973.

[32] Q. Teruel, H. Chen , A. Rubio, G. Gok, A. Grbic, G. Minatti, E. Martini, S. Maci, G. Eleftheriades, M. Chen *et al.*, " Roadmap to metasurfaces ," *Journal of Optics*, vol. 21, no. 073002, pp. 1-44, 2019

[33] W. Zhu, *Electromagnetic Metamaterial Absorbers: From Narrowband to Broadband*. New York: IntechOpen, 2018, ch.7.

[34] A. Elakkiya, S. Radha, B. Sreeja, and E. Manikandan, "Terahertz single dual multi-band metamaterial absorber," Pramana – *J Phys*, vol.95, no.163, pp. 1-8, 2021.

[35] K. P. Kaur, and T. Upadhyaya, "Investigation of polarization-independent wide-angle metamaterial inspired ISM-band absorber," *Indian Journal of Pure & Appl. Phys.*, vol. 57, no. 1, pp.63-73, 2019.

[36] K.P Kaur, and T. Upadhyaya, "Performance evaluation of wide-angle ultrathin microwave metamaterial absorber with polarization independence," *Advanced Electromagnetics*, vol. 7, no. 4, pp. 71-77, 2018.

[37] F. Bagci, and F. Medina, "Design of a dual-band metamaterial absorber in WLAN bands with high stability over incidence angle and polarization," *10th International Congress on Advanced Electromagnetic Materials in Microwaves and Optics (METAMATERIALS)*, 2016, pp. 46-48.

[38] N. Mishra, K. Kumari, and R. Chaudhary, "A dual resonator-based polarisation-independent dual-band metamaterial absorber," *International Journal of Electronics Letters, Taylor & Francis Journals*, vol. 7, no. 3 pp. 338-351, 2018.

[39] P. Jain, A. Singh, J. Pandey, S. Bansal, N. Gupta, A. Singh, S. Kumar, and N. Sardana, "Ultra-thin and Dual Band Metamaterial Absorber for Terahertz Applications," *2018 6th Edition of International Conference on Wireless Networks & Embedded Systems (WECON)*, 2018, pp. 148-151.

[40] T. Wu, Y. Ma, J. Chen, and L. Wang, "Triple-band polarization-insensitive metamaterial absorber with low profile," *International Journal RF and Microwave Computer Aided Engineering*, vol. 30, no. 9, pp. 1-9, 2020.

[41] K.P. Kaur, T. Upadhyaya, M. Palandoken, and C. Gocen, "Ultrathin dual-layer triple-band flexible microwave metamaterial absorber for energy harvesting applications," *International Journal RF and Microwave Computer Aided Engineering*, vol. 29, no. 1, pp. 1-7, 2019.

[42] K. Kumari, N. Mishra, and R.K.Chaudhary, "Wide-Angle Polarization Independent Triple Band Absorber Based on Metamaterial Structure for Microwave Frequency Applications," *Progress In Electromagnetics Research-C (PIER-C)*, vol. 76, pp. 119-127, 2017.

[43] S. Bhattacharyya, S.Ghosh, D. Chaurasiya D, and K.V. Srivastava, "A Broadband Wide Angle Metamaterial Absorber for Defence Applications," *IEEE International Microwave and RF Conference (IMaRC)*, Bangalore, 2014, pp. 33-36.

[44] S. Kalraiya, R. K. Chaudhary, and M. A. Abdalla, "Design and analysis of polarization independent conformal wideband metamaterial absorber using resistor loaded sector shaped resonators," *Journal of Applied Physics*, vol. 125, no. 134904, pp. 1-10, 2014.

[45] T. T. Nguyen, and S. Lim, "Design of metamaterial absorber using Eight- Resistive-Arm Cell for simultaneous broadband a Wide-Incidence-Angle Absorption conformal wideband metamaterial absorber using resistor loaded sector shaped resonators," *Scientific Reports*, vol. 8, no. 6633, 2018.

[46] P. Munaga, S. Ghosh, S. Bhattacharyya, and K.V. Srivastava, "A fractal-based compact broadband polarization insensitive metamaterial absorber using lumped resistors," *Microwave and Optical Technology Letters*, pp. 343-347, 2016.

[47] D.U Zhiqiang, L. Liang, T. Cai, X. Wang, Q. Zhang, T. Deng, B. Wu, R. Mao, and D. Wang, "Ultra-light planar meta-absorber with wideband and full-polarization properties," *Optic Express*, vol. 29, pp. 6434-6444, 2021.

[48] J. H. Winters, "On the capacity of radio communication systems with diversity in a Rayleigh fading environment," *IEEE Journal on Selected Areas Commun*ication, vol. SAC-5, pp. 871-878, 1987.

[49] G. Foschini, and M. Gans, "On limits of wireless communication in a fading environment when using multiple antennas," *Wireless Personal Communication*, pp. 311-335, 1998.

[50] W. Ni, Y. Meng, W. Wang, and G. Shen, "Experimental verification of decoupling on channel capacity for MIMO communications," *Journal of Electromagnetic Waves and Applications*, vol. 26, pp. 1986-19992, 2012.

[51] M. Agarwal, A. Behera, and M. Meshram, "MIMO-configured WLAN access point antenna with high port isolation," *Journal of Electromagnetic Waves and Applications*, vol. 3, pp. 1-12, 2017.

[52] Y. L. Ban, Z. X. Chen, Z. Chen, K. Kang, and L. Li, "Decoupled heptaband antenna array for WWAN/LTE smartphone applications," *IEEE Antennas Wireless Propagation Letters*, vol. 13, pp. 999-1002, 2014.

[53] H. Singh, G. Pandey, P. Bharti, and M. Meshram, "A compact dual-band diversity antenna for WLAN applications with high isolation," *Microwave and Optical Technology Lett*ers, vol. 57, pp. 906-912, 2015.

[54] M. Meshram, R. Animeh, A. Pimpale, and N. Nikolova, "A novel quad-band diversity antenna for LTE and Wi-Fi applications with high isolation," *IEEE Transactions on Antennas and Propagation*, vol. 60, pp. 4360-4371, 2012.

[55] H. Li, J. Xiong, and S. He, "A compact planar MIMO antenna system of four elements with similar radiation characteristics and isolation structure," *IEEE Antennas Wireless Propagation Letters*, vol. 8, pp. 1107-1110, 2009.

[56] C.H. Lee, S. Y. Chen, and P. Hsu, "Integrated dual planar inverted-F antenna with enhanced isolation," *IEEE Antenna Wireless Propagation Lett*ers, vol. 8, pp. 963-965, 2009.

[57] M.A.J. Al-Hasan, T.A. Denidni, and A.R. Sebak, "Millimeterwave compact EBG structure for mutual coupling reduction applications," *IEEE Transactions on Antennas and Propagation*, vol. 63, pp. 823-828, 2015.

[58] Z. Xu, Q. Zhang, and L. Guo, "A compact 5G decoupling MIMO antenna based on split-ring resonators," *Hindawi International Journal of Antennas and Propagation*, Article ID 3782528, 2019.

[59] Z. Ren, and A. Zhao, "Dual-band MIMO antenna with compact self-decoupled antenna pairs for 5G mobile applications," *IEEE Access*, vol. 7, pp. 82288-82296, 2019.

[60] J. Hu, and J. Li, "Compact microstrip antennas using CSRR structure ground plane," *Microwave and Optical Technology Letters*, vol. 56, no.1, pp.117-20, 2014.

[61] A. Malathi, and D. Thiripurasundari, "Review on Isolation Techniques in MIMO Antenna Systems," *Indian Journal of Science and Technology*, vol. 9, no. 35, pp. 1-10, 2016.

[62] Y. Cheng, and H. Yang, "Design, simulation and measurement of metamaterial absorber," *Microwave and Optical Technology letters*, vol. 52, no. 4, pp. 877-880, 2010.

[63] M. Li, H. Yang, X. Hou, Y. Tian, D. Hou, "Perfect metamaterial absorber with dual bands," *Progress In Electromagnetics Research*, vol. 108, pp. 37–49, 2010.

[64] W. Zhu, and X. Zhaoa "Metamaterial absorber with random dendritic cells," *European Physical Journal of Applied Physics*, vol. 50, 2010.

[65] J. Sun, L. Liu, G. Dong, and J. Zhou, "An extremely broad band metamaterial absorber based on destructive interference," *Optic express*, vol. 19, no. 22, pp. 21155, 2011

[66] H. Li, L. Yuan, B. Zhou, X. Shen, and Q. Cheng, "Ultrathin multiband gigahertz metamaterial absorbers," *Journal of Applied. Physics*, vol. 110, no.1, pp. 014909-12, 2011.

[67] L. Huang, and H. Chen, "Multi-band and polarization insensitive metamaterial absorber," *Progress In Electromagnetics Research*, vol.113, pp. 103-110, 2011.

[68] H. Lee, and H. Lee, "A Method for Extending the Bandwidth of Metamaterial Absorber," *Hindawi Publishing Corporation International Journal of Antennas and Propagation*, Article ID 859429, 2012.

[69] M. Abdalla, and L. Hu, "on the study of development of X-band metamaterial radar absorber," *Journal of Advanced Electromagnetics*, vol. 1, no. 3, pp. 94-98, 2012.

[70] Y. Cheng, Y. Nie, and R. Gong, "Metamaterial absorber and extending absorbance bandwidth based on multi-cross resonators," *Journal of Applied Physics*, pp. 483–488, 2013.

[71] Y. Feng, B. Zhu, H. Yuan, J. Zhao, and T. Jiang, "Controllable metamaterial absorbers," *IEEE International Workshop on Electromagnetics, Applications and Student Innovation Competition*, pp. 13-15, 2013.

[72] S. Bhattacharyya, S. Ghosh, and K. Srivastava, "Bandwidth-enhanced metamaterial absorber using electric field–driven LC resonator for airborne radar applications," *Microwave and Optical Technology Letters*, vol. 55, no. 9, pp. 2131-2137, 2013.

[73] D. Wen, H. Yang, Q. Ye, M. Li, L. Guo, and J. Zhang, "Broadband metamaterial absorber based on a multi-layer structure," *IOP publishing Physica Scripta*, vol. 88, pp. 1-7, 2013.

[74] J.Y Lee, M. Yoo, and S. Lim, "A Study of Ultra-Thin Single Layer Frequency Selective Surface Microwave Absorbers with Three Different Bandwidths using Double Resonance," *IEEE Transactions On Antennas And Propagation*, vol. 63, pp. 221-230, 2013.

[75] S. Ghosh, S. Bhattacharyya, and K. V. Srivastava, "Bandwidth-enhancement of an ultrathin polarization insensitive metamaterial absorber," *Microwave and Optical Technology Letters*, vol. 56, no. 2, pp. 350-355, 2014.

[76] D. Shrekenhamer, W. Chen, and W. Padilla, "Liquid crystal tunable metamaterial absorber," *Physical review letters*, vol. 110, no. 177403, pp. 1-5, 2013.

[77] J. Park, P. Tuong, J. Rhee, K. Kim, W. Jang, E. Choi, L. Chen, and Y. Lee, "Multi-band metamaterial absorber based on the arrangement of donut-type resonators," *Optics Express*, vol. 21, no. 8, pp. 1-12, 2013.

[78] F. Dincer, M. Karaaslan, E. Unal, and C. Saba, "Dual-band polarization independent metamaterial absorber based on omega resoanator and octa-starstrip configuration," *Progress In Electromagnetics Research*, vol. 141, pp. 219–231, 2013.

[79] O. Ayop, M. Rahim, and N. Murad, "Double layer circular ring metamaterial absorber for dual-directional application at 10 GHz," *IEEE International RF and Microwave Conference (RFM)*, Penang Malaysia, 9-11 Dec. 2013.

[80] B. Ma, S. Liu, B. Bian, X. Kong, H. Zhang, Z. Mao, and B. Wang, "Novel three band microwave metamaterial absorbers," *Journal of Electromagnetic waves and application*, vol. 28, no. 12, pp. 1478-1486, 2014.

[81] A. Bhattacharya, S. Bhattacharya, S. Ghosh, D. Chaurasiya, and K. Shrivastava, "An ultrathin pentaband polarization insensitive compact metamaterial absorber for airborne radar applications," *Microwave and Optical Technology letters,* vol. 57, no. 11, pp. 2519-2524, 2015.

[82] H. Zhai, C. Zhan, Z. Li, and C. Liang, "A Triple-Band Ultrathin Metamaterial Absorber with Wide-Angle and Polarization Stability," *IEEE Antennas and Wireless Propagation Letters*, vol. 14, pp. 241-244, 2015.

[83] S. Ramya, and I. Rao, "Design of Polarization-Insensitive Dual Band Metamaterial Absorber," *Progress In Electromagnetics Research,* vol. 50, pp. 23–31, 2016.

[84] K. Ozden, O. Yucedag, and H. Kocer "Metamaterial based broadband RF absorber at X-band," *International Journal of Electronics and Communication Elsevier*, vol. 70, pp. 1062–1070, 2016.

[85] M. Aggarwal, A. Behara, and M. Meshram, "Dual resonating C-band with enhanced bandwidth and broad X-band metamaterial absorber," *Journal of Applied Physics A,* vol. 166, pp. 1-9, 2016.

[86] M. Ahmed, and A. Montaser, "Design of metamaterial absorber for all bands from microwave to terahertz ranges," *International Journal of Advanced Research in Electronics and Communication Engineering*, vol. 5, no. 5, pp. 1475-8, 2016.

[87] J. Tak, Y. Jin, and J. Choi, "A dual-band metamaterial microwave absorber," *Microwave and Optical Technology letters*, vol. 58, no. 9, pp. 2052-57, 2016.

[88] K. Ozden, A. Ozer, O. Yucedag, and H. Kocer, "Polarization-independent metamaterial based dual band absorber for stealth applications in microwave bands," *Istanbul University IU-JEEE*, vol. 16, no. 2, pp. 3001-3006, 2016.

[89] G. Sen, S. Islam, A. Banerjee, and S. Das, "Broadband perfect metamaterial absorber on thin substrate for X-band and Ku-band applications," *Progress In Electromagnetics Research C*, vol. 73, pp. 9–16, 2017.

[90] A. Agrawal, M. Misra, and A. Singh, "Oblique incidence and polarization insensitive multiband metamaterial absorber with quad paired concentric continuous ring resonators," *Progress In Electromagnetics Research M*, vol. 60, pp. 33–46, 2017.

[91] D. Marathe, and K. Kulat, "A compact triple-band negative permittivity metamaterial for C, X-band applications," *Hindawi International Journal of Antennas and Propagation*, vol. 2017, pp. 1-13, 2017.

[92] W. Xin, Z. Binzhen, W. Wanjun, W. Junlin, and D. Junping, "Design and characterization of an ultrabroadband metamaterial microwave absorber," *IEEE Photonics Journal*, vol. 9, no. 3, 2017.

[93] F. Bagci, and F. Medina, "Design of a wide-angle, polarization-insensitive, dual-band metamaterial-inspired absorber with the aid of equivalent circuit model," *Springer Journal of Computational Electronics,* vol, 16, no. 3, pp. 913-921, 2017.

[94] M. Naser, A. Niaa, M. Toolabia, and S. Heydarib, "Microwave metamaterial absorber based on jerusalem cross with meandered load for bandwidth enhancement," *Elsevier Optik Journal*, vol. 140, pp. 515-523, 2017.

[95] S. Thummaluru, N. Mishra, and R. Chaudhary, "Design and analysis of an ultrathin triple-band polarization independent metamaterial absorber," *International Journal of Electronics and Communication*, vol. 82, pp. 508-515, 2017.

[96] J. Tak, E. Jeong, and J. Choim, "Metamaterial absorbers for 24-GHz automotive radar applications," *Journal of Electromagnetic Waves and Applications*, pp. 18-23, 2017.

[97] N. Mishra, D. Chaudhary, R. Chowdhury, K. Kumari, and R. Chaudhary, "An Investigation on Compact Ultra-Thin Triple Band Polarization Independent Metamaterial Absorber for Microwave Frequency Applications*," IEEE Access*, vol. 5, pp. 4370-76, 2017

[98] R. Sekar, and S. Rao, "An ultra-thin compact wideband metamaterial absorber," *Radio Engineering*, vol. 27, no. 2, pp. 364-73, 2018.

[99] C. Sabah, B Mulla, H. Altan, and L. Ozyuzer, "Cross-like terahertz metamaterial absorber for sensing applications," *Paramana Journal of Physics,* vol. 91, pp. 17-21, 2018.

[100] X. Huang, C. Lu, C. Rong, S. Wang, and M. Liu, "Wide angle of incidence-insensitive polarization-independent THz metamaterial absorber for both TE and TM mode based on plasmon hybridizations," *MDPI Journal of Materials*, vol. 11, no. 671, pp. 1-12, 2018.

[101] H. Cao, M. Shan, T. Chao, J. Lei, L. Yang, and X. Tan, "Triple-Band Polarization Independent Ultrathin Metamaterial Absorber," *Progress In Electromagnetics Research M,* vol. 77, pp. 93–102, 2019.

[102] M. Amiri, F. Tofigh, N. Shariati, J. Lipman, and M. Abolhasan, "Wide-angle metamaterial absorber with highly insensitive absorption for TE and TM modes," *Scientific Reports*, vol. 10, pp. 1-12, 2020.

[103] H. Wu, S. Ji, J. Zhao, C. Jiang, and H. Dai, “Design and Analysis of a Five-Band Polarization-Insensitive Metamaterial Absorber,” *Hindawi International Journal of Antennas and Propagation*, vol. 2020, no. 8827517, pp. 1-12, 2020.

[104] H. Jaradat, “Ultra-thin single band metamaterial inspired absorber with suppressed higher order modes for terahertz applications,” *Optical Material Express*, vol. 11, no. 10, pp. 3341-3354, 2021.

[105] M. Hakim, T. Alam, M. Islam, M. Baharuddin, and A. Alzamil, “Quad-Band Polarization-Insensitive Square Split-Ring Resonator (SSRR) with an Inner Jerusalem Cross Metamaterial Absorber for Ku- and K-Band Sensing Applications,” *Sensors*, vol. 22, no.4489, pp. 1-20, 2022.

[106] B. Wang, C. Xu, and H. Zhou, “Realization of broadband terahertz metamaterial absorber using an antisymmetric resonator consisting of two mutually perpendicular metallic strips,” *APL Materials*, vol. 10, no. 050701, pp. 1-8, 2022.

[107] S. Banerjee, P. Dutta, A. Jha, P. Tripathi, A. Srinivasulu, B. Appasani, and C. Ravariu, “A Triple Band Highly Sensitive Refractive Index Sensor Using Terahertz Metamaterial Perfect Absorber,” *Progress In Electromagnetics Research M*, vol. 107, pp. 13-23, 2022.

[108] S. Gu, B. Su, and X. Zhaoa, “Planar isotropic broadband metamaterial absorber,” *Journal of Applied Physics*, vol. 114, pp. 1637021-6, 2013.

[109] G. D. Wang, M. H. Liu, X. W. Hu, L. H. Kong, L.L. Cheng, and Z.Q. Chen, “Broadband and ultra-thin terahertz metamaterial absorber based on multi-circular patches,” *The European Physical Journal B*, vol. 86, pp. 304-313, 2013.

[110] F. Dincer, O. Akgol, M. Karaaslan, E. Unal, and C. Saba, “Polarization angle independent perfect metamaterial absorbers for solar cell applications in the microwave, infrared, and visible regime,” *Progress In Electromagnetics Research*, vol. 144, pp. 93–101, 2014.

[111] S. Bhattacharyya, S. Ghosh, D. Chaurasiya, and K.Srivastava, “Bandwidth-enhanced dual-band dual-layer polarization-independent ultra-thin metamaterial absorber,” *Journal of Applied physics A*, pp. 207-15, 2014.

[112] G. Wang, J. Chen, X. Hu, Z. Chen, and M. Liu, “Polarization-insensitive triple-band microwave metamaterial absorber based on rotated square rings,” *Progress In Electromagnetics Research*, vol. 145, pp. 175–183, 2014.

[113] B. Wang, S. Liu, B. Bian, Z. Mao, X. Liu, B. Ma, and L. Chen, "A novel ultrathin and broadband microwave metamaterial absorber," *Journal of Applied Physics*, vol. 116, pp. 0945041-0945047, 2014.

[114] O. Ayop, M. Kamal, A. R. Noor, A. Murad, and N. Asmawati, "Wideband polarization-insensitive metamaterial absorber with perfect dual resonances," *Applied Physics A*, vol. 316, pp. 4-7, 2015.

[115] M. Agarwal, and M. Meshram, "X-band Metamaterial Absorber with Dual band / Broadband Absorption Characteristics," *2015 IEEE MTT-S International Microwave and RF Conference (IMaRC)*, 2015, pp. 121-124.

[116] Y. Song, J. Ding, and C. Guo, "A semi-analytical numerical method for fast metamaterial absorber design," *AIP Advances*, vol. 5, no. 9, pp. 971081-11, 2015.

[117] X. Kong, J. Xu, J. Jun, and S. Liu, "Broadband and conformal metamaterial absorber," *Frontier of Optoelectronics*, vol. 10, no. 2, pp. 124–131, 2017.

[118] D. Lee, H. Jeong, and S. Lim, "Electronically switchable broadband metamaterial absorber," *Scientific Reports, Nature*, pp. 1-10, 2017.

[119] D. Sood, and C. Tripathi, "A compact ultrathin ultra-wideband metamaterial microwave absorber," *Journal of Microwaves, Optoelectronics and Electromagnetic applications*, vol. 16, no.2, pp. 514-528, 2017.

[120] H. Huang, H. Xia, W. Xie, Z. Guo, H. Li, and D. Xie, "Design of broadband grapheme metamaterial absorbers for permittivity sensing at mid-infrared regions," *Scientific Reports Nature*, pp. 1-10, 2018.

[121] F. Alkurt, O. Altinatus, M. Bakir, A. Tamer, F. Karadag, M. Bagmanci, M. Karaaslan, E. Unal, and O. Akgol, "Octagonal shaped metamaterial Absorber Based Energy Harvester," *Journal of Materials science*, vol. 24, no. 3, 2018.

[122] L. Lei, S. Li, H. Huang, K. Tao, and P. Xu, "Ultra-broadband absorber from visible to near-infrared using plasmonic metamaterial," *Optics Express*, vol. 26, no. 5, 2018.

[123] B. Wang, C. Tang, Q. Niu, Y. He, and R. Chen, "A broadband terahertz metamaterial absorber enabled by the simple design of a rectangular shaped resonator with an elongated slot," *Nanoscale*, vol. 1, pp. 3621-25, 2019.

[124] P. Ranjan, A. Choubey, S. Mahato, R. Sinha, and C. Barde, "A novel ultrathin wideband metamaterial absorber for X-band applications," *Journal of Electromagnetic Waves and applications*, vol. 33, no. 17, pp. 2341-2353, 2019

[125] G. Zhang, J. Gao, X. Cao, H. Yang, and L. Jidi, “An Ultra-Thin Low-Frequency Tunable Metamaterial Absorber Based on Lumped Element,” *Radioengineering*, vol. 28, no. 3, pp. 579-584,2019.

[126] L. Qi, and C. Liu, “Broadband multilayer graphene metamaterial absorbers,” *Optical Materials Express*, vol. 9, no. 3, pp. 1298-1309, 2019.

[127] P. Nochain, and Z. Atlasbaf, “A Novel Single Layer Ultra-Wideband Metamaterial Absorber,” *Progress In Electromagnetics Research Letters*, vol. 93, pp. 107–114, 2020.

[128] C. Barde, A. Choubey, and R. Sinha, “Wideband metamaterial absorber for Ku and K band applications,” *Journal of Applied Physics*, vol. 126, no. 175104, pp. 1-9,2020

[129] L. Wang, D. Xia, Q. Fu, X. Ding, and Y. Wang, “A Switchable Ultra-Wideband Metamaterial Absorber with Polarization-Insensitivity and Wide-incident Angle at THz Band,” *Frontiers in Materials*, vol. 8, no. 729495, pp. 1-6,2021.

[130] Z. Luo, S. Ji, J. Zhao, and H. Dai, “A multiband metamaterial absorber for GHz and THz simultaneously,” *Results in Physics*, vol. 30, no. 104893, pp. 1-8, 2021.

[131] Y. Kim, P. Park, J. Jo, J. Lee, L. Jeong, J. Shin, J. Lee, and H. Lee, “Ultrawideband electromagnetic metamaterial absorber utilizing coherent absorptions and surface plasmon polaritons based on double layer carbon metapatterns,” *Scientific Reports*, vol. 11, no. 23045, pp. 1-13, 2021.

[132] M. Kaur, and H. Singh, “Experimental verification of super-compact ultra-wideband (UWB) polarization and incident angle-independent metamaterial absorber,” *International Journal of Microwave and Wireless Technologies*, vol. 13, no. 8, pp. 1-11, 2021.

[133] C. Chiu, and C. Cheng, “Reduction of mutual coupling between closely-packed antenna elements,” *IEEE Transactions on Antennas and Propagation*, vol. 55, no. 6, pp.1732–1738, 2007.

[134] S. Chen, Y. Wang, and J. Chung, “A decoupling technique for increasing the port isolation between two strongly coupled antennas,” *IEEE Transactions on Antennas and Propagation*, vol. 56, no.12, pp. 3650–3658, 2008.

[135] H. Wang, D. Fang, and X. Wang, “Mutual coupling reduction between two microstrip patch antennas by using the parasitic elements,” *2008 Asia-Pacific Microwave Conference*, 2008, pp. 1-4.

[136] R. M. Sharma, A. Gautam, N. Agarwal, and N. Singh, "Design of MIMO planar antenna at 24 GHz band for radar, communication and sensors applications", International Journal of Electronics and Communication,vol.136,no.153747,pp.1-8,2021.

[137] H. S. Lee, and H. M. Lee, "Isolation improvement between loop antennas with absorber cells," *IEEE International Symposium on Antennas and Propagation (APSURSI)*, 2011, pp. 1735-1738.

[138] S. Su, C. Lee, and F. Chang, "Printed MIMO-Antenna System Using Neutralization-Line Technique for Wireless USB dongle application," *IEEE Transactions on Antennas Propagation*, vol. 60, no. 2, pp. 456–463, 2012.

[139] K. Lin, C. Wu, and T. Ma, "Novel Dual Band decoupling network for two-element closely spaced array using synthesized microstrip lines," *IEEE Transactions on Antenna and Wave Propogation*, vol. 60, no.11, pp. 5118-5128, 2012.

[140] Y. Li, W. Li, C. Liu, and T. Jiang, "Two UWB-MIMO antennas with high isolation using sleeve coupled stepped impedance resonators," *2012 IEEE Asia-Pacific Conference on Antennas and Propagation,* 2012, pp. 21-22.

[141] D. Margaret, M. Subasree, S. Susithra, S. Keerthika, and B. Manimegalai, "Mutual coupling reduction in MIMO antenna system using EBG structures," *2012 International Conference on Signal Processing and Communications (SPCOM)*, 2012, pp. 1-5.

[142] X. Zhou, X. Quan, and R. Li, "A dual-broadband MIMO antenna system for GSM/ UMTS/LTE and WLAN handsets," *IEEE Antennas Wireless Propagation Letters,* vol. 11, pp. 551-554, 2012.

[143] T. Dabas, D. Gangwar, B. Kanaujia, and A. Gautam, "Mutual coupling reduction between elements of UWB MIMO antenna using small size uniplanar EBG exhibiting multiple stop bands" *International Journal of Electronics and Communication,* vol. 93, pp. 32-38, 2018

[144] W. Yu, and Q. Chu, "Dual-band multiple input multiple output antenna with slitted ground," Microwaves, Antennas and Propagation, vol.8, no.13, pp. 1007-1013,2014.

[145] H. Singh, B. Meruva, G. Pandey, P. Bharti, and M. Meshram, "Low mutual coupling between MIMO antennas by using two folded shorting strips," *Progress In Electromagnetics Research B,* vol. 53, pp. 205-221, 2013.

[146] A. Suntives, and R. Abhari, "Miniaturization and isolation improvement of a multiple-patch antenna system using electromagnetic bandgap structures," *Microwave and Optical Technology Letters*, vol. 55, no. 7, pp. 1609–1612, 2013.

[147] R. Xia, S. Qu, Q. Jiang, P. Li, and Z. Nie, “An efficient decoupling feeding network for two-element microstrip antenna array,” *IEEE Transactions on Antennas and Wireless Propagation letters*, vol. 14, pp. 871-874, 2015.

[148] M. Benzaghata, B. Er, G. Bilgin, E. Ydin, A. Kara, “A miniaturized multi-layer microstrip antenna for linear wireless sensor network monitoring systems,” *Journal of Science*, vol. 35, no.4, pp. 875-884, 2022

[149] J. Marin, A. Bab, D. Cuence, J. Hasselbarth, R. Hashmi, K. Esselle, “High-gain lowprofile chip-fed resonant cavity antennas for millimeter-wave bands,” *IEEE Antennas and Wireless Propagation letters*, vol.18, no.11, pp. 2394-2398, 2019.

[150] M. Khan, A, Capobianco, A. Najam, I. Shoaib, E. Autizi, and M. Shafique, “Compact ultra-wideband diversity antenna with a floating parasitic digitated decoupling structure,” *IET Microwaves, Antennas and Propagation*, vol. 8, no. 10, pp. 747-753, 2014.

[151] W. Chen, and H. Lin, “LTE700/WWAN MIMO antenna system integrated with decoupling structure for isolation improvement,” *2014 IEEE Antennas and Propagation Society International Symposium (APSURSI)*, 2014, pp. 689-690.

[152] L. Liu, S. Cheung, and T. Yuk, “Compact MIMO antenna for portable UWB applications with band-notched characteristic,” *IEEE Transactions on Antennas Propag*ation, vol.63, no.5, pp. 1917-1924, 2015.

[153] K. Jha, Z. Jibran, C. Singh, S. Sharma, “4-Port MIMO antenna using common radiator on a flexible substrate for sub-1GHz, sub-6GHz, 5G NR, and Wi-Fi 6 applications,” *IEEE Open Journal of Antennas and Propagation*, vol. 2, pp. 689- 701, 2021.

[154] L. Zhao, and K. L. Wu, “A Dual-Band Coupled Resonator Decoupling Network for Two Coupled Antennas,” *IEEE Transactions on Antennas and Propagation*, vol. 63, no. 7, pp. 2843–2850, Jul. 2015

[155] T. Roshna, U. Deepak, V. Sajitha, K. Vasudevan, and P. Mohanan, “A Compact UWB MIMO Antenna With Reflector to Enhance Isolation,” *IEEE Transactions on Antennas and Propagation*, vol. 63, no. 4, pp. 1873–1877, 2015.

[156] H. Singh, G. Pandey, P. Bharti, and M. Meshram, “A low profile tri-band diversity antenna for WLAN/WiMAX/HIPERLAN applications with high isolation,” Microwave and Optical Technology Letters, vol. 57, no. 2, pp. 452-457, 2015.

[157] Y. Yu, X. Liu, G. Zhaoki, and R. Nadia, “Dual-frequency two-element antenna array with suppressed mutual coupling,” *International Journal of Antennas and Propagation*, vol. 2015, no. 912934, pp. 1-6, 2015.

[158] S. Zhang, and G. Pedersen, “Mutual coupling reduction for UWB MIMO antennas with a wideband neutralization line,” *IEEE Antennas and Wireless Propagation Letter*, vol. 15, pp. 166-169, 2015.

[159] S. Wang, and Z. Du, “Decoupled Dual-Antenna System Using Crossed Neutralization Lines for LTE/WWAN Smartphone Applications,” *IEEE Antennas and Wireless Propagation Letters*, vol. 14, pp. 523–526, 2015.

[160] J. Lee, S. Kim, and J. Jang, “Reduction of Mutual Coupling in Planar Multiple Antenna by Using 1-D EBG and SRR Structures,” *IEEE Transactions on Antennas and Propagation*, vol. 63, no. 9, pp. 4194–4198,2015.

[161] G. Zhai, Z. N. Chen, and X. Qing, “Enhanced Isolation of a Closely Spaced Four-Element MIMO Antenna System Using Metamaterial Mushroom,” *IEEE Transactions on Antennas and Propagation*, vol. 63, no. 8, pp. 3362–3370,2015.

[162] H. Singh, G. Pandey, P. Bharti, and M. Meshram, “Design and performance investigation of a low profile MIMO/Diversity antenna for WLAN/ WiMAX/ HIPERLAN applications with high isolation,” *International Journal of RF and Microwave Computer-Aided Engineering*, vol. 25, no. 6, pp. 510-521, 2015.

[163] M. Aggarwal, and M. Meshram, “Isolation improvement of 5GHz WLAN antenna array using metamaterial absorber,” *2016 URSI Asia-Pacific Radio Science Conference (URSI AP-RASC)*,2016, pp. 1050-1053.

[164] K. Wei, J. Li, L. Wang, Z. Xing, and R. Xu, “S-shaped periodic defected ground structures to reduce microstrip antenna array mutual coupling,” *Electronics Letters*, vol. 52, no. 15, pp. 1288–1290, 2016

[165] Y. Chen, and C. Chang, “Design of a four-element multiple input multiple-output antenna for compact long-term evolution small-cell base stations,” *IET Microwaves, Antennas & Propagation*, vol. 10, no. 4, pp. 385–392, 2016.

[166] A. Ibrahim, and A. Abdalla, “CRLH MIMO antenna with reversal configuration,” *AEU-International Journal of Electronics and Communications*, vol. 70, no. 9, pp. 1134-1141, 2016.

[167] R. Krishna, and R. Kumar, “A Dual-Polarized Square-Ring Slot Antenna for UWB, Imaging, and Radar Applications,” *IEEE Antennas and Wireless Propagation Letters*, vol. 15, pp. 195–198, 2016.

[168] G. Srivastava, and A. Mohan, “Compact MIMO Slot Antenna for UWB Applications,” *IEEE Antennas and Wireless Propagation Letters*, vol. 15, pp. 1057-1060, 2016

[169] A. Diallo, and C. Luxey, "Study and reduction of the mutual coupling between two mobile phone PIFAs operating in the DCS 1800 and UMTS bands*," IEEE Transaction on Antennas and Propagation*, vol. 54, no. 11, pp. 3063-3074, 2006.

[170] A. Kumar, G. Reddy, J. Padhi, R. Jawale, and S. Narayan, "Wideband, polarization independent electromagnetic wave absorber using cross arrow resonator and lumped SMD resistors for C and X band applications," *RF and Microwave Computer Aided Engineering*, vol. 32, no. 7, pp. 1-13, 2022.

[171] N. Kishore, G. Upadhyay, V. Tripathi, and A. Prakash, "Dual band rectangular patch antenna array with defected ground structure for its application," *International Journal of Electronics and Communication*, vol. 9, pp.228-237, 2018

[172] K. Suman, R. Gangwar, and V. Gangwar, "A compact, low-profile, and high performance monopulse for missle seeker," Journal of Electromagnetic Waves and Applications, August 2022, https://doi.org/10.1080/09205071.2022.2109068.

[173] S. Xu, M. Zhang, H. Wen, and J. Wang, "Deep-subwavelength Decoupling for MIMO Antennas in Mobile Handsets with Singular Medium," *Scientific Reports*, vol. 7, no. 1, pp. 12162, 2017

[174] D. Wu, S. Cheung, Q. Li, and T. Yuk, "Decoupling using diamond-shaped patterned ground resonator for small MIMO antennas," *Antennas Propagation IET Microwaves*, vol. 11, no. 2, pp. 177-183, 2017.

[175] M. Khan, A. Capobianco, A. Iftikhar, R. Shubair, D. Anagnostou, and B. Braaten, "Ultra-compact dual-polarised UWB MIMO antenna with meandered feeding lines," *Antennas Propagation IET Microwaves*, vol. 11, no. 7, pp. 997–1002, 2017.

[176] J. Li, J. Zhao, J. Liang, L. Zhong, and J. Song, "Metamaterial-Based Planar Compact MIMO Antenna with Low Mutual Coupling," *Microwave Journal*, vol.61, no.5, pp.116-126, 2018.

[177] C. Ding, X. Zhang, C. Xue, and C. Sim, "Novel Pattern-Diversity-Based Decoupling Method and its Application to Multi-Element MIMO Antenna," *IEEE Transactions on Antennas and Propagation*, vol. 66, no. 10, pp. 4976-4985, 2018.

[178] M. Rezapour, J. Mohassel, A.Keshtkar, and M.Moghadasi, "Suppression of mutual coupling in rectangular dielectric resonator antenna arrays using Epsilon-Negative metamaterials (ENG)," *Journal of Electromagnetic Waves and Applications*, vol. 33, no.9, pp. 1-13, 2019.

[179] A. Khan, S. Geng, X. Zhao, Z. Shah, M. Jan, and M. Abdelbaky, “Design of MIMO antenna with enhanced isolation technique,” *Electronics*, vol.9, no.1217, pp.1-17, 2020.

[180] D. Hadri, A. Zakriti, A. Zugairi, M. Ouahabi, and J. Aoufi, “High isolation and ideal correlation using spatial diversity in compact MIMO antenna for fifth generation applications,” *Hindawi International Journal of Antennas and Propagation*, vol. 2020, no. 2740920, pp.1-10, 2020.

[181] M. Kaur, and H. Singh, “Isolation Improvement of the MIMO PIFA using Metamaterial Absorber Array,” *2020 International Symposium on Antennas & Propagation (APSYM)*, 2020, pp. 29-31.

[182] S. Dey, S. Dey, and S. Koul, “Isolation improvement of MIMO antenna using novel EBG and hair pin shaped DGS at 5G millimetre wave band,” *IEEE Access*, vol. 9, pp. 162820-162834, 2021.

[183] R. Rajmohan, K. Vishavksenan, and R. Kalidoss, “Compact four port slot based MIMO antenna with isolation enhancement,” *International Journal of Electronics*, vol. 108, no. 7, pp. 1-12, 2021.

[184] S. Roy, A. Biswas, S. Ghosh, U. Chakraborty, and A. Sarkhel, “Isolation improvement of dual-/quad-element textile MIMO antenna for 5G application,” *Journal of Electromagnetic Waves and Applications*, vol. 35, no. 10, pp. 1-18, 2021.

[185] A. Kurshid, J. Dong, M. Ahmad, and R. Shi, “Optimized Super-Wideband MIMO antenna with high isolation for IoT applications,” *Micromachines*, vol. 13, no. 514, pp. 1-13, 2022.

[186] W. Mu, H. Lin, Z. Wang, C. Li, M. Yang, W. Nie, and J. Wu, “A flower shaped miniaturized UWB-MIMO antenna with high isolation,” *Electronics*, vol. 1, no. 2190, pp. 1-13, 2022.

[187] S. Nithya, and V. Seethalakshmi, “MIMO antenna with isolation enrichment for 5G mobile information,” *Hindawi Mobile Information Systems*, vol. 2022, no. 1802352, pp. 1-14, 2022.

[188] H. Kaur, and H. Singh, “A High-Isolated CPW-Fed Multi-Band Metamaterial Inspired MIMO Antenna for Wireless Applications,” in Handbook of Metamaterial-Derived Frequency Selective Surfaces, vol. 3, Singapore: Springer, 2022.

[189] T. Wang, H. Wang, G. Tan, L. Wang and L. Qiao, "The Relationship of Permeability and Permittivity at the Perfect Matching Point of Electromagnetic Wave Absorption for

the Absorber Filled by Metallic Magnetic Particles," *IEEE Transactions on Magnetics*, vol. 51, no. 6, pp. 1-5, 2015.

[190] T. Wanghuang, W. Chen, Y. Huang, and G. Wen, "Analysis of metamaterial absorber in normal and oblique incidence by using interference theory," *AIP Adv.*, vol. 3, pp. 102118-1-102118-3, 2013.

[191] S. Shang, S. Yang, L. Tao, L. Yang, and H. Cao, "Ultrathin triple-band polarization insensitive wide angle compact metamaterial absorber," *AIP Adv.,* vol. 6, pp. 075203-1-075203-8, 2016.

[192] C. A. Balanis, *Antenna Theory Analysis and Design*, John Wiley and Sons. New Jersey. New Jersey, 2005.